Vibrational Sum-Frequency Scattering Studies of Oil-in-Water Emulsions

THÈSE N^{O} 5074 (2011)

PRÉSENTÉE LE 29 SEPTEMBRE 2011

À LA FACULTÉ DES SCIENCES ET TECHNIQUES DE L'INGENIEUR
CHAIRE JULIA JACOBI DE PHOTOMÉDECINE - LABORATOIRE DE BIOPHOTONIQUE FONDAMENTALE
INSTITUT INTERFACULTAIRE DE BIOINGENIERIE

ÉCOLE POLYTECHNIQUE FÉDÉRALE DE LAUSANNE

POUR L'OBTENTION DU GRADE DE DOCTEUR ÈS SCIENCES

PAR

Hilton BARBOSA DE AGUIAR

acceptée sur proposition du jury:

Prof. O. Martin, président du jury
Prof. S. Roke , directrice de thèse
Prof. M. Bonn, rapporteur
Prof. C. Moser, rapporteur
Dr A. Petukhov, rapporteur

ÉCOLE POLYTECHNIQUE
FÉDÉRALE DE LAUSANNE

Suisse
2011

Abstract

Oil-in-water emulsions consist of oil droplets dispersed in an aqueous phase. Interfacial properties of the droplets determine the stability of emulsions. Even though this statement is widely accepted, a molecular level picture of the droplet interface is yet to be determined. In this thesis, we use Vibrational Sum-Frequency Scattering (SFS), an interface specific technique, to probe the interface of the droplets with chemical specificity. We start with a detailed description of how SFS measurements can be performed in water and what the effects of penetration depth, pulse energy and particle density are. This is followed by a comparison between non phase-matched SF scattering and phase-matched SF Generation from planar interfaces. We then show studies on hexadecane oil droplets stabilized by the anionic surfactant sodium dodecylsulfate (SDS) dipersed in D_2O. We measure the interfacial activity of SDS by probing the response of symmetric SO_3 stretch of the headgroup. Surprisingly, the results show that the interfacial density of SDS is very low, namely one order of magnitude lower than what would be expected at the corresponding planar interface. As a consequence of such a low interfacial density, the interfacial tension barely changes from the value of the pristine oil-water interface. Moreover, we use SFS to retrieve molecular order of the alkyl chains from the CH stretch responses of either SDS or oil using a selective deuteration scheme. The spectral analysis shows that the SDS alkyl chains are highly disordered at the droplets interface. In contrast, the alkyl chains of the oil molecules at the interface are more ordered than SDS. Interference experiments show that the oil molecules are, in contrast to what is seen on most planar interface, oriented predominantly parallel with respect to the interface. We also probe the alkyl chain order of SDS adsorbed at interfaces of dispersions of polymer particles. Regardless of the chemical structure of the dispersed phase the SDS molecules are always very disordered. We can therefore conclude that SDS does not show any specific interaction with the droplets or particles. In the last part of this thesis, we use SFS to probe electrostatic properties of the droplets interfaces. Adsorption of charged surfactants at the droplet interface creates a strong electrostatic field that is screened by water and counter ions in the solution. The electrostatic field, together with the incoming laser fields, excite the OD vibrational stretch of the water molecules in the vicinity of the interface with a strength proportional to the surface potential. The surface charge densities are probed by the response of the symmetric SO_3 stretch of the SDS headgroup. Therefore, we are able to independently measure the surface potential and the surface charge density. We show that it is essential to separate the changes of surface potential due to charging of the interface from changes due to screening effects. The results are in agreement with the Gouy-Chapman model.

Key words: nonlinear optics, sum-frequency generation, vibrational spectroscopy, nonlinear light scattering, nanodroplets, soft matter, photonics, liquid-liquid interfaces, oil-in-water emulsions, surfactant adsorption, electrical double-layer.

Résumé

Une émulsions huile-dans-eau est composée de gouttelettes d'huile dispersées dans une phase aqueuse. Les propriétés interfaciales des les gouttelettes jouent un rôle determinant dans la stabilité des émulsions. Même si cette affirmation est largement acceptée, une representation de l'interface au niveau moléculaire reste á formuler. Dans cette thèse, nous utilisons une méthode optique de generation vibrationelle de fréquence somme (SFS). Cette méthode spectroscopique permet d'analyser spécifiquement l'interface des gouttelettes. Après une description détaillée de l'expérience SFS et une caractérisation du signal de SFS, nous montrons des études sur les gouttelettes d'huile hexadécane disperses dans D_2O, stabilisées par un surfactant: dodécylsulfate de sodium (SDS). Nous avons mesuré l'activité interfaciale de SDS en sondant la réponse du mode SO_3 symétrique du groupe de tête du surfactant. Étonnamment, les résultats montrent que la densité interfaciale de SDS est très faible, à savoir un ordre de grandeur plus faible que ce qui était attendu pour une interface planaire correspondante. En conséquence de cette faible densité interfaciale, la tension interfaciale change à peine de la valeur de l'interface huile-eau vierge de SDS. En outre, nous utilisons SFS pour reconstituer la conformation moléculaire des chaînes alkyle à partir des réponses des mode CH du SDS ou de l'huile à l'aide de deutération sélective. L'analyse spectrale montre que les chaînes alkyle SDS sont fortement désordonnés à l'interface de la gouttelette. En revanche, les chaînes alkyle des molécules d'huile à l'interface sont plus ordonnées que celle du SDS. Nous avons également sonder de l'ordre des chaînes alkyle de SDS adsorbées à l'interface de dispersions de particules polymère. Quelle que soit la structure chimique de la phase dispersée les molécules de SDS sont toujours très désordonnées. Nous pouvons donc conclure que le SDS ne subit aucune interaction spécifique avec les gouttelettes ou les particules. Dans la dernière partie de cette thèse, nous utilisons SFS pour sonder les propriétés électrostatiques des interfaces des gouttelettes. L'adsorption de surfactants chargés à l'interface des gouttelettes crée un fort champ électrostatique qui est écranté dans la solution. Le champ électrostatique, ainsi que les champs laser entrant, excitent les mode de vibration OD des molécules d'eau dans le voisinage de l'interface avec une amplitude proportionnelle au potentiel de surface. Les densités de charges de surface (ou la densité interfaciale) sont détectés par la réponse SO_3 du groupe de tête de SDS. Par conséquent, nous sommes capables de mesurer indépendamment le potentiel de surface et la densité de charge de surface. Nous montrons qu'il est essentiel de séparer les modifications du potentiel duent au changement de la surface et de ceux duent au changement dans l'effet décrantage dans la solution. Les résultats sont conformes au modèle de Gouy-Chapman.

Mots clés: optique non linéaire, génération de fréquence somme, spectroscopie vibrationnelle, diffusion non linéaire de la lumière, nanogouttelettes, matière molle, photonique, interface liquide-liquide, émulsions huile-dans-eau, adsorption de surfactant, double couche

électrique.

Contents

Chapter 1

Introduction

1.1 Emulsions and interfacial science

Emulsions

Emulsions are a particular type of colloidal systems: Emulsions consist of two immiscible liquid phases with one liquid (dispersed phase) as droplets in the other (continuous phase) [1, 2]. Emulsions are present around us in our daily lives in many different forms or products. Milk, butter, ice-cream, mayonnaise, salad dressing are typical food emulsions. Detergent, shampoo and soap are not originally emulsions, but as soon as they are used for their cleaning purpose, they form an emulsion system, which consists of oil droplets stabilized by surfactants adsorbed at the interface. In petroleum industry emulsions are one of the main products and the separation of the oil from the water in a more effective way is constantly pursued.

There are different types of emulsions. Emulsions are subdivided into emulsions, microemulsions and nanoemulsions. The name emulsion is used for systems that have droplet sizes in the range 0.1-100 μm. Ref. [3, 4] are comprehensive reviews. Other definitions exist, but for the purpose of this thesis we shall only discuss about these last three above-mentioned and not have a comprehensive description of emulsions. In these systems, there can be some overlap of the size range of the droplets, which leads to some confusion in definitions in literature, but these systems are fundamentally different. Emulsions and nanoemulsions are inherently nonequilibrium systems, meaning that one needs energy to form the droplets. This leads the system to a state that is out of thermodynamic equilibrium. In contrast, microemulsions are formed spontaneously upon mixing of the constituents. Therefore, microemulsions are in thermodynamic equilibrium and are not comparable to emulsions or nanoemulsions. It has been suggested that the term swollen micelles is more appropriate to microemulsions.

The creation of an emulsion (or nanoemulsion) is energetically unfavorable, meaning that in order to make an emulsion one needs energy. The reason lies on the the interfacial tension which exists between two liquids. The interfacial tension γ is the change in free energy F that accompanies a change in interfacial area A and can be written as [5]

$$\gamma = \frac{\partial F}{\partial A}. \tag{1.1}$$

Since γ is a positive quantity for the oil-water interface, an increase in interfacial area will increase the free energy of the system. Therefore, once an emulsion is created, its lifetime is very short and the system tends to its state of minimum energy: the phase separated bulk oil and bulk water. However, with addition of the surfactants one can readily observe emulsion stability for hours, days, months or even years! Consequently, emulsions and nanoemulsions are considered metastable systems.

Surfactants are amphiphilic molecules that have a hydrophobic part (like oil) and a hydrophilic part (like water) and reside at the oil-water interface of the droplets. The simplest chemical structure of surfactants consists of an alkyl chain chemically bound to a water-soluble chemical group. The hydrophilic part can carry a net charge and therefore these type

of surfactants are called ionic surfactants. A non-ionic surfactant is a surfactant that does not carry a net charge. Typical surfactants used for preparation of oil-in-water emulsions are shown in Fig. 1.1. Surfactants are the species responsible for the stability of an emulsion. The explanation for emulsion (meta) stability is due to the adsorption of surfactants at the interface which creates a repulsive interaction between droplets. This repulsive interaction will be explained in more details in Chapter 6.

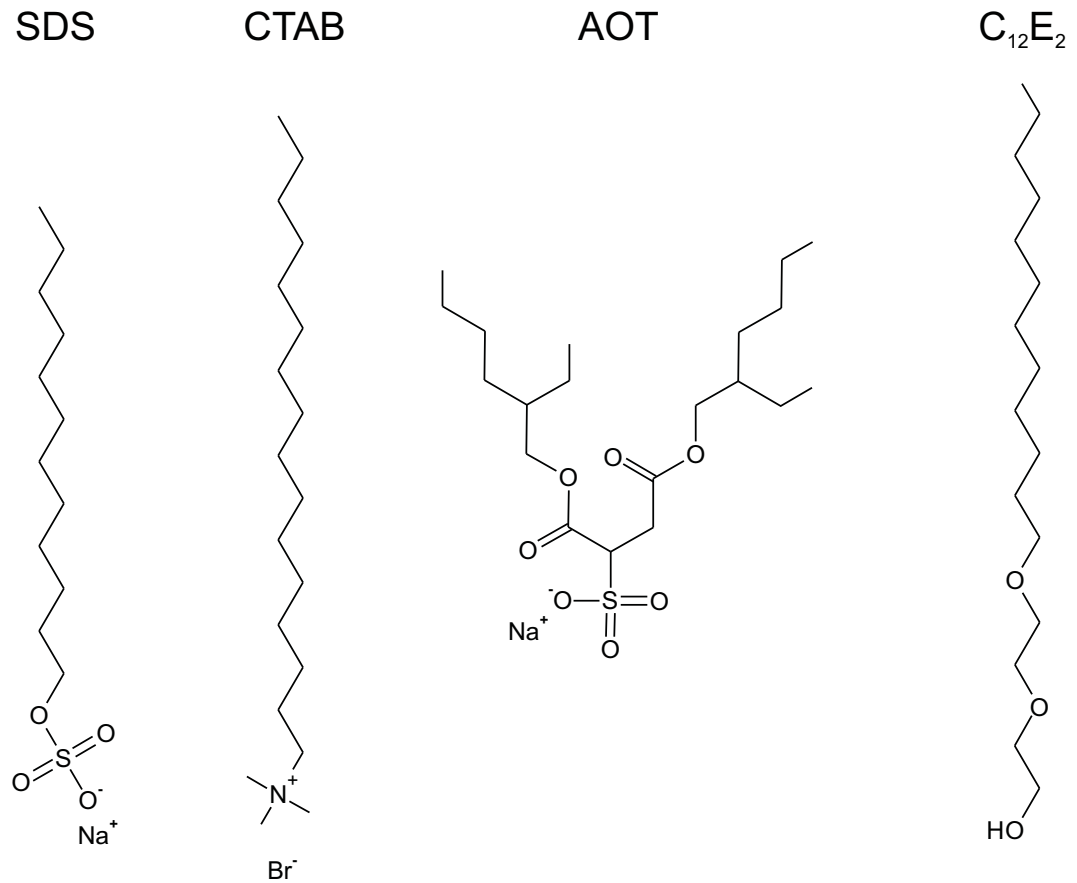

Figure 1.1: Typical surfactants used in oil-in-water emulsions. Anionic: sodium dodecylsulfate (SDS). Cationic: hexadecyltrimethylammonium bromide (CTAB). Anionic: sodium bis(2-ethylhexyl) sulfosuccinate (AOT). Non-ionic: Diethyleneglycol dodecylether ($C_{12}E_2$).

Once an emulsion is created the destabilization can be through different mechanisms: flocculation, creaming, coalescence and/or Ostwald ripening. Some of these destabilization mechanism are easily reversible, with no destruction of the droplets. Flocculation is simply the formation of aggregates of droplets without fusion of them. Creaming is the action of gravitational forces on the droplets forcing them to go to the top (oil of lower density than water) or to the bottom (oil of higher density) of the emulsion. Coalescence is the fusion of droplets upon impact, forming a bigger droplet. Ostwald ripening is the increase of the size of bigger droplets at the expense of the smaller ones. Ostwald ripening occurs through diffusion of the molecules of the smaller droplets through the continuous phase towards the

bigger droplets. Note that these destabilization mechanisms can occur independently of each other or even be additive. For instance, flocculation can lead to faster creaming rate, since the effective droplet (a floc) has a heavier mass, or to a faster Ostwald ripening rate, since the droplets are closer and therefore the diffusion of molecules is faster.

One can see that a molecular level description of the interface of the droplets is of extreme importance since the interfacial properties determine emulsions stability. Unfortunately, to probe droplets interfaces at a molecular level is an experimental challenge for many reasons, from which we highlight two. (*i*) The experimental probe needs to distinguish the response of the interfacial species from the bulk ones, in other words, the probe needs to be interface specific. Only in the last decades few techniques became available and capable of discerning interfacial response from the outnumbering bulk response. It should be noted here that the interface specificity of a technique is proved by performing experiments on planar interfaces, not directly on emulsions system. (*ii*) An emulsion is an inhomogeneous liquid, therefore the experimental probe needs to penetrate both phases (the dispersed one and the continuous one) without extinction in order to impinge on the interface of the droplets.

Interfacial science

Since the droplet interfaces are buried in the continuous phase and direct probing was not possible, historically, experiments on planar model interfaces were used to gain insight in emulsion properties. Planar interfaces experiments showed that amphiphilic molecules can form a single molecule thick layer at planar interfaces [6, 7]. Shortly after, Harkins and others tried to correlate the stability of emulsions with the molecular properties of surfactants [8] (geometry of the surfactant, valency of the hydrophilic moiety etc) with the observations from planar interface experiments [9]. One of the outcomes of these studies of emulsions was that the interfacial density of surfactants at the oil droplets interface had a limiting value close to the value of a close packed monolayer [9–11]. Since similar values were also observed on experiments performed at planar interfaces, they concluded that the interfacial molecules in both systems, droplets and planar interfaces, behave similarly.

Correlations between planar interface experiments and emulsion stability were one of the motivations for studying planar interfaces and, consequently, triggered a numerous amount of studies. However, the techniques used are macroscopically averaged (*e. g.* interfacial tension, contact angle) and by means of thermodynamics analysis a tentative molecular-level picture of the interface was inferred [5, 7].

On the pursuit to obtain a molecular level description of interfaces, new techniques that can retrieve molecular level information were adapted to study liquid planar interfaces. For instance, X-Ray Reflectivity, Neutron reflectivity [12] and Nonlinear Optical techiniques, such as Second-Harmonic and Sum-Frequency Generation [13], were developed in the past decades and demonstrated to be interface-specific techniques with molecular resolution. Although these techniques had given a molecular level description of the air-liquid interfaces,

there was a lag until these techniques started probing the liquid-liquid interface. The main challenge was to design an experiment where the probe can impinge on the liquid-liquid interface without extinction [14].

The majority of studies on liquid-liquid interfaces were done on CCl_4-water, 1,2-dichloroethane-water and alkane-water [15, 16] interfaces. In particular, the CCl_4-water interface has been extensively studied by SFG because CCl_4 is infrared-transparent allowing the beam to impinge at the interface, even though CCl_4 is not an oil. The alkane-water interface is the main subject of this thesis, therefore we shall focus on this interface. The neat interface has been probed with X-Ray Reflectivity (XRR) [17–19], Neutron Reflectivity (NR) [20, 21], Second-Harmonic Generation (SHG) [22], Sum-Frequency Generation (SFG) [23] and Ellipsometry [24]. XRR and NR studies have shown that the width of the interface is larger than expected based solely on capillary wave theory. The width could be explained by considering an intrinsic width, based on the radius of gyration of the alkane, plus the capillary wave width. SHG measurements concluded that the alkane-water interface is highly structured (ordered). The authors of the XRR studies discussed that this ordering of the alkane-water interface measured by SHG should be somewhat related to the larger width measured by XRR and NR. The structuring of the water at the alkane-water interface was partly confirmed by SFG measurements [23] since a recorded spectrum of the water response necessarily requires a noncentrossymetric arrangement of the molecule at interface. Note that none of these techniques, except SFG, can determine if the ordering of the interface is due to the alkane or water molecules. Therefore, it is not excluded that ordering is due to the alkane molecules.

The presence of surface active species strongly changes the properties of liquid-liquid interfaces. The neat alkane-water interface does not show interfacial freezing [18]. However, the presence of surfactants at the interface can readily induce interface-freezing [25, 26]. It has also been observed that surfactants soluble in water are highly disordered at the CCl_4-water interface [27, 28], but more ordered at the hexadecane-water interface [29]. Surfactants soluble in the alkane phase showed that mixing of the alkyl chains of the surfactants with the alkanes is not as strong as previously thought [30]. It also has been observed that multilayer coverage could be achieved by changing the chain length difference between surfactant and alkane [31]. The lack of more experimental results in a systematic way among different systems (surfactant chain length, oil chain length etc) makes it difficult to obtain a trend among all different systems studied. One could try however to relate the results of air-water systems directly to the alkane-water systems, but there are fundamental differences between the two systems which makes questionable whether a correlation is useful [29, 30, 32]. These few examples covered here are not meant to be comprehensive, but rather to illustrate that molecular level studies of liquid-liquid interfaces are still in its infancy.

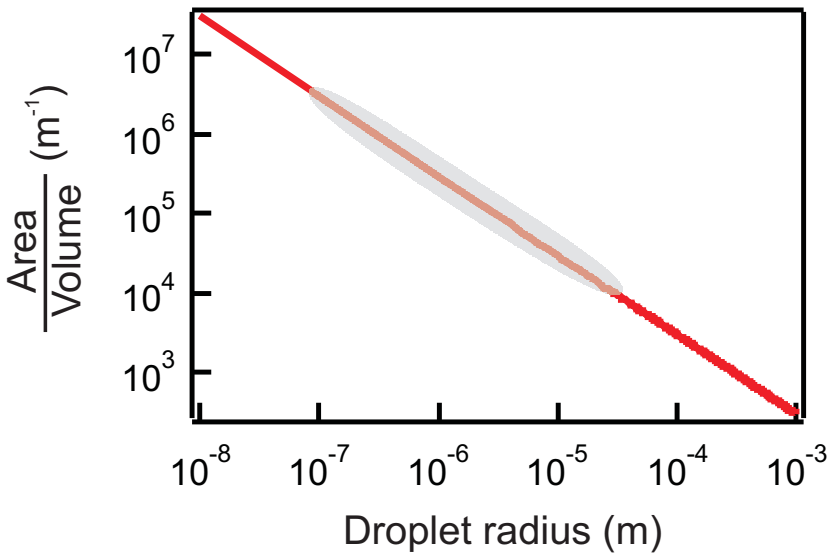

Figure 1.2: Total intefacial area per volume of a dispersion as a function of particle radius for a 10% volume fraction. The shaded area correspons to the drople size range commonly found in emulsions.

The gap between emulsions and interfacial science

Although our understanding at a molecular level of planar liquid-liquid interfaces has advanced recently, very few studies [33, 34] have actually tried to relate the results of planar interfaces to the emulsion stability. Because now we have a more refined picture of the liquid-liquid interface, it is suggestive to make an update of the original experiments performed by Harkins and others from the beginning of the last century. Therefore, we raise the question to which extent the planar liquid interfaces are similar to the droplets interface of emulsion systems at a molecular level? We give some reasonings for this question below.

There are orders of magnitudes difference in the total interfacial area between the phase separated system (planar) and an emulsion system. Fig. 1.2 illustrates this point where we plot the total interfacial area-to-volume ratio as a function of size of the droplets for an emulsion. Typically, the area in a planar interface experiment would be comparable to the values in the lowest range (mm) of the area-to-volume ratio, whereas emulsion systems, illustrated by the shaded area in Fig. 1.2, can easily vary from 100 nm to 10 μm in droplet radii.

Another fundamental difference is in the timescale of droplet movement compared to timescale of equilibrium adsorption. For planar interface systems, equilibrium between adsorbed and bulk species is achieved in the timescale of hundreds of ms [35, 36]. However, droplets in emulsions are not static interfaces. Droplets are in constant movement due to thermal (Brownian) and/or gravitational forces. Would an interface that is constantly moving arrive at the same equilibrium as observed for a planar system?

In planar interface systems there is just one liquid-liquid interface. Droplets in emulsions

are constantly moving and eventually, the interfaces of different droplets start to interact with each other as the droplets approach. The effects of this interactions cannot me mimicked in a planar interface experiment.

1.2 Sum-Frequency Generation (SFG)

Since the first experimental demonstration of (reflection) Infrared-Visible Sum-Frequency Generation in the late 80's [37, 38], the technique has rapidly spread. Nowadays, SFG is a powerful technique to probe interfaces due to its inherent interface specificity with chemical selectivity (a similarity shared with other vibrational spectroscopies). For instance, solid-liquid, solid-solid [39], vapour-liquid [40] and biologically relevant interfaces [41] are among the systems most explored by SFG. It has also advanced to new applications/modes, not being limited to a static spectroscopy. Considerable advances have been achieved in the field of dynamics of interfaces due to its ultrafast time resolution [42]. New applications include SFG microscopy [43] and sum-frequency scattering [44]. In the next section we explain the basics of the technique and the origin of the interface specificity. In the following chapters, there will be an introduction to the specific application of the technique.

Interface specificity

If electromagnetic fields impinging on matter are strong enough, they can excite higher-order polarization terms [45]. The polarization $\mathbf{P}$ can be expanded in a power series of the driving (electric) fields $\mathbf{E}$ as

$$\begin{aligned}\mathbf{P}_i &= \chi^{(1)}_{ij}\mathbf{E}_j + \chi^{(2)}_{ijk}\mathbf{E}_k\mathbf{E}_l + \chi^{(3)}_{ijkl}\mathbf{E}_j\mathbf{E}_k\mathbf{E}_l + \dots \\ &= \mathbf{P}^{(1)} + \mathbf{P}^{(2)} + \mathbf{P}^{(3)} + \dots,\end{aligned}$$

where $\chi^{(n)}$ is the nth-order electrical susceptibility. $\mathbf{P}^{(1)}$ is the first-order polarization responsible for phenomena like refraction, reflection and (linear) scattering. $\mathbf{P}^{(2)}$ is the second-order polarization responsible for phenomena like Second-Harmonic Generation and Sum-Frequency Generation. $\mathbf{P}^{(3)}$ is the third-order polarization responsible for phenomena like Intensity-Dependent Refractive Index and Third-Harmonic Generation.

Here, we focus on the description and properties of the second-order process Sum-Frequency Generation (SFG) [13, 46]. Second-Harmonic Generation is a particular case where the exciting fields are degenerate. Two electric fields $\mathbf{E}(\omega_1)$ and $\mathbf{E}(\omega_2)$, oscillating at frequencies ω_1 and ω_2, respectively, can induce a second-order nonlinear polarization that oscillates at their sum-frequency $\omega_0 = \omega_1 + \omega_2$

$$\mathbf{P}^{(2)}_i(\omega_0) = \chi^{(2)}_{ijk}(\omega_0, \omega_1, \omega_2)\mathbf{E}_k(\omega_1)\mathbf{E}_l(\omega_2), \tag{1.2}$$

where $\chi^{(2)}_{ijk}$ is the second-order electrical susceptibility. For a centrossymetric material, *e. g.* liquids, glasses, $\chi^{(2)}_{ijk}$ is invariant under the inversion operation. If the fields change sign in a centrossymetric material, the polarization must also change sign as

$$-\mathbf{P}^{(2)}_i(\omega_0) = \chi^{(2)}_{ijk}(\omega_0,\omega_1,\omega_2)(-\mathbf{E}_k(\omega_1))(-\mathbf{E}_l(\omega_2)) \tag{1.3}$$

$$= \chi^{(2)}_{ijk}(\omega_0,\omega_1,\omega_2)\mathbf{E}_k(\omega_1)\mathbf{E}_l(\omega_2). \tag{1.4}$$

The only possible solution to Eqs. 1.2 and 1.4 is $\chi^{(2)}_{ijk} = 0$. This means that an SFG process is not allowed in centrossymetric material. However, at interfaces between two centrossymetric materials the centrossymetry is broken leading to a nonzero $\chi^{(2)}_{ijk}$. Because the second-order polarization is nonzero, it oscillates at ω_0 thus acting as source to generate a photon at the sum-frequency.

$\chi^{(2)}_{ijk}$ is a third-rank tensor with 27 possible non-zero elements. Due to additional symmetry constraints, the number of elements can be greatly reduced. For an interface that has cylindrical symmetry (C_∞) the number of independent elements reduce to only 4. They are

$$\chi^{(2)}_{\parallel\parallel\perp}, \chi^{(2)}_{\parallel\perp\parallel}, \chi^{(2)}_{\perp\parallel\parallel}, \chi^{(2)}_{\perp\perp\perp},$$

where the $\chi^{(2)}$ components are defined in respect to the perpendicular ($\perp$) or parallel ($\parallel$) directions to the interface (see inset of Fig. 1.3). $\chi^{(2)}_{ijk}$ is a macroscopic physical quantity and is related to the molecular hyperpolarizability $\beta^{(2)}_{abc}$ as

$$\chi^{(2)}_{ijk} = N_s\langle T_{ia}T_{jb}T_{kc}\rangle\beta^{(2)}_{abc}, \tag{1.5}$$

where N_s is the density of molecules, T_{mn} denote a coordinate transformation from the molecular coordinate system (a,b,c) to the lab coordinate system (i,j,k) and $\langle\rangle$ denote average over the molecular orientations.

If the energy of one of the electric fields is equal to a transition between two real quantum levels, $\chi^{(2)}$ is greatly enhanced. This, in turn, will increase the detected SF intensity. In the case of organic molecules, resonant conditions can be achieved by using mid-infrared (IR) radiation. In the frequency range of the mid-IR, molecules have specific vibrational transitions energies for each moiety, which gives chemical specificity to SFG spectroscopy. The strength of $\chi^{(2)}$ under resonant conditions is modeled as a Lorentzian distribution as

$$\chi^{(2)} = A_{NR}e^{i\Delta\phi} + \sum_n \frac{A_n}{(\omega_{IR}-\omega_{0n}) + \mathrm{i}\Upsilon_\mathrm{n}}, \tag{1.6}$$

where A_{NR} refers to the amplitude of the non-resonant (NR) contribution, n refers to a vibrational mode with resonance frequency ω_{0n}, amplitude A_n and half width at half maximum Υ_n. $\Delta\phi$ is the phase difference between the resonant and non-resonant response. The resonant SF cross-section A_n is

$$A_{n,ijk} \propto \frac{\partial\alpha_{ij}}{\partial Q}\frac{\partial\mu_k}{\partial Q}, \tag{1.7}$$

where $\frac{\partial\alpha_{ij}}{\partial Q}$ and $\frac{\partial\mu_k}{\partial Q}$ are the Raman and IR transition cross-sections, respectively. Eq. 1.7 shows that in order for a vibrational mode to be SFG-active it must be *both* IR and Raman active.

1.3 Nonlinear light scattering

1.3.1 General perspective

As seen in the previous section, second-order processes (SHG, SFG) are forbidden in centrosymmetric media. Nevertheless, SHG could be observed for the first time from spherical colloidal particles dispersed in a liquid in 1996 [47]. Since then, a great number of applications of the technique to colloidal systems have been made. These include studies of electrostatic properties of polymer particles surface [48], adsorption of molecules at colloidal interfaces [49–52], surface acid-basic equilibria [53] and molecular transport across liposome bilayers [54–56]. Vibrational Sum-Frequency Scattering (SFS) experiments in colloidal suspensions was first demonstrated in 2003 [44]. Shortly after, SFS was used to probe complex colloidal phase transitions [57, 58] and later on crystalline domains in polymer microspheres [59].

The physical origins of the processes are relatively well understood. For SHG, the radiation pattern, polarization combinations, particle size dependence and particle/ wavelength ratios have been studied using different approaches (approximations or exact solution) [60–63]. In the case of SFG, chiral and nonchiral surfaces [64], radiation pattern [65], polarization combinations and molecular orientation analysis [66] have been documented.

When visible (VIS) and infrared (IR) electric fields are overlapped in a suspension, a second-order polarization cannot be excited from the homogeneous centrossymetric bulk. However, at the interface of the particles, centrossymetry is broken and *at* the interface a second order polarization is excited. This polarization is the source of the SF photons (or SH) At the far field, where the detector is positioned, the SF photons interfere and in some positions they interfere destructively and others constructively. In fact, this interference pattern in the far field is the scattering pattern.

In the next section, we show the formulas needed to describe a scattering pattern, from which we obtain the position where the maximum intensity is expected and therefore where to set the detector and record a spectrum.

1.3.2 Sum-Frequency Scattering (SFS)

Figure 1.3 depicts the geometry of the SFS process at a single-particle level. An IR and a VIS laser beams with wavevectors $\mathbf{k}_1$ and $\mathbf{k}_2$, respectively, are incident on a spherical particle with radius R. At the interface of the particle a second-order polarization is created which oscillates at the sum of IR and VIS frequencies. This oscillating polarization is the source of the SF photons. SF photons are detected at an angle θ which is the angle between the wavevector $\mathbf{k}_0^0$ (the sum of the incoming wave vectors $\mathbf{k}_0^0 = \mathbf{k}_1 + \mathbf{k}_2$) and the wavevector of the scattered $\mathbf{k}_0$. $\mathbf{q}$ is defined as the difference between $\mathbf{k}_0$ and $\mathbf{k}_0^0$ ($\mathbf{q} = \mathbf{k}_0 - \mathbf{k}_0^0$). The polarization state of the electric fields are defined relative to the plane XY with p electric fields polarized parallel and s perpendicular to the XY plane.

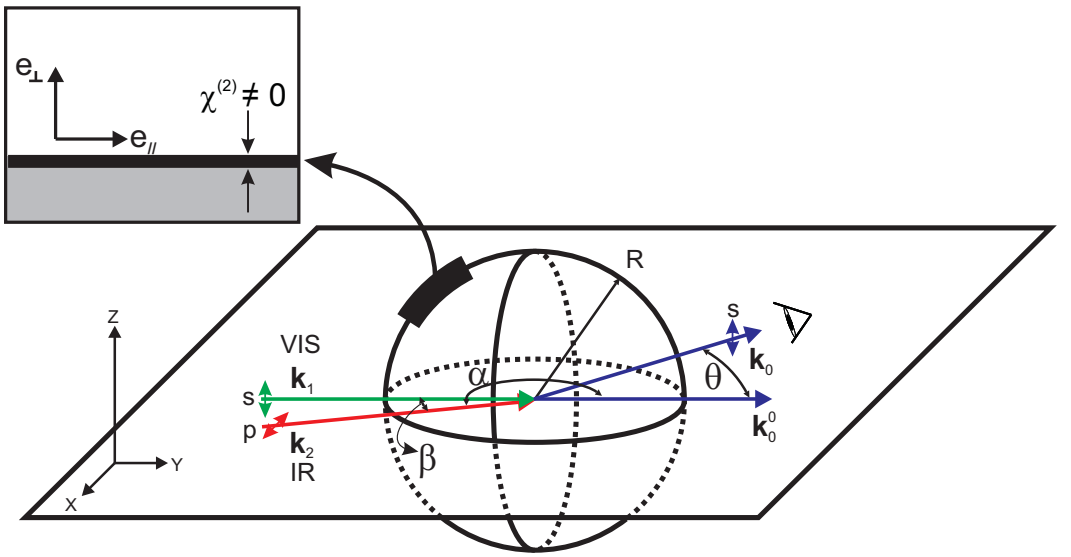

Figure 1.3: Illustration of the SFS scattering geometry at a single particle level. The top left inset depicts the interface coordinate system.

The generated SFS field is given by

$$E_{0,i} \propto \Gamma^{(2)}_{ijk}(\chi^{(2)}, R, \theta) : E_{1,j} E_{2,k}. \tag{1.8}$$

$\Gamma^{(2)}$ is the effective particle susceptibility. It is a quantity that depends on the second-order response of the surface ($\chi^{(2)}$), scattering geometry and particle shape. Refs. [44, 64, 65] show the derivation of the $\Gamma^{(2)}$ expressions for spherical particles.

The relation between the particle interfacial response given by the $\chi^{(2)}$ elements to the measured quantity $\Gamma^{(2)}$ elements is

$$\begin{pmatrix} \Gamma_1 \\ \Gamma_2 \\ \Gamma_3 \\ \Gamma_4 \end{pmatrix} = \begin{pmatrix} 2F_1 - 5F_2 & 0 & 0 & 0 \\ F_2 & 2F_1 & 0 & 0 \\ F_2 & 0 & 2F_1 & 0 \\ F_2 & 0 & 0 & 2F_1 \end{pmatrix} \begin{pmatrix} \chi_1 \\ \chi_2 \\ \chi_3 \\ \chi_4 \end{pmatrix}, \tag{1.9}$$

where the effective susceptibility are redefined as $\Gamma_1 = \Gamma^{(2)}_{zzz} - \Gamma^{(2)}_{xxz} - \Gamma^{(2)}_{xzx} - \Gamma^{(2)}_{zxx}$, $\Gamma_2 = \Gamma^{(2)}_{xxz}$,$\Gamma_3 = \Gamma^{(2)}_{xzx}$ and $\Gamma_4 = \Gamma^{(2)}_{zxx}$. The $\chi^{(2)}$ elements are redefined as $\chi_1 = \chi^{(2)}_{\perp\perp\perp} - \chi^{(2)}_{\parallel\parallel\perp} - \chi^{(2)}_{\parallel\perp\parallel} - \chi^{(2)}_{\perp\parallel\parallel}$, $\chi_2 = \chi^{(2)}_{\parallel\parallel\perp}$,$\chi_3 = \chi^{(2)}_{\parallel\perp\parallel}$ and $\chi_4 = \chi^{(2)}_{\perp\parallel\parallel}$. The form factor functions $F_1(qR)$ and $F_2(qR)$ are given by

$$F_1(qR) = 2\pi i \left(\frac{\sin(qR)}{(qR)^2} - \frac{\cos(qR)}{qR} \right) \tag{1.10}$$

$$F_2(qR) = 4\pi i \left(3\frac{\sin(qR)}{(qR)^4} - 3\frac{\cos(qR)}{(qR)^3} - \frac{\sin(qR)}{(qR)^2} \right). \tag{1.11}$$

The argument of the form factors is the modulus of the scattering vector $q = ||\mathbf{q}|| = 2|\mathbf{k}_0| \sin(\theta/2)$ and the particle radius R.

The scattered electric field amplitudes are:

$$\begin{aligned} E_{ppp} \propto\ & \cos\left(\frac{\theta}{2}\right)\cos\left(\frac{\theta}{2}-\alpha\right)\cos\left(\frac{\theta}{2}-\alpha+\beta\right)\Gamma_1^{(2)} \\ & +\cos\left(\theta-\alpha+\beta\right)E_{ssp} \\ & +\cos\left(\theta-\alpha\right)E_{sps} \\ & +\cos\left(\beta\right)E_{pss}, \end{aligned} \tag{1.12}$$

$$E_{ssp} \propto \cos\left(\frac{\theta}{2}-\alpha\right)\Gamma_2^{(2)}, \tag{1.13}$$

$$E_{sps} \propto \cos\left(\frac{\theta}{2}-\alpha+\beta\right)\Gamma_3^{(2)}, \tag{1.14}$$

$$E_{pss} \propto \cos\left(\frac{\theta}{2}\right)\Gamma_4^{(2)}, \tag{1.15}$$

where the angle between the incoming IR and VIS is β and the angle between $\mathbf{k}_0^0$ and $\mathbf{k}_2$ is α.

1.4 Thesis outline

The aim of this thesis is to explore the buried droplet interface of emulsions at a molecular level. For that purpose, we combine traditional approaches of the two sides of the same coin (colloidal and interfacial science). From the interfacial science side, we use Vibrational Sum-Frequency Generation which is an interface specific technique capable of obtaining a molecularly resolved picture of the interface. From the colloidal science side, we use Nonlinear Light Scattering which is a combination of Sum Frequency Generation and Linear Light Scattering to study droplet interfaces. We also use other techniques like Electrophoretic Mobility measurements to correlate with our results. Using this joint approach we hope to start bridging the gap between the two sides and finally give a molecularly resolved picture of the droplets interface without need of extrapolations.

This thesis uses as model system the hexadecane-in-water emulsions stabilized by the surfactant SDS. In Chapter 2 we present details on emulsions preparation and characterization, as well as details on the laser setup. In Chapter 3 we present experimental details on the implementation of the SFS experiment and its characterization, with emphasis in how to discern the SFS process from possible unwanted responses. In Chapter 4 we use SFS to determine an upper limit for the interfacial density of SDS at the critical micelle concentration by probing the SO_3 stretch vibration of the surfactant headgroup. In Chapter 5 we probe the CH stretch of the alkyl chain of either SDS or the oil molecules in order to infer how ordered they are at the interface. Finally, in Chapter 6 we use SFS to probe the electrostatic properties of the droplets interface by measuring independently the surface potential and surface charge density. A summary of the main conclusions are presented in end of this thesis as well as an outlook for future work.

Bibliography

[1] I. D. Morrison and S. Ross. *Colloidal Dispersions: Suspensions, Emulsions, and Foams*. Wiley-Interscience, 2002.

[2] J. W. Goodwin. *Colloids and interfaces with surfactants and polymers: an introduction*. John Wiley & Sons, 2004.

[3] T Mason, J Wilking, K Meleson, C Chang, and S Graves. Nanoemulsions: formation, structure, and physical properties. *J. Phys.: Condens. Matter*, 18(41):R635, 2006.

[4] D McClements. Critical review of techniques and methodologies for characterization of emulsion stability. *Crit. Rev. Food Sci. Nutr.*, 47:611–649, 2007.

[5] J. T. Davies and E. K. Rideal. *Interfacial Phenomena*. Academic Press, 2nd edition, 1963.

[6] I Langmuir. The constitution and fundamental properties of solids and liquids. II. Liquids. *J. Am. Chem. Soc.*, 39:1848–1906, 1917.

[7] W. D. Harkins. *The Physical Chemistry of Surface Films*. Reinhold Publishing Corporation, 1952.

[8] P Finkle, H Draper, and J Hildebrand. The theory of emulsification. *J. Am. Chem. Soc.*, 45:2780–2788, 1923.

[9] E Fischer and W Harkins. Monomolecular films. the liquid-liquid interface and the stability of emulsions. *J. Phys. Chem.*, 36(1):98–110, 1932.

[10] W Harkins and N Beeman. Emulsions: stability, area per molecule in the interfacial film, distribution of sizes and the oriented wedge theory. *J. Am. Chem. Soc.*, 51:1674, 1929.

[11] A Martin and R Hermann. Emulsions. Part I. Mechanism of emulsification of a standard emulsion in sodium oleate solution and nature of adsorption at the interface. *Trans. Faraday Soc.*, 37:25–29, 1941.

[12] M Schlossman. Liquid-liquid interfaces: studied by x-ray and neutron scattering. *Curr. Opin. Colloid Interface Sci.*, 7(3-4):235, 2002.

[13] Y Shen. Surface-properties probed by 2nd-harmonic and sum-frequency generation. *Nature*, 337(6207):519, 1989.

[14] J. M. Perera and G. W. Stevens. Spectroscopic studies of molecular interaction at the liquid-liquid interface. *Anal. Bioanal. Chem.*, 395(4):1019, 2009.

[15] C McFearin, D Beaman, F Moore, and G Richmond. From franklin to today: Toward a molecular level understanding of bonding and adsorption at the oil-water interface. *J. Phys. Chem. C*, 113(4):1171, 2009.

[16] M. L. Schlossman and A. M. Tikhonov. Molecular ordering and phase behavior of surfactants at water-oil interfaces as probed by x-ray surface scattering. *Annu. Rev. Phys. Chem.*, 59(1):153–177, 2008.

[17] D. Mitrinovic, A. M. Tikhonov, M. Liand Z. Q. Huang, and M. L. Schlossman. Noncapillary-wave structure at the water-alkane interface. *Phys. Rev. Lett.*, 85(3):582–585, 2000.

[18] A Tikhonov, D Mitrinovic, M Li, Z Huang, and M Schlossman. An x-ray reflectivity study of the water-docosane interface. *J. Phys. Chem. B*, 104(27):6336–6339, 2000.

[19] K Kashimoto, J Yoon, B Hou, C Chen, B Lin, M Aratono, T Takiue, and M Schlossman. Structure and depletion at fluorocarbon and hydrocarbon/water liquid/liquid interfaces. *Phys. Rev. Lett.*, 101(7):076102, 2008.

[20] J Bowers, A Zarbakhsh, J Webster, L Hutchings, and R Richards. Neutron reflectivity studies at liquid-liquid interfaces: Methodology and analysis. *Langmuir*, 17(1):140–145, 2001.

[21] A Zarbakhsh, J Bowers, and J Webster. Width of the hexadecane-water interface: A discrepancy resolved. *Langmuir*, 21(25):11596–11598, 2005.

[22] J Conboy, J Daschbach, and G Richmond. Studies of alkane water interfaces by total internal-reflection 2nd-harmonic generation. *J. Phys. Chem.*, 98(39):9688, 1994.

[23] M Brown, D Walker, E Raymond, and G Richmond. Vibrational sum-frequency spectroscopy of akane/water interfaces: Experiment and theoretical simulation. *J. Phys. Chem. B*, 107(1):237–244, 2003.

[24] J Day and C Bain. Ellipsometric study of depletion at oil-water interfaces. *Phys. Rev. E*, 76(4):041601, 2007.

[25] Q Lei and C Bain. Surfactant-induced surface freezing at the alkane-water interface. *Phys. Rev. Lett.*, 92(17):176103, 2004.

[26] E Sloutskin, C Bain, B Ocko, and M Deutsch. Surface freezing of chain molecules at the liquid-liquid and liquid-air interfaces. *Faraday Discuss. Chem. Soc.*, 129:339–352, 2005.

[27] M Messmer, J Conboy, and G Richmond. Observation of molecular ordering at the liquid-liquid interface by resonant sum-frequency generation. *J. Am. Chem. Soc.*, 117(30):8039, 1995.

[28] J. C. Conboy, M. C. Messmer, and G. L. Richmond. Investigation of surfactant conformation and order at the liquid-liquid interface by total internal reflection sum-frequency vibrational spectroscopy. *J. Phys. Chem.*, 100(18):7617–7622, 1996.

[29] M. M. Knock, G. R. Bell, E. K. Hill, H. J. Turner, and C. D. Bain. Sum-frequency spectroscopy of surfactant monolayers at the oil-water interface. *J. Phys. Chem. B*, 107(39):10801–10814, 2003.

[30] A Tikhonov and M Schlossman. Surfactant and water ordering in triacontanol monolayers at the water-hexane interface. *J. Phys. Chem. B*, 107(15):3344–3347, 2003.

[31] A Tikhonov and M Schlossman. Vaporization and layering of alkanols at the oil/water interface. *J. Phys.: Condens. Matter*, 19:375101, 2007.

[32] R. A. Walker, J. A. Gruetzmacher, and G. L. Richmond. Phosphatidylcholine monolayer structure at a liquid-liquid interface. *J. Am. Chem. Soc.*, 120(28):6991, July 1998.

[33] S. A. Nespolo, M. A. Bevan, D. Y. C. Chan, F. Grieser, and G. W. Stevens. Hydrodynamic and electrokinetic properties of decane droplets in aqueous sodium dodecyl sulfate solutions. *Langmuir*, 17(23):7210, 2001.

[34] D Georgieva, V Schmitt, F Leal-Calderon, and D Langevin. On the possible role of surface elasticity in emulsion stability. *Langmuir*, 25(10):5565–5573, 2009.

[35] V Fainerman. Adsorption-kinetics from concentrated micellar solutions of ionic surfactants at the water air interface. *Colloids Surf.*, 62(4):333–347, 1992.

[36] A Javadi, N Mucic, D Vollhardt, V Fainerman, and R Miller. Effects of dodecanol on the adsorption kinetics of SDS at the water-hexane interface. *J. Colloid Interface Sci.*, 351(2):537–541, 2010.

[37] X Zhu, H Suhr, and Y Shen. Surface vibrational spectroscopy by infrared-visible sum frequency generation. *Phys. Rev. B*, 35(6):3047–3050, 1987.

[38] J Hunt, P Guyotsionnest, and Y Shen. Observation of C-H stretch vibrations of monolayers of molecules optical sum-frequency generation. *Chem. Phys. Lett.*, 133(3):189–192, 1987.

[39] F. Vidal and A. Tadjeddine. Sum-frequency generation spectroscopy of interfaces. *Rep. Prog. Phys*, 68(5):1095–1127, 2005.

[40] P. B. Miranda and Y. R. Shen. Liquid interfaces: A study by sum-frequency vibrational spectroscopy. *J. Phys. Chem. B*, 103(17):3292, 1999.

[41] S. Roke. Nonlinear optical spectroscopy of soft matter interfaces. *ChemPhysChem*, 10(9-10):1380–1388, 2009.

[42] H Arnolds and M Bonn. Ultrafast surface vibrational dynamics. *Surf. Sci. Rep.*, 65(2):45–66, 2010.

[43] K Cimatu and S Baldelli. Chemical microscopy of surfaces by sum frequency generation imaging. *J. Phys. Chem. C*, 113(38):16575–16588, 2009.

[44] S. Roke, W. G. Roeterdink, J. E.G. J.Wijnhoven, A. V. Petukhov, A. W. Kleyn, and M. Bonn. Vibrational sum frequency scattering from a submicron suspension. *Phys. Rev. Lett.*, 91:258302, 2003.

[45] Robert W. Boyd. *Nonlinear Optics*. Academic Press, 2nd edition, 2003.

[46] A. Lambert, P. B. Davies, and D. J. Neivandt. Implementing the theory of sum frequency generation vibrational spectroscopy: A tutorial review. *Appl. Spectrosc. Rev.*, 40(2):103, 2005.

[47] H. Wang, E. C. Y. Yan, E. Borguet, and K. B. Eisenthal. Second harmonic generation from the surface of centrosymmetric particles in bulk solution. *Chem. Phys. Lett.*, 259(1-2):15–20, 1996.

[48] E Yan, Y Liu, and K Eisenthal. New method for determination of surface potential of microscopic particles by second harmonic generation. *J. Phys. Chem. B*, 102(33):6331, 1998.

[49] H Wang, E Yan, Y Liu, and K Eisenthal. Energetics and population of molecules at microscopic liquid and solid surfaces. *J. Phys. Chem. B*, 102(23):4446, 1998.

[50] S. H. Jen and H. L. Dai. Probing molecules adsorbed at the surface of nanometer colloidal particles by optical second-harmonic generation. *J. Phys. Chem. B*, 110(46):23000–23003, 2006.

[51] H. F. Wang, T. Troxler, A. G. Yeh, and H. L. Dai. Adsorption at a carbon black microparticle surface in aqueous colloids probed by optical second-harmonic generation. *J. Phys. Chem. C*, 111(25):8708–8715, 2007.

[52] S Jen, G Gonella, and H Dai. The effect of particle size in second harmonic generation from the surface of spherical colloidal particles. I: Experimental observations. *J. Phys. Chem. A*, 113(16):4758, 2009.

[53] M Subir, J Liu, and K Eisenthal. Protonation at the aqueous interface of polymer nanoparticles with second harmonic generation. *J. Phys. Chem. C*, 112(40):15809, 2008.

[54] X. M. Shang, Y. Liu, E. Yan, and K. B. Eisenthal. Effects of counterions on molecular transport across liposome bilayer: Probed by second harmonic generation. *J. Phys. Chem. B*, 105(51):12816–12822, 2001.

[55] J Liu, X Shang, R Pompano, and K Eisenthal. Antibiotic assisted molecular ion transport across a membrane in real time. *Faraday Discuss.*, 129:291–299, 2005.

[56] J Liu, M Subir, K Nguyen, and K Eisenthal. Second harmonic studies of ions crossing liposome membranes in real time. *J. Phys. Chem. B*, 112(48):15263–15266, 2008.

[57] S Roke, J Buitenhuis, J van Miltenburg, M Bonn, and A van Blaaderen. Interface-solvent effects during colloidal phase transitions. *J. Phys.: Condens. Matter*, 17(45):S3469, 2005.

[58] S. Roke, O. Berg, J. Buitenhuis, A. van Blaaderen, and M. Bonn. Surface molecular view of colloidal gelation. *Proc. Natl. Acad. Sci. U. S. A.*, 103(36):13310–13314, 2006.

[59] A. G. F. de Beer, H. B. de Aguiar, J. F. W. Nijsen, A. B. Sugiharto, and S. Roke. Detection of buried microstructures by nonlinear light scattering spectroscopy. *Phys. Rev. Lett.*, 102(9):095502, 2009.

[60] J Dadap, J Shan, K Eisenthal, and T Heinz. Second-harmonic Rayleigh scattering from a sphere of centrosymmetric material. *Phys. Rev. Lett.*, 83(20):4045, 1999.

[61] J. I. Dadap, J. Shan, and T. F. Heinz. Theory of optical second-harmonic generation from a sphere of centrosymmetric material: small-particle limit. *J. Opt. Soc. Am. B*, 21(7):1328, 2004.

[62] E. C. Y. Yan, Y. Liu, and K. B. Eisenthal. In situ studies of molecular transfer between microparticles by second-harmonic generation. *J. Phys. Chem. B*, 105(36):8531–8537, 2001.

[63] Y. Pavlyukh and W. Hubner. Nonlinear Mie scattering from spherical particles. *Phys. Rev. B*, 70:245434, 2004.

[64] A. G. F. de Beer and S. Roke. Sum frequency generation scattering from the interface of an isotropic particle: Geometrical and chiral effects. *Phys. Rev. B*, 75:245438, 2007.

[65] S. Roke, M. Bonn, and A. V. Petukhov. Nonlinear optical scattering: The concept of effective susceptibility. *Phys. Rev. B*, 70:115106, 2004.

[66] A de Beer and S Roke. Obtaining molecular orientation from second harmonic and sum frequency scattering experiments in water: Angular distribution and polarization dependence. *J. Chem. Phys.*, 132(23):234702, 2010.

Chapter 2

Experimental details

In this chapter, we present sample preparation and experimental details. We first describe the preparation and characterization of an emulsion system that is stable for months. We explain the laser setup used for the SFS experiment: The amplification of ultrashort laser pulses, the frequency conversion and finally the detection of the SF light.

2.1 Introduction

Here, we describe the procedure to make a stable oil-in-water emulsion, and characterize it as a function of time with electrophoresis and dynamic light scattering. It is shown that the chosen emulsion system is stable against creaming and Ostwald Ripening destabilization effects.

In the second section, we describe the laser system setup used for the SFS experiments. Due to the very low signal levels of the SFS signal, strong electric fields are needed to create a nonlinear polarization. High peak powers can be achieved using short pulses with high energies. This is done by using lasers that can generate ultrashort pulses (typical pulse duration $10^{-13} - 10^{-11}$ s) together with laser amplifiers. We further describe another fundamental part of the laser system which is the generation of ultrashort mid-infrared pulses using nonlinear optical processes with highly efficient nonlinear crystals.

2.2 Emulsion systems

2.2.1 Emulsion preparation

The oil-in-water emulsions prepared for the studies performed in this thesis were done using two different approaches which we will label as "constant size approach" or "standard approach". The constant size approach was used to keep the size distribution constant while we changed other parameters, *e.g.* surfactant and/or salt concentration. The standard approach is the one often used in colloidal science, which results in different size distribution of droplets for every emulsion sample. Fig. 2.1 is a sketch that shows the steps involved in the emulsification procedures.

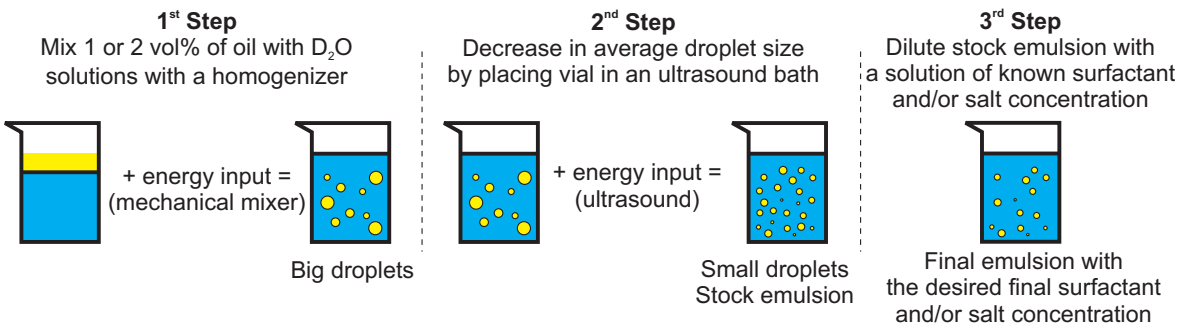

Figure 2.1: Schematic representation of the steps involved in the emulsion preparation procedure. The standard emulsification approach ends in the 2nd step.

Standard approach

1 vol% of oil and D_2O solution, with a known concentration of surfactant and/or salt, were mixed in a 4 mL vial using a handheld homogenizer (TH, OMNI International) for 5 min.

The homogenizer consisted of a motor driven plastic tip that spun inside a fixed plastic tube. The tip and the tube were immersed in the vial containing the oil and the water and spun at variable angular velocities that could be changed from 5 to 35 RPM. The angular velocity determined how fast the emulsion was prepared and the resulting average droplet size. When working with surfactants one should avoid creating foams to not deplete the surfactant from the solution. For this reason, we always used the slowest angular velocity (5 RPM) and let the system homogenize for a longer time. This procedure produced an emulsion with droplets in the micrometer size range which creams in a few minutes. To avoid creaming, the droplet size was reduced by placing the vial containing the emulsion in an ultrasound bath (35 kHz, 400 W, Bandelin) for 15 min. We noticed that the final droplet size distribution changed according to the time it was immersed in the ultrasound bath: longer times resulted smaller average droplets. Using this methodology, we could obtain droplets that had an average size ranging from 50 to 500 nm (radius). Unfortunately, we could not control the final droplet size distribution better than sub-micron sizes, presumably due to the low quality of the probe used in the ultrasound bath. Even samples prepared in exactly the same way, but with different type of surfactants, did not show any correlation among them in the final droplet size distribution. A solution to this problem was achieved using the "constant size approach" presented below.

Constant size approach

The constant size approach starts in the same way as the standard one, but with a 2 vol% of oil and D_2O solution. This resulting emulsion was used as a "stock" sample, which was further diluted with D_2O of a known concentration of surfactant and/or salt. This approach resulted in multiple emulsion samples with the same droplet size distribution and volume fraction (1 vol%), but different final surfactant/salt concentration. In this way, changes in SFS signal can only be due to changes in the concentration and/or conformation of species in the interfacial region of the oil droplets, not by different droplet concentrations or size. The characterization of the emulsions prepared with a constant size approach is in section 2.2.3.

Chemicals and glassware cleaning

All chemicals were used as received. The oils used were n-hexadecane (C16), n-dodecane (C12). n-hexane (C6) ($\geq$99%, Merck), d_{34}-hexadecane (dC16), d_{26}-dodecane (dC12) (98% D, Cambridge Isotope). Aqueous solutions were prepared with D_2O (99% D, Aldrich) or ultra pure water. The surfactants used were sodium dodecyl sulfate (SDS) ($\geq$99%, Alfa Aesar), perdeuterated SDS (dSDS) (98% D, Cambridge Isotope) and sodium bis(2-ethylhexyl) sulfosuccinate or Aerosol OT (AOT) (98%, Aldrich). Sodium chloride ($\geq$ 99.5%) was provided by Roth.

Glassware was cleaned with 3:7 H_2O_2:H_2SO_4 piranha solution (*be extremely careful when*

handling piranha solutions!) and then thoroughly rinsed with ultra pure water (0.053 μS/cm, TKA) to remove residual chemicals.

2.2.2 Emulsion characterization methods

We used Dynamic Light Scattering and ζ-Potential measurements to corroborate and/or control possible variables in the emulsions samples that could affect the size changes or surface potential. Here, we present a basic background of the additional characterization techniques used. Refs. [1] and [2] give a rigorous mathematical demonstration and the experimental details for the measurements.

Dynamic light scattering

In Dynamic Light Scattering (DLS), or Photon Correlation Spectroscopy, a 632 nm laser beam is steered into a cuvette containing a diluted dispersion. The particles in the dispersion scatters the light which is further detected at different time intervals [1]. A digital signal processor compares how the signal changes at successive time intervals and computes an intensity autocorrelation spectrum. A fit to the autocorrelation spectrum is made which has the particle size as a fitting parameter.

The intensity-intensity autocorrelation function $G(q,\tau)$ is

$$G(q,\tau) = \langle I(q,t)I(q,t+\tau)\rangle\,. \tag{2.1}$$

$G(q,\tau)$ can be related to the electric field-field autocorrelation function $g(q,\tau)$ by

$$G(q,\tau) = A(1 + B\ |g(q,\tau)|^2), \tag{2.2}$$

where A is the baseline of the correlation function and B the intercept. For a monodisperse distribution of particles

$$g(q,\tau) \propto \exp(-Dq^2\tau) \tag{2.3}$$

$$q = \frac{4\pi}{\lambda}\sin(\theta/2), \tag{2.4}$$

where D is the diffusion constant and q is the wave vector related to the scattering angle θ and wavelength λ. The diffusion constant is related to the particle hydrodynamic radius R by the Stokes-Einstein formula

$$D = \frac{k_B T}{6\pi\,\eta R}, \tag{2.5}$$

where k_B is the Boltzmann constant, T the temperature and η the solvent viscosity.

In summary, the measurement of the intensity autocorrelation can be fit to Eq. 2.2 to obtain the diffusion constant D, from which Eq. 2.5 can be used to retrieve the particle size.

Electrophoresis

Electrophoresis is the phenomenon of a charged particle movement due to an external electric field [2]. This happens if the particle carries a net excess charge. The particle movement is called electrophoretic mobility μ_e, which is a proportionality constant between the attained particle velocity v_e due to an external electric field E_{ext} [2]

$$\mu_e = \frac{v_e}{E_{ext}}. \tag{2.6}$$

v_e can be measured by the technique Laser Doppler Velocimetry (LDV). The technique relies in the Doppler effect where a particle in movement changes the frequency of the scattered light. The change in frequency Δf is [1]

$$\Delta f = \frac{2\, v_e \sin \theta/2}{\lambda}, \tag{2.7}$$

where θ is the scattering angle and λ the laser wavelength.

At the particle surface, there can be an excess of charges. These interfacial charges are related to the electrostatic potential through the Poisson equation. The relation between μ_e and the electrostatic potential ϕ_ζ measured at a position ζ from the particle surface is

$$\mu_e = \frac{\phi_\zeta\, \epsilon}{\eta}, \tag{2.8}$$

where ϵ is the dielectric constant and η is the viscosity of the fluid where the particle is embedded. ϕ_ζ is the so-called ζ-potential. The ζ-potential is defined as the potential measured at a distance from the particle surface where the fluid velocity attains the same value as the particle velocity.

Experimental details

The droplet size distribution was determined by DLS measurements using a Malvern ZS Nanosizer. The device has a software which converts the autocorrelation data into intensity-weighted droplet size distribution. Using a light scattering algorithm, and with the knowledge of the optical properties of the materials, a number- or volume-weighted size distribution can be retrieved. Prior to measurements, the emulsions were diluted by a factor 100 in disposable polystyrene cuvettes.

ζ-potential measurements were done using the same device used for the DLS measurements. Solutions were measured with disposable electrophoretic cells. The electrodes of the cell were made out of Au. The device uses the Phase Analysis Light Scattering technique to retrieve electrophoretic mobility [1]. Using Eq. 2.8 the measured electrophoretic mobility v_e can be converted into a ζ-potential.

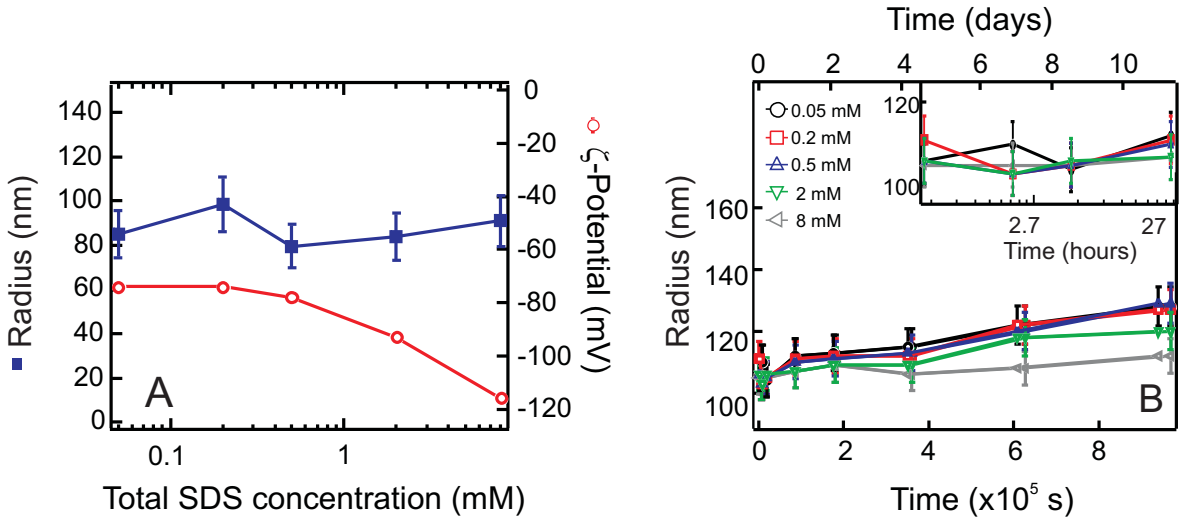

Figure 2.2: Droplet stability and size evolution. A) Average radius (left scale, squares) and ζ-potential (right scale, circles) for droplets prepared with constant size approach and varying final SDS concentration. B) Size measurements as function of time for different SDS concentration. The inset zooms in on the first 27 hours. Note that the sample presented in A is different from B.

2.2.3 Emulsions characterization

The chosen oil was hexadecane due to its low solubility in the water. Fig. 2.2.A shows the average radius (left scale, squares) obtained for a concentration series that was used in the SFS experiments of Chapter 4. The data points are averages of 5 Dynamic Light Scattering measurements, and error bars represent the width of the distribution. It can be seen that the droplet radius does not correlate to the SDS concentration using the constant size approach. The average droplet radius was 83 nm, with a standard deviation of 10 nm. The stability of the emulsion was further corroborated by ζ-potential measurements. In Fig. 2.2.A the ζ-potential is plotted (right scale, circles) for different SDS concentration. As it can be seen, the modulus of the ζ-potential increased as the surfactant concentration increased. These values are within the range for colloidal stability [2].

In order to measure the long-term size stability of the emulsions we have prepared an emulsion using the constant size approach where we have used non-deuterated hexadecane and water. At various time interval a small volume from the emulsions was diluted 100 times, after which the average droplet radius was measured. Fig. 2.2.B shows radius data as a function of time for samples with varying SDS concentrations, over a time span of 10 days. The inset of Fig 2.2.B shows the short term stability of the droplets which was constant within one day. It can be seen that the size increase is very slow. Since our SFS measurements were typically performed in a time span of several hours the droplet sizes in a concentration series are constant and do not vary on the time scale of the SFS measurement. Furthermore, it can be seen that there is a correlation of the size change rate and SDS concentration. This

is related to the interfacial tension of the oil droplets-water interface. These results are in qualitative agreement with previous studies on Ostwald Ripening measurements [3] and we will return to this in Chapter 4.

We can conclude that by using the constant size approach we obtain emulsion samples with different final salt/surfactant concentration but the same droplet size distribution among the samples, at least for the timescale of the SFS experiments. Thus, changes observed in SFS spectra as we change surfactant/salt concentration can only be associated to changes in interfacial species (Chapter 4 and 6) and/or conformation (Chapter 5) at the interface, not by different size distribution.

2.3 The SFS system

Our SFS experimental setup consists of a laser system to generate the excitation pump pulses, a SFS sample stage and a detection part. The laser system generates broad-band ultrashort pulses and involves three major parts: oscillator, amplifiers, optical parametric generation/amplification. The SFS sample stage and detection system consist of a cuvette holder, optical elements that are convenient to use in scattering experiments, a spectrometer and an intensified charged-couple device (I-CCD) to detect the SFS photons. We describe the details of each of these parts in the following.

Laser system

A scheme of the laser system is depicted in Fig 2.3 [4]. An ocillator (Integral 50, Femtolasers) generates ultrashort pulses (50 fs, 800 nm, 20 nm bandwidth, 85 MHz repetition rate) with pulse energies of 1-2 nJ. These pulses are first stretched in time then amplified in a three-stage amplifier system (Integra-C, Quantronix). After the pulse lengthening, the 800 nm pulses are sent into a regenerative amplifier (RGA) with a Ti:Sapphire crystal as gain medium. A second amplification is done by passing the 800 nm pulse through a second Ti:Sapphire crystal (MPA, multi-pass amplifier). Both RGA and MPA are pumped by 2.5 and 12.5 mJ, respectively, 150 ns, 527 nm pulses at 1 kHz repetition rate laser. This results in a 10^6 increase in pulse energy. The 800 nm pulses passes through a Pockels cell to optimize pulse contrast ratio. In the last amplification step, the 800 nm pulses passes through a Ti:Sapphire crystal pumped by two lasers pulses (15 mJ, 150 ns, 527 nm). The Ti:Sapphire crystal is kept in a base pressure of 2×10^{-6} mbar thermally stabilized at 87 K, in order to minimize thermal lensing effects. After the last amplification step, the resulting pulse energy is $\sim$9 mJ which after compresion to 130 fs (intensity auto-correlation) reduces to 6 mJ of output pulse energy.

90% of the amplified beam pumps a customized commercial optical parametric generator/amplifier (OPA/OPG) (HE-TOPAS, Light Conversion). This OPA/OPG generates near-IR pulses so-called signal (1.1-1.6 μm) and idler (1.6-2.6 μm). These signal and idler pulses

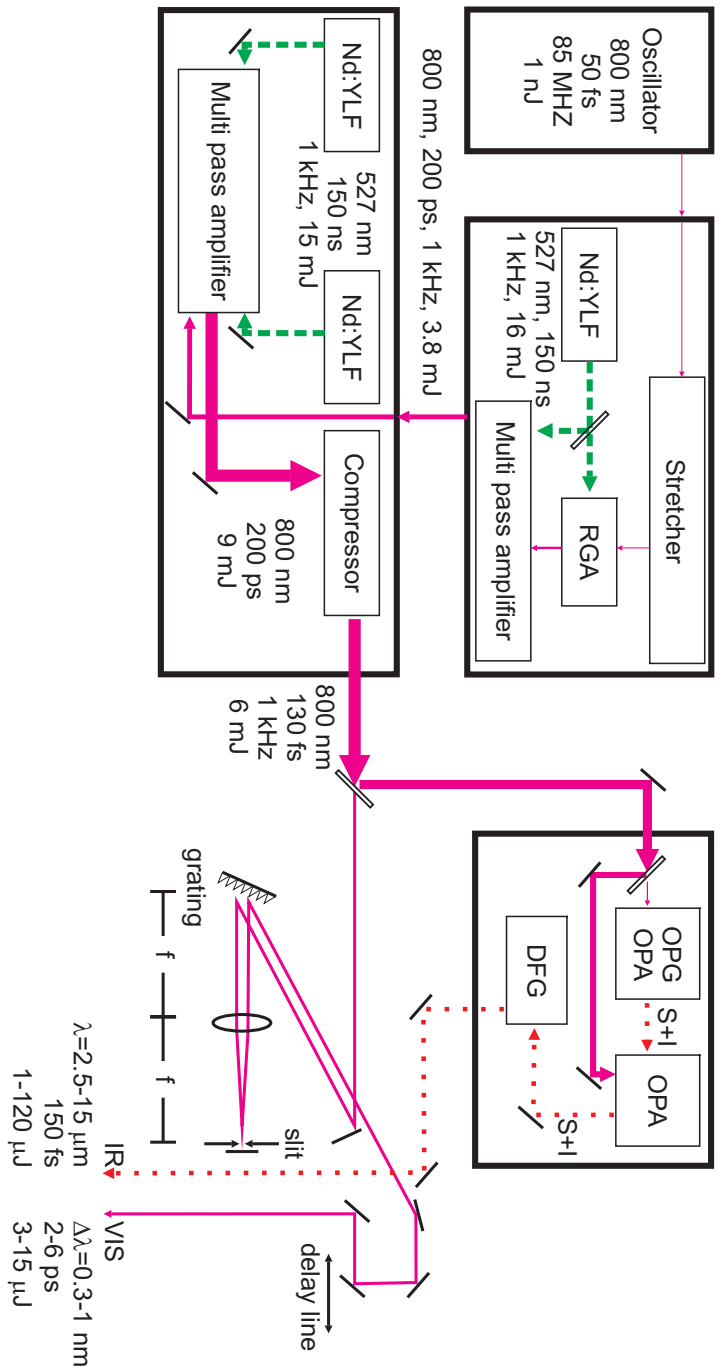

Figure 2.3: Laser setup for performing SFS experiments. It consists of an oscillator to generate ultrashort pulses, three amplification stages, optical parametric generator/amplifier (OPG/OPA) together with difference-frequency generation (DFG) stages to generate ultrashort IR pulses and a spectral pulse shaper for the VIS pulse. Continuous lines denote the beam path for 800 nm, dashed lines for 527 nm and dotted lines for IR wavelengths.

overlap in a $AgGaS_2$ crystal where difference frequency generation (DFG) process generates tunable mid-IR pulses with wavelengths ranging from 2.6 μm to 20 μm. The mid-IR pulse energies vary from few μJ up to 120 μJ.

The remaining 10% of the amplified beam is spectrally shaped in a pulse shaper. This stage reduces the bandwidth of the visible (VIS) beam in order to increase the resolution of the SF spectrum. The spectrally broad incoming beam is dispersed by a 1200-groves/mm grating (Spectrogon, Sweden) with an efficiency $\geq$90% for 800 nm. The diverging light from the grating is collimated by a plane-convex lens (f=50 mm). At the focal plane of the lens, a mirror reflects the light back to the grating with a small offset in the beam direction. A slit placed close to the mirror selects the spectral range of interest. After a second reflection from the grating the beam restores its original (incoming) spatial profile, but now having a narrow bandwidth.

Reflection SFG experiment

Typical reflection SFG spectra of the system are shown in Fig. 2.4 for the two IR spectral regions studied in this thesis. The mid-IR generated from the DFG stage and the VIS from the pulse shaper are overlapped in space and time on the surface of a substrate. The incidence angles are 43° and 58° with respect to the surface normal, respectively. The generated SFG beam from the surface is steered to the spectrometer equipped with intensified CCD camera (i-Star DH742, Andor Technologies). The spectra are plotted as a function of IR wavenumber by subtracting the VIS energy from the original SF energy (raw data). The black lines in Fig. 2.4 are fits with a Gaussian centered at 1100 cm^{-1} (left spectrum) and 2890 cm^{-1} (right spectrum). For these particular experiments Au was used as substrate for experiments with IR central frequency around 1100 cm^{-1} and Z-cut Quartz for IR central frequency around 2890 cm^{-1}.

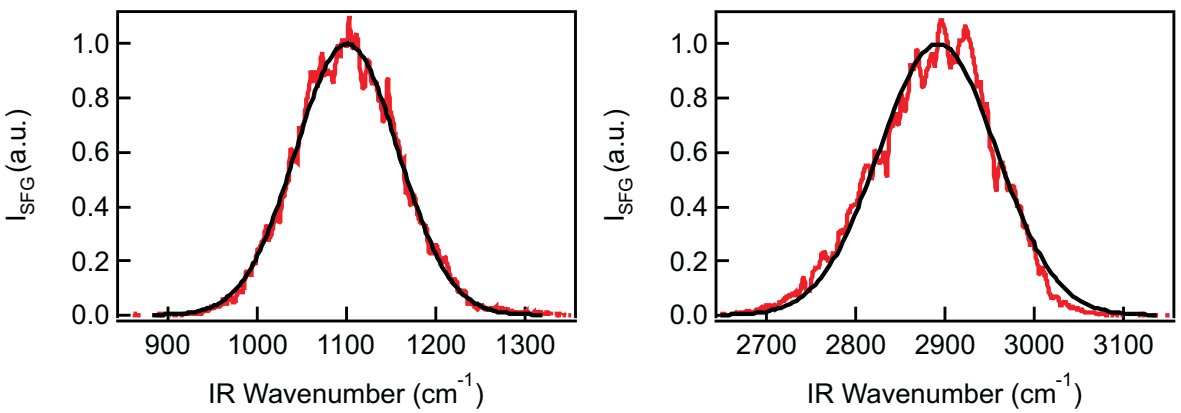

Figure 2.4: Reflection SFG experiment. IR and VIS beams are overlapped on the surface of a Au (left) or Z-cut Quartz (right) to generate a SF beam. These spectra represent the spectrum of the IR beam used throughout this thesis.

Throughout this thesis we use the sequence polarization combinations defined as a three letters code with the SF polarization in the first, the VIS in the middle and the IR polarization in the last position. For instance, ssp are s-polarized SF, s-polarized VIS and p-polarized IR beams.

Bibliography

[1] R. Borsali and R. Pecora, editors. *Soft-Matter Characterization*, volume 1. Springer, 2008.

[2] R J Hunter. *Zeta Potential in Colloid Science: Principles and Applications*. Colloid Science. Academic Press, 1981.

[3] J. Weiss, N. Herrmann, and D. J. McClements. Ostwald ripening of hydrocarbon emulsion droplets in surfactant solutions. *Langmuir*, 15:6652, 1999.

[4] A. B. Sugiharto, C. M. Johnson, H. B. De Aguiar, L. Alloatti, and S. Roke. Generation and application of high power femtosecond pulses in the vibrational fingerprint region. *Appl. Phys. B*, 91(2):315–318, 2008.

Chapter 3

SFS implementation and characterization

Droplet interfaces of emulsion systems are notoriously difficult to probe at a molecular level. Vibrational Sum-Frequency Generation (SFG) is an interface-specific technique that can provide a molecular-level picture of planar interfaces. Vibrational Sum-Frequency Scattering (SFS) is a combination of Light Scattering and SFG which allows the application to probe colloidal systems. Here, we present a detailed description of the SFS experiment to probe the interfacial vibrational spectrum of nanoscopic oil droplets dispersed in water. We have measured scattering spectra at different scattering angles to determine if, and under which conditions, competing processes might play a role. We have compared SFS experiments to reflection and transmission phase matched sum frequency generation measurements of the same samples. This chapter concludes with SFS measurements as a function of optical path length, particle density and pulse energy. They show that the SFS process follows the principles of nonlinear light scattering.

3.1 Introduction

Interfacial phenomena are defining for the properties of dispersions consisting of sub-micron sized particles or droplets [1, 2]. Ionic surfactants adsorbed at the droplet/oil interface can prolong the stability of droplets in emulsions and chemically crafted polymers or alkanes can stabilize particles by means of steric stabilization [3]. Although such processes are well understood on the macroscopic scale the study of molecular properties of droplet or particle interfaces in solution is a challenge because it is difficult to distinguish bulk molecules from surface molecules. A probe also needs to penetrate the liquid phase, which is not always transparent. Furthermore, small particles undergo Brownian motion.

Second-Harmonic Scattering (SHS) and Vibrational Sum-Frequency Scattering (SFS) are recently developed nonlinear Light Scattering (NLS) techniques, capable of selectively probing the interfaces of particles or droplets in a dispersion [4, 5]. SHS has been pioneered by the Eisenthal group and has been applied to study a number of colloidal phenomena such as electrostatic properties of polymer particle surfaces [6, 7], adsorption of molecules at colloidal interfaces [8–11], surface acid-basic equilibria [12] and molecular transport across liposome bilayers [13–15]. SFS offers additional chemical specificity, since it allows to probe the vibrational spectrum of molecules on the particle/solution interface [16]. SFS has been used to probe colloidal phase transitions [17, 18] in apolar solvents, to probe crystalline domains in amorphous polymer microspheres [19] and to probe asymmetry in catanionic vesicles dispersed in water [20].

In this chapter, we show details of the implementation of the SFS experiment to study oil droplets in water. We first introduce the basic background for the SFS technique and also discuss other light/matter processes that occur in a dispersion, such as absorption and linear scattering. A detailed description of the experiment is followed by experiments aimed to describe in detail various aspects of sum frequency scattering. We performed SFS measurements on emulsions consisting of $\sim$100 nm sized oil droplets dispersed in SDS/D_2O solutions. We have measured scattering spectra at two different scattering angles. This measurement can be used to verify that the droplet interfaces are probed. To determine if and under which conditions competing processes might play a role, we have compared scattering experiments to reflection and transmission phase matched measurements. The manuscript concludes with SF scattering measurements as a function of optical path length, pulse energy and particle density. They show that the SF scattering processes follows the principles of nonlinear light scattering.

3.2 Sum Frequency Scattering Background

In an SFS experiment, mid-infrared (IR) and visible (VIS) pulsed laser beams are overlapped inside a cuvette containing dispersed particles in a liquid or solid matrix [17, 19].

Fig. 3.1.A illustrates the process at a single particle level. At the particle interface, a second-order nonlinear polarization is created which oscillates at the sum of IR and VIS frequencies ($\omega_{SF} = \omega_{VIS} + \omega_{IR}$). This polarization is small but does not vanish because there is a phase difference between the polarization components generated on different parts of the sphere. The SF photons generated at the surface coherently interfere at the detector position interface and generate a scattering pattern. The scattering pattern depends on droplet size, experimental geometry and surface structure [11, 21–23].

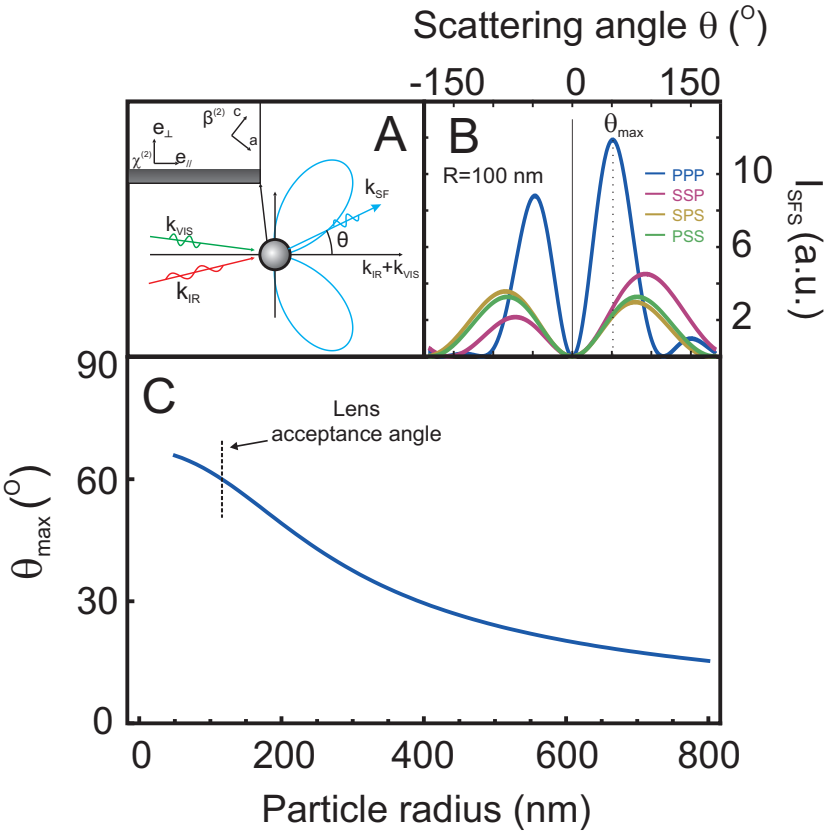

Figure 3.1: Sum frequency scattering. A) Important parameters for the sum frequency scattering experiment. The $\chi^{(2)}$ components are defined as perpendicular ($\perp$) or parallel ($\parallel$) to the droplet interface. B) Scattering pattern for a droplet with a 100 nm radius (R) in different polarization combinations, assuming that $\chi^{(2)} = 0$, except $\chi^{(2)}_{\perp\perp\perp}$=1. C) Angle of the maximum SF intensity as a function of particle radius for the polarization combination *ppp*, assuming the same parameters. The dashed line has a length of 20° and depicts the acceptance angle of the lens used in the SFS experiments.

The SFS spectrum detected at an angle θ from a single particle can be described by the following equation:

$$I_{SFS}(\theta, R, \omega) \propto \frac{k_0^4}{r_0^2} |\Gamma^{(2)}(\theta, R, \omega)|^2 \, I_{IR} \, I_{VIS} \tag{3.1}$$

$$\Gamma^{(2)}(\theta, R, \omega) \propto N_s G \left[F_1(\theta, R), F_2(\theta, R), \chi^{(2)}(\omega) \right].$$

The scattered intensity depends on the distance between the particle and the detector (r_0), the scattered wave vector ($\mathbf{k}_0$), the (local) intensity of the IR (I_{IR}) and VIS (I_{VIS}) beams, and on the effective susceptibility $\Gamma^{(2)}$. The magnitude of $\Gamma^{(2)}$ depends on the nonlinear optical surface response ($\chi^{(2)}$), scattering geometry, particle size (R), the surface density of vibrational groups (N_s) and on the scattering form factor functions F_1 and F_2, which are given in Chapter 1.

3.2.1 Angular distribution of the SFS process

The angular direction in which the SFS intensity is peaked changes with particle size [9, 11, 21, 23–26]. Therefore, knowledge of the particle size distribution in the sample is key to a successful experiment. Once the particle size distribution is available, the position of the detection system can be chosen, whereby we use a calculated scattering pattern for the particular size distribution as a guide to determine the optimal detection angle. Fig. 3.1.B shows a scattering pattern of a particle with a radius of 100 nm, for different polarization combinations, using the formulas given in Section 1.3.2. p refers to beams polarized parallel to the plane of the wave vectors and s refers to a polarization direction perpendicular to that. It can be seen that different polarization combinations are peaked at different scattering angles. For all polarization combinations, however, the signal vanishes in the forward direction.

Fig. 3.1.C shows the scattering angle of maximum intensity as a function of particle radius. For particle with a bulk refractive index close to the bulk refractive index of the surrounding medium the size dependence of the scattered intensity per particle is: $I_{SF} \propto R^6$ [25]. For n particles the intensity of each particle needs to be added. If we have a constant IR and VIS intensities through the overlap volume and no correlations between the particles, this will result in a total signal (S_{SFS}) of

$$S_{SFS} = \sum_{i=0}^{n} I_{SF,i} = nI_{SF} \propto \phi R^3, \tag{3.2}$$

for spherical particles with ϕ the volume fraction of the sample (dispersion). As the sample consists of particles in solution, linear light scattering and absorption of the incoming fields may also play a role. These effects are described next.

3.2.2 Effects of optical path length on the generated signal

The intensity of the IR and VIS beams will vary along the optical axis due to absorption and/or scattering processes. In the case of D_2O, the IR beam is mainly attenuated by absorption . As D_2O is transparent for visible light attenuation the extinction of the VIS beam is due to linear scattering. The extinction of IR and VIS beams therefore have a different dependence on sample cell path length. For the emulsions considered here the $1/e$ extinction path length of the VIS beam is several hundreds of micrometer. If we use a cuvette with path length d, and

optical axis z we need to take into account that the IR, the VIS and the generated SF intensity are all changing along the optical axis (along $\mathbf{k}_0$). We thus have for the signal $S_{SFS}(d)$:

$$\begin{aligned} I_{IR}(z) &\propto e^{-\alpha_{IR}\, z} e^{-\tau_{IR}\, z} I_{IR,0} \\ I_{VIS}(z) &\propto e^{-\tau_{VIS}\, z} I_{VIS,0} \\ S_{SFS}(d) &\propto \int_0^d \left|\Gamma^{(2)}\right|^2 I_{VIS}(z) I_{IR}(z) e^{-\tau_{SF}\,(d-z)} dz, \end{aligned} \tag{3.3}$$

where α is the absorption coefficient, τ the extinction due to scattering, $I_{VIS,0}$ and $I_{IR,0}$ the incoming VIS and IR intensities, respectively. Fig. 3.2.A shows a sketch of the IR and VIS beam intensities as a function of propagation distance. Fig. 3.2.B illustrates the combined effects on a nonlinear light scattering experiment. As a comparison sample cell path length dependence for linear scattering is also given. Consequently, the total signal measured as a function of the optical path length is different for nonlinear light scattering (SFS, SHS) and linear scattering.

3.2.3 Competing processes

There are two interfaces in a sample cell: the droplet interfaces and the interface of the sample cell window. Since both interfaces have a nonzero surface susceptibility $\chi^{(2)}$ they can both generate SF photons. The SF photons from the SFS process are generated inside the liquid phase and appear with a typical scattering pattern (Fig. 3.2.C), which most notable feature is the absence of scattered light in the forward direction (θ=0). This forward direction is the same direction as the phase matched direction ($\mathbf{k}_0^{SF} = \mathbf{k}_{IR} + \mathbf{k}_{VIS}$) for the SFG process of the sample cell window/solution interface. SF photons generated from the window will travel through the emulsion and undergo linear scattering. Both processes are illustrated in Fig. 3.2.C and 3.2.D. If photons are generated from the window/solution interface this signal is generated in the direction that is forbidden for SFS.

SF photons generated in a SFS process will have a certain polarization dependence and an angular scattering pattern. The frequencies that appear in the spectrum are originating from the specific chemical structure at the droplet interface. The polarization dependence can be calculated and depends on the droplet size and surface structure [26]. The polarization dependence from the SF photons from the window/solution interface is also determined by the molecular surface structure at the interface. It follows a different dependence on the surface structure than for SFS. The spectrum is determined by the molecular conformation and local dielectric environment [5].

Thus, there are fundamental differences between SFS of the droplets and transmission SFG from the window/solution interface. Based on the above description, differences are expected in polarization combination, spectral shape, angular intensity distribution and sample cell path length.

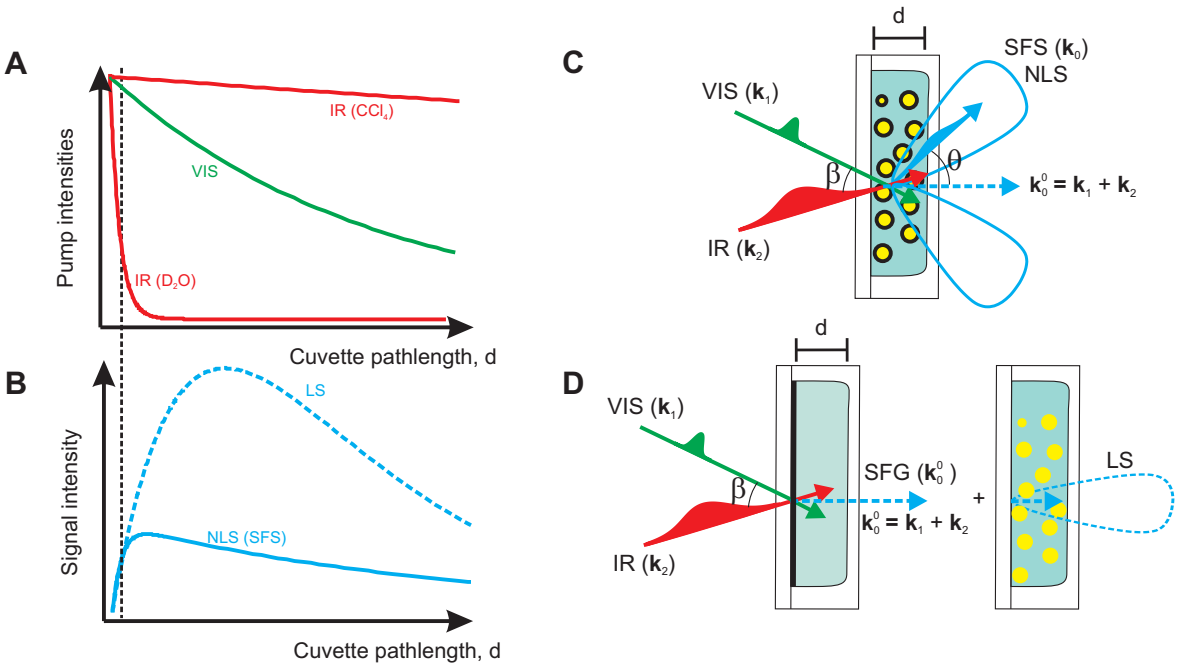

Figure 3.2: Linear Light Scattering (LS) and Nonlinear Light Scattering (NLS) processes. A: Sketch of the spatial intensity dependence of the exciting IR and VIS beams for IR transparent media and IR absorbing media (such as water). B: Expected intensity dependence on the optical path length. The overall SFS intensity continuously increases with sample cell path length due to incoherent addition of radiation from separate droplets. The added signal from probing a larger volume levels off as a consequence of extinction of both incoming beams. The extinction occurs due to absorption of IR or VIS light by the medium or linear light scattering in the sample. The signal intensity further is reduced because of secondary linear scattering events. C: Experimental geometry of the SFS process where IR and VIS beams overlap inside a cuvette with a path length d containing scatterers. The SFS signal is detected at an angle θ, and has a scattering pattern illustrated by the straight line. The SFS process is generated at the droplet-solution interface, illustrated by the black thick lines around the droplets. D: A sketch of the SFG + LS process: SFG signal is generated at the window-solution interface in the phase matched direction (i.e. at θ=0). This SF light is then scattered linearly by the droplets in a wide angular range. The scattering pattern of the LS process is illustrated by the dashed lines.

The effect of micelles

Throughout this thesis, we study dispersions with surfactants that can form aggregate structures called micelles [1]. These structures are in equilibrium with free surfactant in solution. As the surfactant concentrations increases the relative population between free surfactants to micelles decreases until it reachs a concentration called critical micelle concentration (cmc). Above the cmc, additional surfactant will mostly form micelles [27].

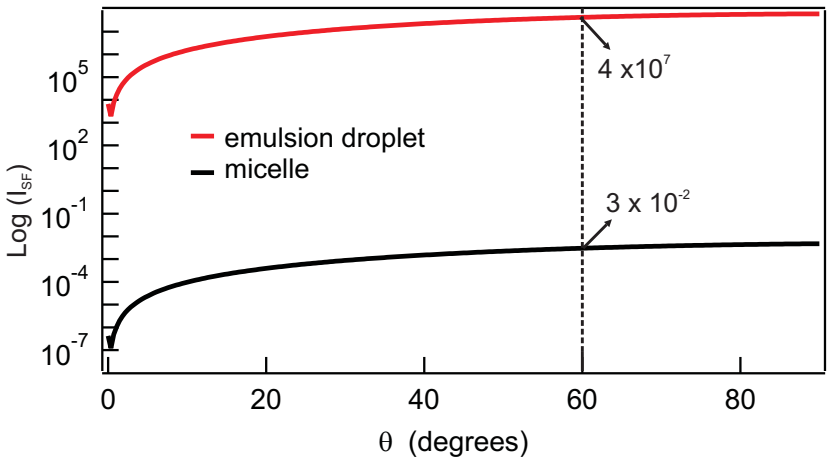

Figure 3.3: Calculated SFS pattern for micelles (R=2 nm) and an emulsion droplet (R=80 nm).

Emulsion systems can be composed of droplets and micelles. Because the droplets size in the emulsions used throughout this thesis are relatively small ($R \cong$100 nm), the micelles scattering intensity could make an additional contribution to the signal. To estimate the contribution of micelles to the scattering signal we have calculated the scattered intensity of both a micelles and an emulsion droplets using Eq.1.13. The result is shown in Fig. 3.3. The calculated SFS intensity as a function of scattering angle for an emulsion droplet (R=80 nm, upper curve) and a micelle (R=2 nm, lower curve). The intensity was calculated for polarization combination ssp. It can be seen that the signal of an emulsion droplet measured at θ=60° (indicated by the vertical line) is 9 orders of magnitude larger than that of a micelle.

It can be seen that in our experiment a single micelle scatters 9 orders of magnitude less than an emulsion droplet. We perform most of our SFS measurements below or at the CMC. To give any estimate in terms of number density of micelles compared to oil droplets, we assume that a solution containing 8 mM of a surfactant is in the form of a micelle. Then we have (per ml of solution) 4.8×10^{16} micelles and 4.6×10^{12} emulsion droplets. Because the total scattered intensity increases linearly with the number of droplets or micelles the total difference in scattering intensity between droplets and micelles amounts to a factor of $\frac{4.8\times10^{16}}{4.6\times10^{12}}10^{-9} \approx 10^{-5}$. Thus, we can neglect any contribution of scattering from micelles to our signal. Futhermore, we were not able to detect any scattered SFS light from solutions containing only micelles (no droplets).

3.3 Experimental

3.3.1 Emulsions

In order to have a suitable emulsion system to study by SFS, it needs to be stable for the time scale of the SFS experiment. The two main issues are droplet density changes within the overlapping region of the IR and VIS pulse and droplet size changes due to coalescence and/or Ostwald Ripening. The first issue can be avoided by either using density-matched liquids or by decreasing the droplet size. The second issue can be avoided if one uses an oil that has a very low solubility in water to suppres Ostwald Ripening. Thus, we used hexadecane as the oil due to its low solubility in the water [28].

Emulsions were prepared using the Standard approach (see Chapter 2) with concentration of surfactants close to their critical micelle concentration (8 mM for SDS) and perdeuterated hexadecane as oil.

3.3.2 Details on SFS implementation

The SFS stage

In order to measure scattered sum frequency photons it is necessary to use pulses of ps or fs duration in the mid-IR and VIS frequency range. A description of our laser system was given in Chapter 2. Here we focus only on the details of the SFS setup. Fig. 3.4.A depicts a scheme of the SFS sample stage and detection system. The SFS experiments are performed using IR pulses (8-12 μJ, $\sim$150 fs, FWHM bandwidth 120 cm^{-1}) spatially and temporally overlapped with 800 nm VIS pulses (8-15 μJ, FWHM bandwidth 5-13 cm^{-1}) in a cuvette containing the emulsion. A 90° off-axis parabolic Au mirror (f=5 cm) focuses the IR beam down to a $\sim$150 μm beam waist diameter. Two BaF_2 wire grid polarizers control the energy and polarization of the IR beam. The VIS beam polarization is cleaned by a polarizer cube and changed by a $\lambda/2$ plate. The VIS beam is gently focused with a bi-convex lens (f=50 cm). At the overlapping position, the VIS beam diameter is 240 μm, bigger than the IR beam. The angle between VIS and IR beams is set to 15° in a nearly collinear geometry.

The cuvettes (Hellma GmbH, 106 O.20-40, Germany) with various optical path lengths consisted of two detachable windows with one side made out of CaF_2 and the other side made out of quartz. The SF scattered beam was collimated with a 0.5" diameter plano-convex lens (f=18 mm, Thorlabs), and directed towards the detection system using two 2" Ag mirrors. The lens was placed at a scattering angle of 60° with the cuvette exit window (quartz side) oriented parallel to the collimating lens. The polarization of the SF signal was selected with a Glan-Taylor CaF_2 prism. Two short-pass spectral filters (FES750, Thorlabs and 3RD-770, Omega Optical) were placed before the entrance of the spectrometer (Shamrock 303i, Andor Technologies).

The SF signal was spectrally dispersed onto an intensified CCD camera (i-Star DH742,

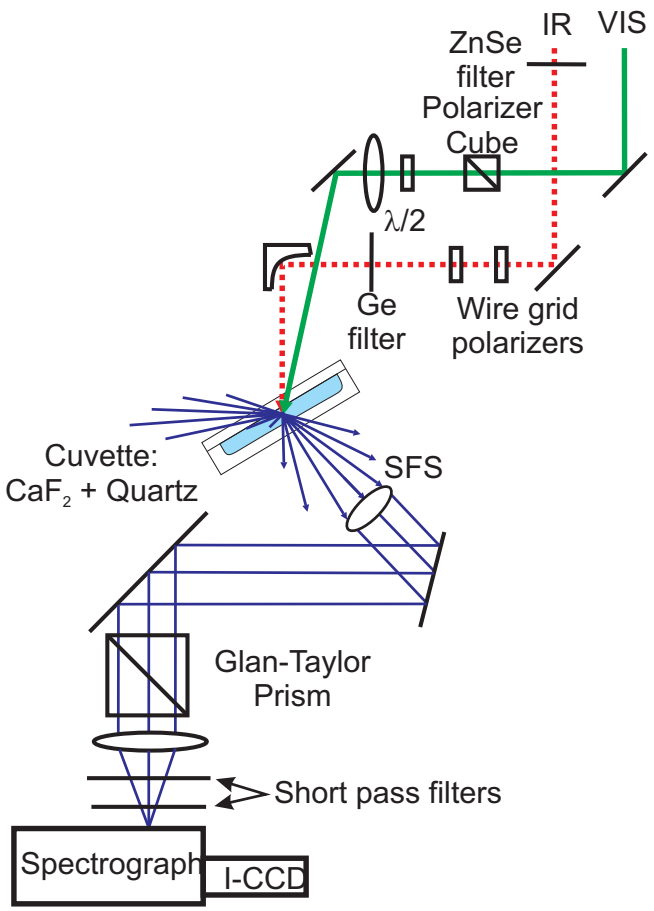

Figure 3.4: SFS sample stage and detection system. IR (dashed red line) and VIS (green line) are overlapped in the cuvette containing an emulsion. In the overlap volume, SF light is generated in a wide angular range which is collimated and steered into the detection system.

Andor Technologies). The intensifier was triggered by the laser system with a gate time of 8 ns. The acquisition time of a single spectrum was 300 s. The presented SF spectra in this thesis were plotted as a function of IR wavenumber. The y-axis units of all were background subtracted data that has been subsequently divided by the VIS and IR input energies (measured before the sample) and acquisition time. Graphs labeled I_{SFS}/I_{IR} represent spectra that have been normalized by the IR pulse spectrum.

System stability

We measured the SFS spectrum of a stable reference sample between measurements of the sample of interest in order to compensate for changes in overlap volume and/or IR spectrum. This sample consisted of an emulsion with very small droplet size ensuring that the changes in droplets density in the overlapping volume (of IR and VIS beams), due to creaming, was negligible in comparison to the timescale of a taken spectrum. To estimate what would be the effect of creaming in the intensity, we calculated the terminal velocity of a droplet [29]. An oil droplet with a radius of 100 nm dispersed in D_2O moves 1.3 μm h^{-1}, thus negligible for measurements correction since the overlapping region diameter was limited by the IR beam size ($\sim$100 μm).

The above mentioned estimation was experimentally corroborated. Fig. 3.5 shows the spectra of a reference sample taken at different times. It can be seen that only a small drift in intensity occurred within 7 hours. A detailed explanation of the spectral features is given in the following chapters.

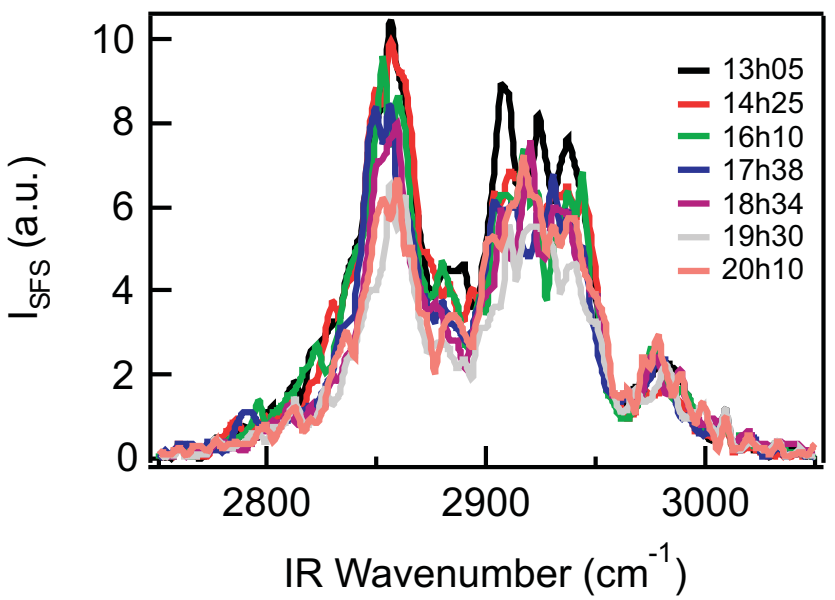

Figure 3.5: SFS spectra of a stable reference sample obtained at different times. The sample consisted of 1 vol% dC16-in-D_2O with 8 mM SDS. Detailed spectral assignments are given in the Chapter 5.

3.4 Results and discussion

3.4.1 Different scattering angles

In order to examine the scattering process we have taken spectra of an emulsion containing a 1 vol% dC16-in-D_2O emulsion with 8 mM SDS and 100 nm average droplet radius at different scattering angles. We measured spectra at θ=60°, the angle at which maximum intensity is expected, and at θ=0°, the phase matched direction. It can be seen from Fig. 3.6 that an SF spectrum can be recorded at θ=60°, but not at θ=0°. The process that gives rise to our signal therefore corresponds to an SF scattering process (see Fig. 3.1.B).

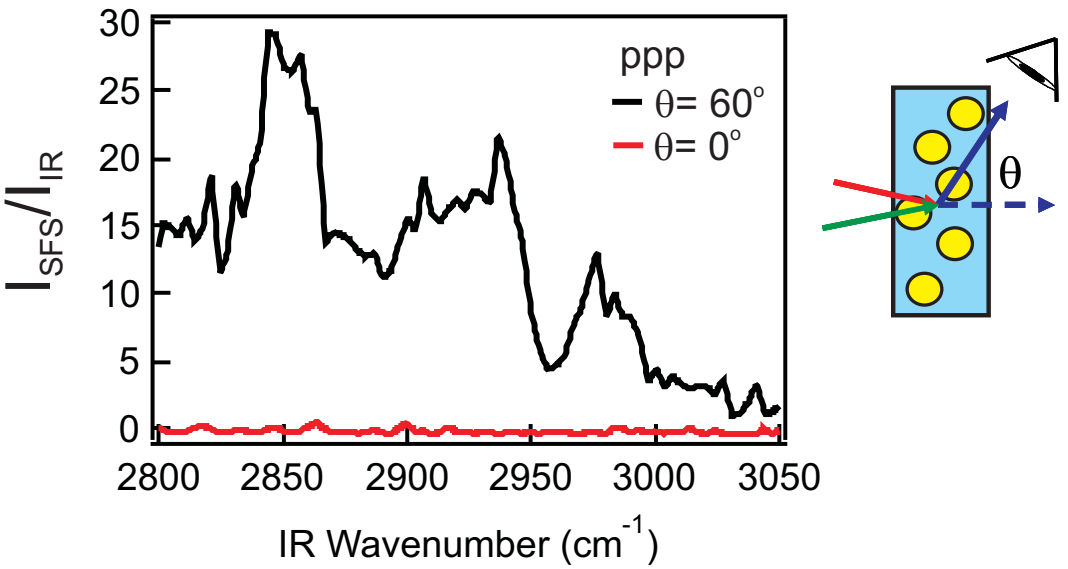

Figure 3.6: SFS spectra taken at a scattering angle θ of 60° and and at 0°, which corresponds to the phase matched direction. The data was taken from a 1 vol% dC16-in-D_2O emulsion with 8 mM SDS and 105 nm average droplet radius. The polarization combination was *ppp* and the sample cell path length was 200 μm.

3.4.2 Comparison of the droplet/D_2O solution interface and CaF_2/D_2O solution interface

Since it is known that SDS adsorbs on the CaF_2/D_2O it can be asked to what extent such an interface might be probed in the SFS experiment. We have therefore performed a number of measurements. First, we made an emulsion solution containing 1 vol% oil and 8 mM SDS. We then inserted the solution in a sample cell with a 200 μm path length. This was done in the same setup and beam geometry as was used when varying the scattering angle. The beam overlap was centered on the surface of the CaF_2/solution interface. The phase matched reflected SFG signal was detected, and is displayed in the upper panel of Fig. 3.7. This spectrum is composed of the well-known spectral features of the C-H stretch modes of SDS: The symmet-

ric methylene stretch vibration (d^+, at 2855 cm^{-1}), the symmetric methyl stretch mode (r^+, at 2878 cm^{-1}), the Fermi resonance of the CH_3 bending mode overtone with the CH_3 stretch mode (r^{FR+}, at 2939 cm^{-1}) and the asymmetric methyl stretch mode (r^-, at 2959 cm^{-1}). The spectrum is indeed identical to the SFG spectrum from the SDS/D_2O/CaF_2 interface as measured by Moore et al [30]. Scattered SF photons can be detected in this geometry, but only when the beam overlap is placed *inside* the sample cell. When this is done, the spectrum in the bottom panel of Fig. 3.7 is measured. As can be seen, this spectrum consists of the same resonances but the relative intensities are very different, as indicated by the vertical lines. It is therefore cleat that the SFS spectrum originate from the droplet interfaces.

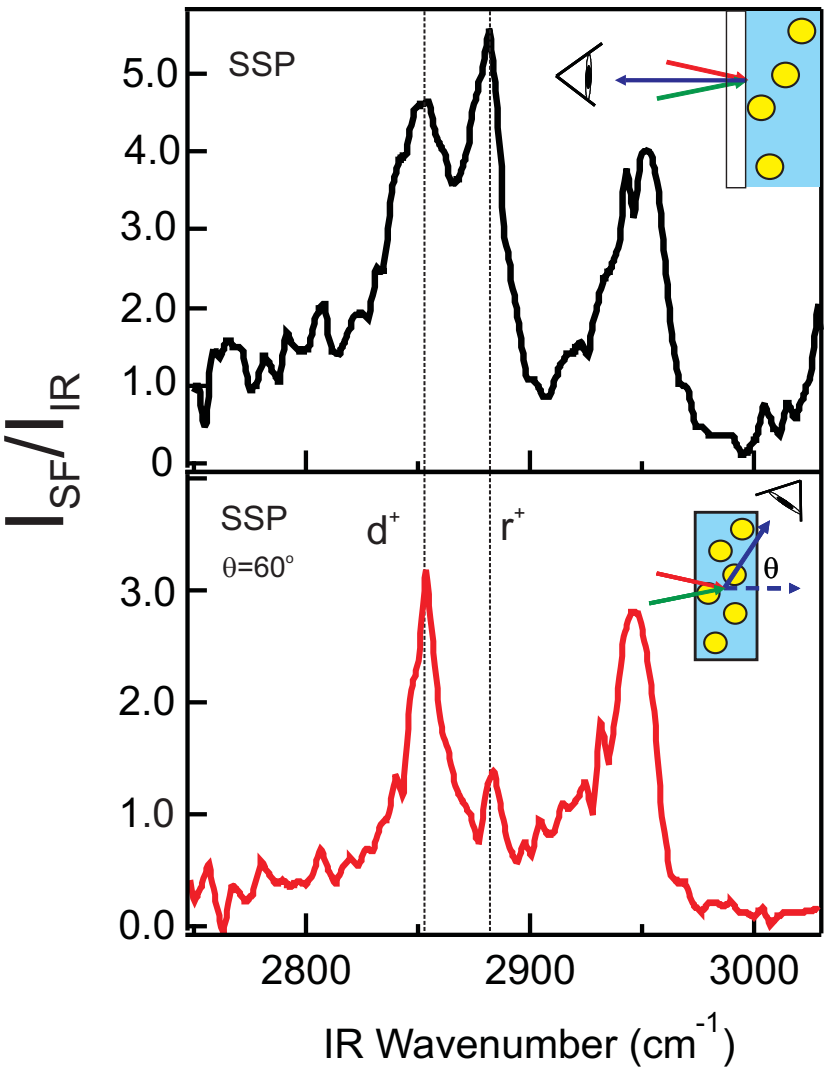

Figure 3.7: Top: Reflection SFG spectrum recorded from the CaF_2/D_2O SDS solution interface. Bottom: SFS spectra taken at a scattering angle of 60°. The data was taken from a 1 vol% dC16-in-D_2O emulsion with 8 mM SDS and 100 nm average droplet radius. The polarization combination was *ppp* and the sample cell path length was 200 μm.

3.4.3 Quantifying competing processes

To identify under which conditions there might be a response from phase matched SFG from the entrance window of the cuvette, we have deposited a water insoluble crystalized layer of poly-(D-Lactic Acid) (PDLA) on the inside of the CaF_2 window. The film had a thickness of a few microns (see [31] for the procedure) and the crystalline structure belongs to the $P2_12_12_1$ space group, so that a bulk signal occurs at polarization combination *spp*. We then measured (i) signal in the phase matched transmission direction from the bare window, (ii) signal in transmission in the phase matched θ=0° direction, with an emulsion sample present in the sample cell, and (iii) signal at θ=60°, with an emulsion sample present in the sample cell. The result is shown in Fig. 3.8. It can be seen that $<$ 1 % of the bulk PDLA signal reaches the detector if we measure at θ=60°. This number further decreases because the beam overlap position is optimized to create signal from the window surface.

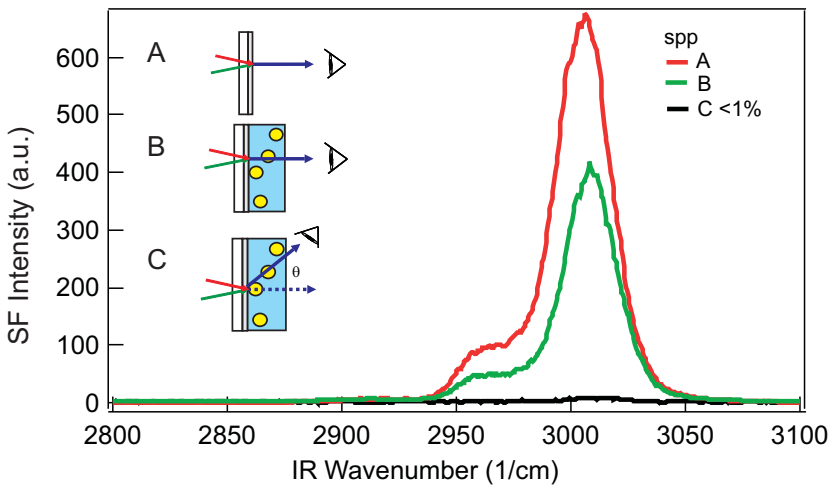

Figure 3.8: SF spectra recorded from a sample cell with a crystalline PDLA film on top of the CaF_2 entrance window. The spectra display the bulk window signal in phase matched transmission (A), the bulk window signal in the same direction but transmitted through an emulsion sample (B) and the signal that can be detected at a scattering angle of θ=60° (C). The emulsion consisted of a 1 vol% dC16-in-D_2O emulsion with 8 mM SDS with a 100 nm average droplet radius. The polarization combination was *spp* and the sample cell path length was 200 μm.

3.4.4 Path length effects

Having now characterized the process we have studied the signal dependence of the sample cell path length, the particle density, and the IR energy. Starting with the path length dependence, we measured the SFS intensity at θ=60° using sample cells with different thicknesses. Spectra taken in the SO_3 stretching region display a single resonant feature at 1070 cm^{-1} and are shown in Fig. 3.9. It can be seen that for this spectral region there is an optimal cell

length of $\sim$ 100 μm. Increasing the cell length results in a smaller intensity. The integrated intensities for both the SO_3 and CH spectral region are plotted as well. It can be seen that for both modes there is a different path length dependence. The graph also shows that the maximum corresponds very well with the extinction of the IR pulse. This is in agreement with our theoretical description in the background section.

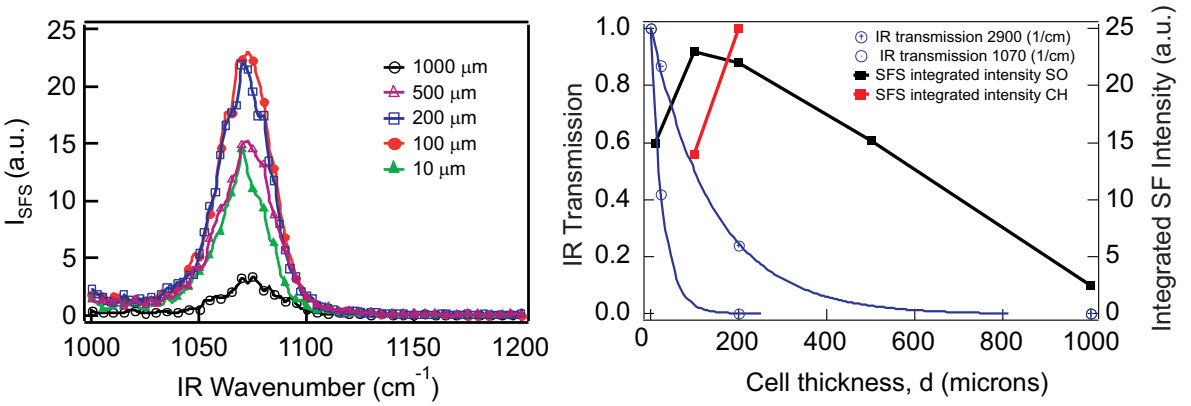

Figure 3.9: Left: SFS spectra in the SO_3 stretch region taken at θ=60° in ssp polarization combination for emulsions using sample cells with different thickness. Right: Integrated intensity as a function of cell thickness. The IR intensity transmitted through a sample cell with different thickness is also shown. The SFS data was taken from a 1 vol% dC16-in-D_2O emulsion with 8 mM SDS. The polarization combination was ssp.

3.4.5 Particle density

Fig. 3.10 shows the signal strength as a function of particle density. The integrated intensity of the collected spectra display a linear dependence on the particle density in the sample. Such a dependence has also been observed for second harmonic scattering [8, 32]. The intensities of the individual particles are additive so that there is no phase relationship between the individual particles. This shows that the process we measure is indeed a scattering process. Schneider et al [9] measured the SHS intensity dependence on particle density. Using a sample cell with a path length of 2 mm they observed a linear dependence for malachite green covered polystyrene beads with a diameter of 202 nm up to particles densities of $\sim 40 \times 10^{10}$ particles/ml. At higher densities the intensity decreases. This decrease can be explained by the occurrence of multiple light scattering. The linear increase of our signal indicates that there are no multiple light scattering effects that need to be taken into account.

3.4.6 Dependence on IR pulse energy

Finally, we measured SF scattering spectra as a function of IR energy. Fig. 3.11 (left panel) shows the integrated spectral intensity as a function of IR pulse energy. The right panel shows

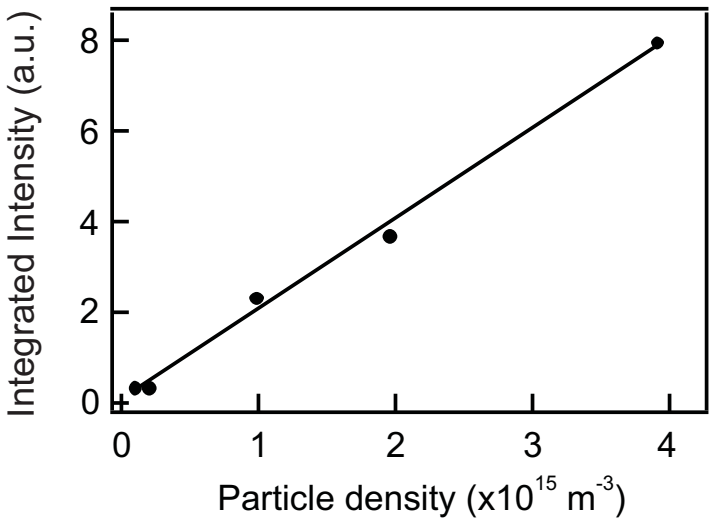

Figure 3.10: Integrated intensity as a function of particle density in the sample. The detection angle is θ=60°.

the normalized spectra for *ppp* polarization. As can be seen the spectral shape does not change with increasing IR power.

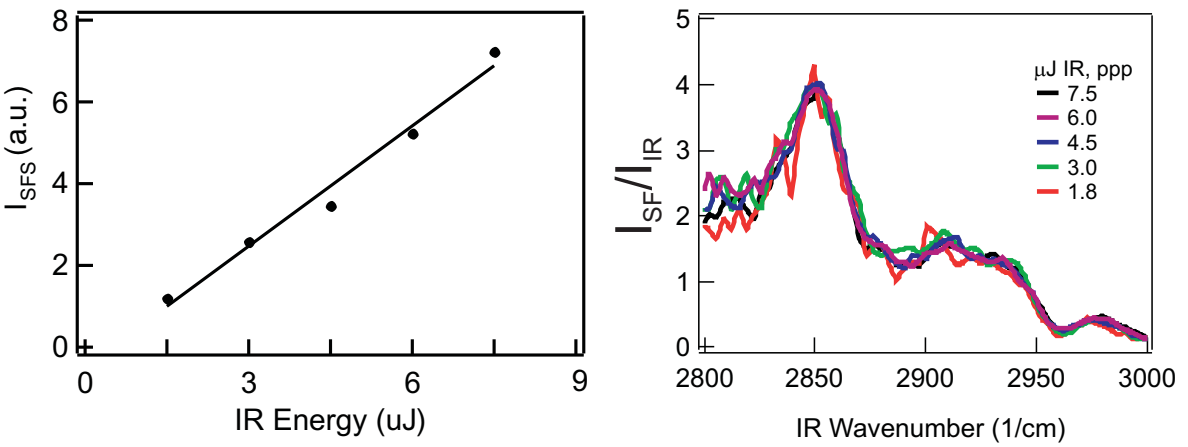

Figure 3.11: Left: Integrated signal as a function of IR pulse energy. Right: Normalized SF scattering spectra for different IR pulse energies showing no dependence of the spectral shape on IR intensity. The data was taken from a 1 vol% dC16-in-D_2O emulsion with 8 mM SDS and 100 nm average droplet radius. The polarization combination was *ppp*.

3.5 Conclusions

We have described in detail various aspects of sum frequency scattering. We performed SF scattering measurements on emulsions consisting of 100 nm sized oil droplets dispersed in SDS/D_2O solutions. We have measured scattering spectra at different scattering angles.

Scattered SF intensity is not detected in the phase matched forward direction. This clearly demonstrates SF scattering nature of the experiment.

To determine if and under which conditions sum frequency generation from the CaF_2/D_2O solution interface might contribute to the measurement we have compared the scattered spectrum to a reflection SFG spectrum from the CaF_2/D_2O solution interface. The alkyl chain conformation of SDS on the CaF_2/D_2O emulsion interface differs from the alkyl chain conformation of SDS on the oil droplet/water interface. To quantify under which conditions the window/solution interface might give rise to comparable signal at a scattering angle of $\theta = 60°$, we have made use of bulk allowed sum frequency generation. The test showed that < 0.1 % of the SF scattered signal can come from the sample cell interface.

The scattered signal was further quantified by measurements with different optical path lengths. The dependence is different for different IR wavelengths and follows the IR absorption behavior of the solvent. The scattered signal increases linearly with droplet density, so that no multiple scattering occurs. Furthermore, the signal depends linearly on IR intensity and the spectral shape does not change with IR pulse energy. This is all in correspondence with predictions for nonlinear scattering theory.

Bibliography

[1] R. J. Hunter. *Foundations of Colloid Science*. Oxford, 2002.

[2] D McClements. Critical review of techniques and methodologies for characterization of emulsion stability. *Crit. Rev. Food Sci. Nutr.*, 47:611–649, 2007.

[3] J. W. Goodwin. *Colloids and interfaces with surfactants and polymers: an introduction*. John Wiley & Sons, 2004.

[4] K. B. Eisenthal. Second harmonic spectroscopy of aqueous nano- and microparticle interfaces. *Chem. Rev.*, 106(4):1462, 2006.

[5] S. Roke. Nonlinear optical spectroscopy of soft matter interfaces. *ChemPhysChem*, 10(9-10):1380–1388, 2009.

[6] E Yan, Y Liu, and K Eisenthal. New method for determination of surface potential of microscopic particles by second harmonic generation. *J. Phys. Chem. B*, 102(33):6331, 1998.

[7] B Schurer, S Wunderlich, C Sauerbeck, U Peschel, and W Peukert. Probing colloidal interfaces by angle-resolved second harmonic light scattering. *Phys. Rev. B*, 82(24):241404, 2010.

[8] H. Wang, E. C. Y. Yan, E. Borguet, and K. B. Eisenthal. Second harmonic generation from the surface of centrosymmetric particles in bulk solution. *Chem. Phys. Lett.*, 259(1-2):15–20, 1996.

[9] L Schneider, H Schmid, and W Peukert. Influence of particle size and concentration on the second-harmonic signal generated at colloidal surfaces. *Appl. Phys. B*, 87(2):333, 2007.

[10] S. H. Jen and H. L. Dai. Probing molecules adsorbed at the surface of nanometer colloidal particles by optical second-harmonic generation. *J. Phys. Chem. B*, 110(46):23000–23003, 2006.

[11] S Jen, G Gonella, and H Dai. The effect of particle size in second harmonic generation from the surface of spherical colloidal particles. I: Experimental observations. *J. Phys. Chem. A*, 113(16):4758, 2009.

[12] M Subir, J Liu, and K Eisenthal. Protonation at the aqueous interface of polymer nanoparticles with second harmonic generation. *J. Phys. Chem. C*, 112(40):15809, 2008.

[13] X. M. Shang, Y. Liu, E. Yan, and K. B. Eisenthal. Effects of counterions on molecular transport across liposome bilayer: Probed by second harmonic generation. *J. Phys. Chem. B*, 105(51):12816–12822, 2001.

[14] J Liu, X Shang, R Pompano, and K Eisenthal. Antibiotic assisted molecular ion transport across a membrane in real time. *Faraday Discuss.*, 129:291–299, 2005.

[15] J Liu, M Subir, K Nguyen, and K Eisenthal. Second harmonic studies of ions crossing liposome membranes in real time. *J. Phys. Chem. B*, 112(48):15263–15266, 2008.

[16] S. Roke, W. G. Roeterdink, J. E.G. J.Wijnhoven, A. V. Petukhov, A. W. Kleyn, and M. Bonn. Vibrational sum frequency scattering from a submicron suspension. *Phys. Rev. Lett.*, 91:258302, 2003.

[17] S Roke, J Buitenhuis, J van Miltenburg, M Bonn, and A van Blaaderen. Interface-solvent effects during colloidal phase transitions. *J. Phys.: Condens. Matter*, 17(45):S3469, 2005.

[18] S. Roke, O. Berg, J. Buitenhuis, A. van Blaaderen, and M. Bonn. Surface molecular view of colloidal gelation. *Proc. Natl. Acad. Sci. U. S. A.*, 103(36):13310–13314, 2006.

[19] A. G. F. de Beer, H. B. de Aguiar, J. F. W. Nijsen, A. B. Sugiharto, and S. Roke. Detection of buried microstructures by nonlinear light scattering spectroscopy. *Phys. Rev. Lett.*, 102(9):095502, 2009.

[20] M. L. Strader, H. B. de Aguiar, A. G. F. de Beer, and S. Roke. Label-free spectroscopic detection of vesicles in water using vibrational sum frequency scattering. *Soft Matter*, 2011.

[21] S. Roke, M. Bonn, and A. V. Petukhov. Nonlinear optical scattering: The concept of effective susceptibility. *Phys. Rev. B*, 70:115106, 2004.

[22] J Dadap, H de Aguiar, and S Roke. Nonlinear light scattering from clusters and single particles. *J. Chem. Phys.*, 130(21):214710, 2009.

[23] S Jen, H Dai, and G Gonella. The effect of particle size in second harmonic generation from the surface of spherical colloidal particles. II: The nonlinear Rayleigh-Gans-Debye model. *J. Phys. Chem. C*, 114(10):4302, 2010.

[24] J. Shan, J. I. Dadap, I. Stiopkin, G. A. Reider, and T. F. Heinz. Experimental study of optical second-harmonic scattering from spherical nanoparticles. *Phys. Rev. A*, 73:023819, 2006.

[25] A. G. F. de Beer and S. Roke. Nonlinear mie theory for second-harmonic and sum-frequency scattering. *Phys. Rev. B*, 79:155420, 2009.

[26] A de Beer and S Roke. Obtaining molecular orientation from second harmonic and sum frequency scattering experiments in water: Angular distribution and polarization dependence. *J. Chem. Phys.*, 132(23):234702, 2010.

[27] Jacob N. Israelachvili. *Intermolecular and Surface Forces*. Academic Press, 2nd edition, 1992.

[28] J. Weiss, N. Herrmann, and D. J. McClements. Ostwald ripening of hydrocarbon emulsion droplets in surfactant solutions. *Langmuir*, 15:6652, 1999.

[29] I. D. Morrison and S. Ross. *Colloidal Dispersions: Suspensions, Emulsions, and Foams*. Wiley-Interscience, 2002.

[30] F Moore, K Becraft, and G Richmond. Challenges in interpreting vibrational sum frequency spectra: Deconvoluting spectral features as demonstrated in the calcium fluoride-water-sodium dodecylsulfate system. *Appl. Spectrosc.*, 56(12):1575–1578, 2002.

[31] C. M. Johnson, A. B. Sugiharto, and S. Roke. Surface and bulk structure of poly-(lactic acid) films studied by vibrational sum frequency generation spectroscopy. *Chem. Phys. Lett.*, 449(1-3):191–195, 2007.

[32] S Viarbitskaya, V Kapshai, P van der Meulen, and T Hansson. Size dependence of second-harmonic generation at the surface of microspheres. *Phys. Rev. A*, 81(5):053850, 2010.

Chapter 4

Adsorption of surfactants at the oil droplets interface

Surfactants such as sodium dodecyl sulfate (SDS) can reduce the interfacial tension between bulk water and bulk hexadecane by 42 mN/m. Although reduction of interfacial tension should also take place on the interface of nanoscopic oil droplets in water, vibrational sum frequency scattering experiments indicate otherwise. In these measurements, we have directly measured the adsorption of SDS onto hexadecane oil droplets with an average radius of 83 nm. We find that the interfacial density of adsorbed SDS is at least one order of magnitude lower than that at a corresponding planar interface. By using the Gibbs equation, the derived maximum decrease in interfacial tension is only 5 mN/m. A similar interfacial density was also found for other ionic surfactant.

4.1 Introduction

The properties of emulsions consisting of nanoscopic oil droplets dispersed in water are primarily determined by the local chemical environment (i.e. molecular structure and charge) of their interfaces [1]. In a detergent-containing emulsion the droplet interface is generally perceived as an interface with a high density of surfactant molecules. This view originates primarily from extrapolating experimental findings on planar interfaces [2]. In a common planar oil/water system such as bulk hexadecane in contact with bulk water, the surfactant SDS reduces the interfacial tension from 52 mN/m (neat hexadecane-water) to 10 mN/m by populating the interface [3–6]. Surfactants resides at the interface with its apolar tail residing in the oil phase, and the polar groups immersed in the water phase [7]. At SDS concentrations approaching the critical micelle concentration (cmc) of 8 mM, the interface is greatly occupied by SDS molecules [6] giving rise to an interfacial excess of 3.3×10^{-6} mol m^{-2}, or equivalently, an occupied molecular interfacial area of 50 Å^2. It is widely assumed that similar behavior can be expected for SDS adsorption on sub micron sized n-hexadecane oil droplets dispersed in water [1, 2, 8, 9]. However, nanoscopic droplets are too small for direct interfacial tension measurements.

As was shown by the Eisenthal group, [10, 11] the electronic structure of the interface can be probed with second harmonic scattering (SHS) [12–15]. The SHS signal depends quadratically on the molecular surface excess (N_s) which can be used to retrieve the interfacial energetics and population [11]. Here, we selectively probe the interfacial SDS molecules using SFS [16, 17] on SDS-stabilized n-hexadecane ($C_{16}D_{34}$) droplets dispersed in D_2O. We have followed the adsorption of SDS onto oil droplets dispersed in D_2O with a constant average radius of 83 nm.

4.2 Experimental details

4.2.1 Emulsions preparation

Emulsions were prepared by using the constant size approach (see Chapter 2) with a stock emulsion made out of 2 vol% perdeuterated n-hexadecane in D_2O solution containing 100 μmol purified SDS (>99%, Alpha Aesar).

4.2.2 SFS experiments

The SFS measurements were done with the emulsions placed in a CaF_2 cuvette with an optical path length of 100 μm. The SFS experiments were performed using 10 μJ IR pulses (150 fs, FWHM bandwidth of $\sim$140 cm^{-1}) centered around 1100 cm^{-1} and 10 μJ, 800 nm VIS pulses with a 12 cm^{-1} FWHM bandwidth (see Chapter 2 for details). The selectively polarized IR and VIS pulses were incident in the horizontal plane in respect to the optical table. The

SF scattered light was measured in the same plane at a scattering angle of 60° with an acceptance angle of 20°. The SF photons were polarization selected and spectrally dispersed onto an intensified CCD camera. Fluctuations in laser power and stability were accounted for by measuring a reference sample between samples (see Fig. 3.5).

4.3 Results

4.3.1 SFS strength as a function of surfactant concentration

The vibrational SFS measurements were performed by overlapping IR and VIS laser pulses [18] inside the cuvette containing an emulsion. Fig. 4.1.A sketches the SFS process in a single-droplet level for a ssp polarization combination. The p-polarized broadband IR field (centered around 1100 cm^{-1}) can excite the IR dipole moment of the symmetric SO_3 stretch mode. Only the sulfate head groups in the first molecular layer around the droplet interface can, upon interaction with the narrow band s-polarized VIS field, simultaneously undergo a change in their electronic charge distribution. This second-order sum-frequency (SF) polarization can emit a sum frequency photon [17, 19, 20]. Thus, SF photons are generated only by the SDS molecules at the oil/water interface of the droplets. Coherent interference on the droplet surface will give rise to a scattering pattern, which is peaked around a scattering angle θ of 60° with respect to the phase-matched direction of the incoming beams [21].

Fig. 4.1.B and 4.1.C displays several SFS spectra recorded at this angle in ppp and ssp polarization combination, respectively. For the other two allowed polarizations sps and pss the SFS signal was below our detection limit. The SFS spectra can be described by scattering theory [16, 17, 21] and fit with a SO_3 symmetric stretch resonance [22, 23] centered at 1080 cm^{-1} with a constant line width for all SDS concentrations with the following equation:

$$I_{SFS}(\omega,\theta) \propto |E_{IR}(\omega)(\sum_n \frac{A(\theta)_n}{(\omega-\omega_{0n})+i\Upsilon_{0n}} + A_{NR}e^{i\Delta\phi})|^2 \tag{4.1}$$

where n refers to a specific vibrational mode, with resonance frequency ω_{0n}, damping constant Υ_{0n}, and angle dependent amplitude A_n. $E_{IR}(\omega)$ is the envelope of the IR pulse and A_{NR} is the amplitude of the non-resonant contribution, which has a relative phase $\Delta\phi$ in respect to the resonances. The fits were made with the SO_3 symmetric stretch resonance at $\omega_{SO_3} = 1080\,cm^{-1}$, with a width of $\Upsilon_{SO_3} = 15\,cm^{-1}$. As can be seen from the spectra, the ppp polarization is not only determined by this resonance but also by a 'non-resonant' background and a broad band around 1215 cm^{-1}, which coincides with the OD bending mode of heavy water. The IR pulse was described by a fitted Gaussian centered around 1109 cm^{-1} with a width of 132 cm^{-1} (see Fig. 2.4).

The obtained amplitudes for both spectra in ppp and ssp polarization combinations are plotted in Fig. 4.1.C. It shows that a change in total SDS concentration of 2 orders of mag-

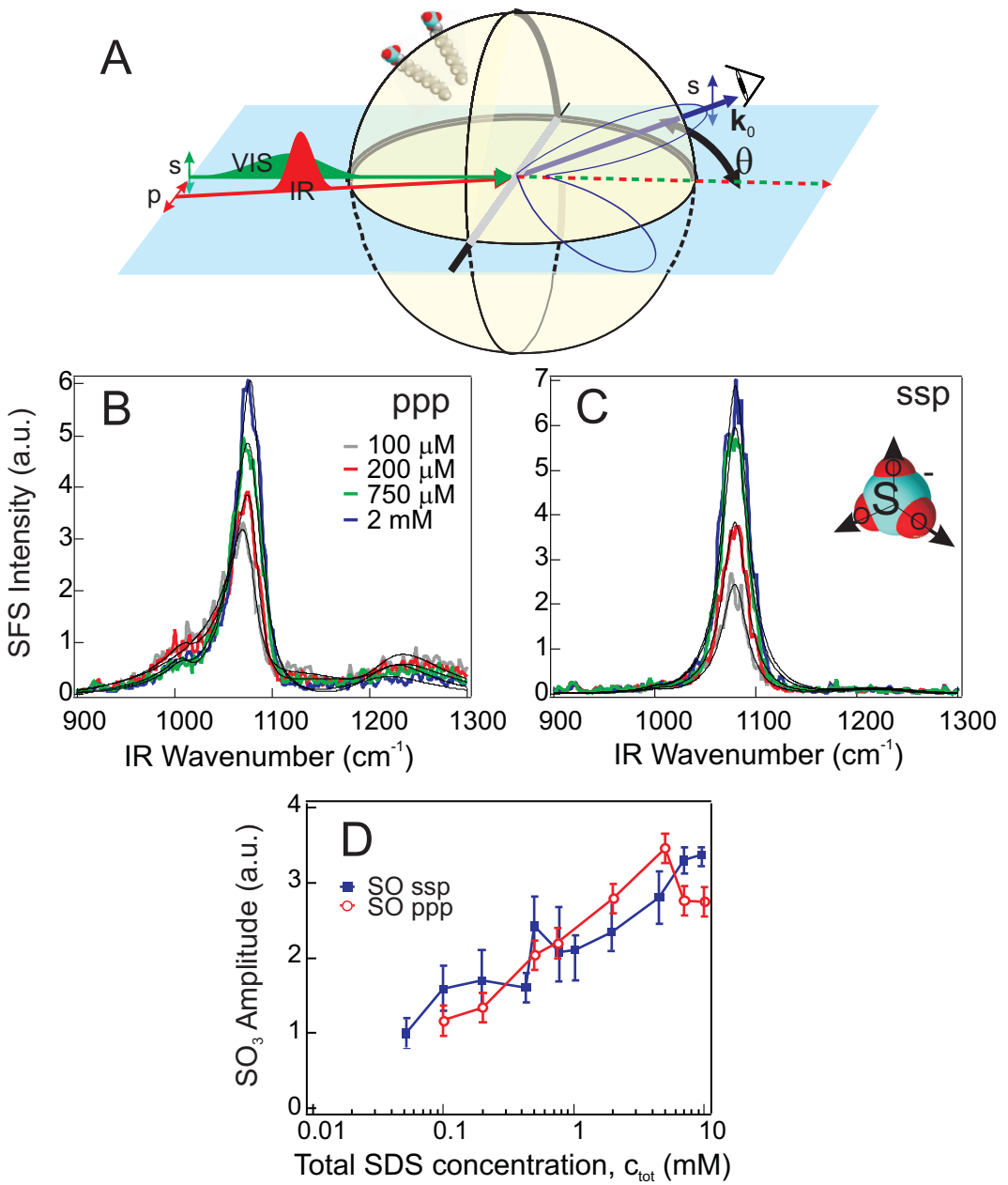

Figure 4.1: SFS spectroscopy to measure the adsorption of SDS molecules on the oil/water droplet interface. A) Illustration of the experiment in which p-polarized IR and s-polarized VIS beams generate s-polarized SF photons. B) ppp polarization combination SFS spectra for various total concentrations of SDS (c_{tot}). C) ssp polarization combination spectra. Continuous lines are fits. D) The resultant amplitudes of the symmetric SO_3 stretch mode for SFS spectra in ssp and ppp polarization plotted against the total SDS concentration. The droplet size distribution is constant for all SDS concentrations.

nitude is accompanied by a change in SF amplitude of only a factor of 3.5. Control experiments with a 40 mM solution of only SDS in D_2O gave no observable signal.

Polarization combination dependence

The SFS amplitude is determined by the orientation of the molecules, the local refractive index at the droplet interface, and the molecular interfacial density. In order to convert the SFS amplitude to an interfacial excess we need to assert that the molecular orientation is not changing as we change the total surfactant concentration. Also, we need to consider how the Fresnel factors are changing if we increase the concentration of SDS. Whether these effects have an influence on the measurements can be established by measuring SFS spectra for both the SO_3 and CH stretches vibrational resonances in multiple polarization combinations. If both ssp and ppp polarization intensities for the SO_3 symmetric stretch mode display the same trend (a constant ssp to ppp ratio), [22] we believe we can conclude that the SFS amplitude from the SO_3 symmetric stretch mode is linearly related to the increase in surface density. Additionally, the CH stretching resonances should display an identical trend as the SO_3 stretch resonances, if there is no considerable changes in alkyl chain conformation.

Since we are working at a very small refractive index difference (0.1), with small droplet radii, and at very low surfactant concentrations, a change in Fresnel factors as the origin of the concentration-dependent amplitude change can be neglected. Changes in Fresnel factors would result in variations of the ssp/ppp intensity ratio (not observed as seen in Fig. 4.1.D).

4.3.2 Counting interfacial molecules

The observations of previous sections indicate that the amplitudes of the SFS signals are directly proportional to SDS interfacial density (interfacial excess) at the oil droplets-water interface.

Since SDS molecules can either reside in the solution (with concentration c) or at the interface, we have total concentration $c_{tot} = N_s A/V + c$, where A is the total surface area (obtained from DLS) and V is the sample volume. Using the modified Langmuir model published by Wang *et al.* [11], in combination with the boundary condition that the interfacial density cannot exceed the total amount of molecules in the solution (*i.e.*, $A \times N_s \leq c_{tot} \times V$) and the known total droplet surface area (from the DLS data), we can estimate the change in interfacial density from the SFS data. The entire N_s vs c curve must therefore lie below the line $N_s = c_{tot}V/A$. Because it is unlikely that all SDS molecules reside at the interface (while none remain in the water phase), we have estimated the surface coverage by fitting the data

in Fig. 4.1.C with the modified Langmuir model presented by Wang *et al.* [11]:

$$A_{SFS} \propto \frac{N_s}{N_s^{max}} = \frac{c_s}{c_s^{max}} = \frac{c_{tot} + c_s^{max} + c^{\ominus}/K - \sqrt{(c_{tot} + c_s^{max} + c^{\ominus}/K)^2 - 4c_{tot}c_s^{max}}}{2c_s^{max}} \tag{4.2}$$

whereby we have imposed the condition that

$$c_{tot}V \geq N_s A \tag{4.3}$$

where c_s is the concentration of absorbed molecules (so that $c_{tot} = c + c_s$), T is temperature, $c^{\ominus}$ is the molarity of D_2O and K is a constant that can be related to the free energy of adsorption by $\Delta G = -R_g T \ln K$, with R_g the molar gas constant. The maximum droplet surface coverage N_s^{max} and the Gibbs free energy of adsorption ΔG are the fitting parameters.

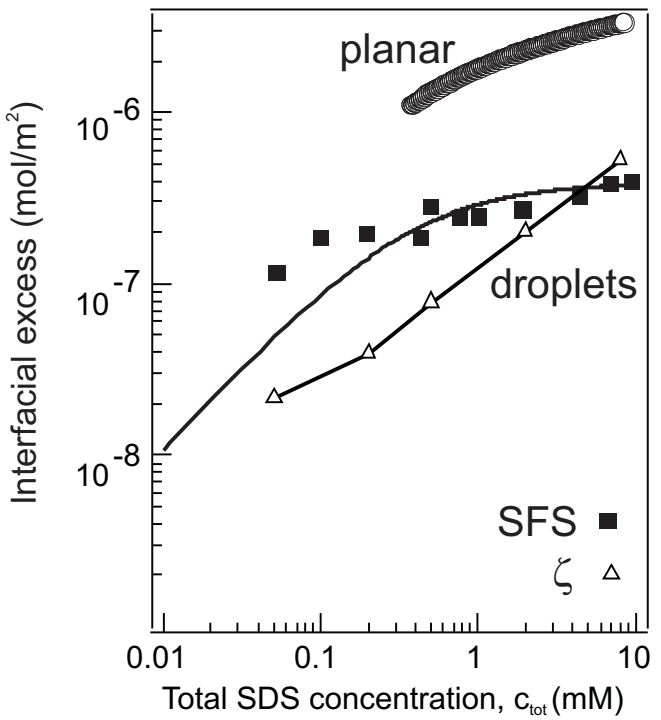

Figure 4.2: Interfacial excess (N_s) of SDS at the n-hexadecane-water interface. (Circles) macroscopic planar interface obtained from interfacial tension data [6]. (squares) n-hexadecane droplets in water measured by SFS amplitudes. (triangles) charge density induced by SDS adsorption on n-hexadecane droplets in water derived from ζ-potential data. The solid line is a fit to the modified Langmuir adsorption model.

The result is shown in Fig. 4.2. From the fit (continuous line) we obtain an upper limit of $3.92 \pm 0.13 \times 10^{-7}$ mol/m^2 for the saturation surface coverage (N_s^{max}) and -29.10$\pm$0.58 kJ/mol for ΔG. Although the quality of the fit is not excellent, it does provide an upper limit for the surface excess. It should be noted that fits with the same accuracy could also be reached with

smaller values of N_s^{max}. This value corresponds to a minimum interfacial area of 425 Å^2 per SDS molecule as opposed to 50 Å^2 for the planar interface. Evidently, there is an enormous difference between the adsorption behavior on a small n-hexadecane droplet and that on a planar interface.

4.3.3 Retrieved interfacial tension

The (curvature corrected) Gibss adsortion equation [7, 8] relates the change in interfacial tension $\delta\gamma$ to the interfacial excess N_s and changes in SDS bulk concentration c:

$$\frac{\delta\gamma(1-2\frac{\delta_t}{R})}{\delta\ln(c)} = -2R_gTN_s \tag{4.4}$$

where R_g is the molar gas constant, T the temperature, R the radius of the droplet and δ_t the Tolman length [24, 25]. The Tolman length is a measure of the interface thickness and is on the order of 1-5 Å. We find that the correction needed for high curvature ($\frac{\delta_t}{R}$) is negligible. Taking upper limit of N_s from our data we can derive the change in interfacial tension ($\delta\gamma$) as a function of bulk concentration by integrating $-2R_gTN_s/c$. The result is plotted in Fig. 4.3 (solid squares). The derived interfacial tension changes only -5 mN/m when the SDS bulk concentration is varied over 3 orders of magnitude. Corresponding data for the equivalent planar interface shows a significantly larger drop in interfacial tension of -42 mN/m (Fig. 4.3, circles).

4.3.4 Extracting the surface tension from SFG data: a test using the planar air/SDS/water system

We have verified that the interfacial tension and molecular surface density obtained from SFG measurements can be related to each other by analyzing SFG data obtained from SDS adsorption on a planar air/water interface. This was achieved by taking the SFG results of Ref. [22], which are in arbitary units, and rescaling the y-axis using the value of the surface excess of SDS at the highest concentration. Once the absolute y-scale is obtained, then we can use Eq. 4.4 to obtain the surface tension.

Fig. 4.4 shows surface tension measurements for the air/water interface as a function of SDS concentration (circles, left axis) [6]. The continuous line plotted on the right axis is the change in surface tension as obtained from the SFG data [22]. As can be seen, the agreement between the SFG and surface tension is considered satisfactory confirming that our approach is reliable.

4.3.5 Correspondence between SFS and ζ-potential data

The retrieved upper limit for the number of SDS molecules at the surface can be compared with surface charge density data, obtained from ζ-potential (ϕ_ζ) measurements [1, 26]. The

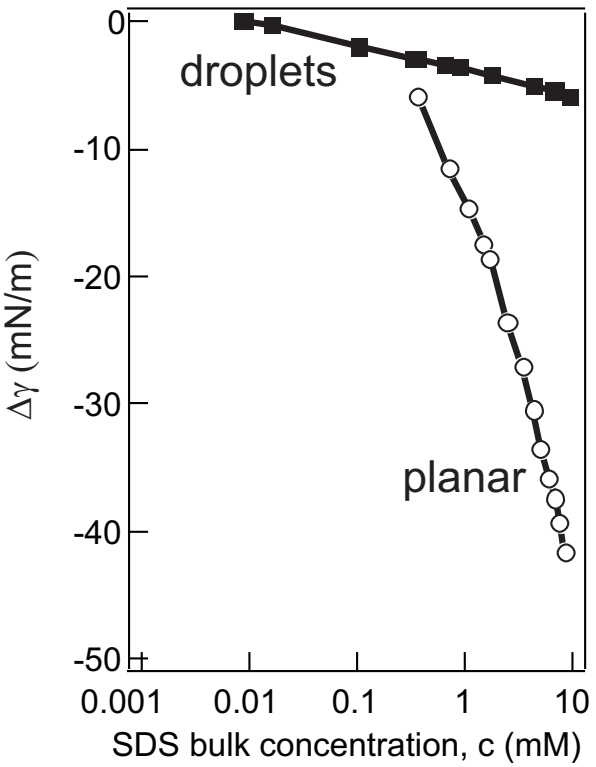

Figure 4.3: Change in interfacial tension ($\delta\gamma$) of the n-hexadecane/water interface due to SDS interfacial activity. (Circles) macroscopic planar interface [6]. (squares) n-hexadecane droplets in water retrieved from the interfacial excess data using the Gibbs Adsorption equation.

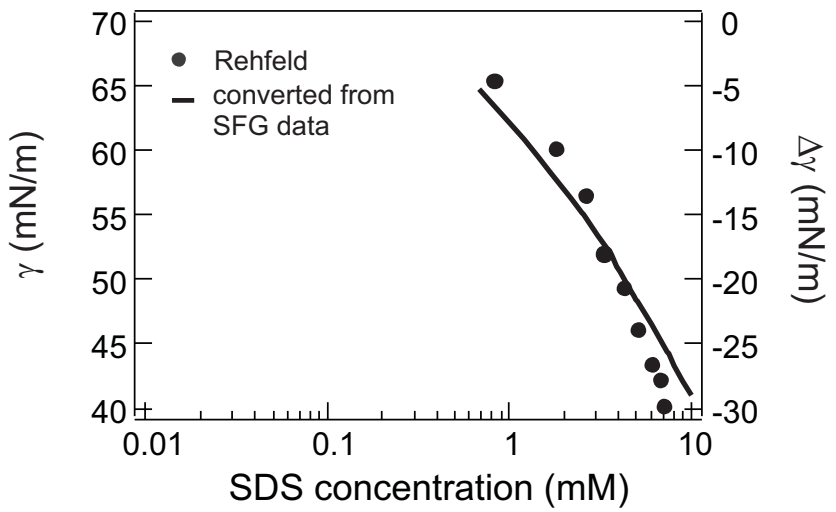

Figure 4.4: Surface tension data as a function of SDS concentration for the air/SDS/water system [6] (circles, left axis), in combination with the retrieved change in surface tension (continuous line, right axis) by using the Gibbs equation and the SFG data from Ref. [22].

surface charge density (σ) can be retrieved from calculating the electrokinetic charge present at the shear plane. Assuming that this plane is very close to the particle interface (a widely used approximation),[1] the surface charge density can be retrieved using the following approximation [1]:

$$\sigma = \epsilon_0 D \frac{kT}{ze} \kappa (2 \sinh(\frac{ze\phi_\zeta}{2kT}) + \frac{4}{\kappa R} \tanh(\frac{ze\phi_\zeta}{4kT})) \tag{4.5}$$

with ϵ_0 the permittivity of free space, D the relative permittivity ($D = \frac{\epsilon}{\epsilon_0}$), κ the Debye-Hückel parameter $\kappa = \sqrt{\frac{e^2 \sum_i n_i^0 z_i^2}{D\epsilon_0 kT}}$, k the Boltzmann constant, T the temperature, e the elementary charge, z the valency, and n_i^0 the number of ions of type i in de bulk solution.

The values of the measured ζ-potentials for different SDS concentrations are shown in Fig. 2.2.A. The calculated charge densities are shown Fig. 4.2 (triangles). It can be seen that the densities from ζ-potential and SFS measurements are of the same order of magnitude, so that both results are in agreement with one another, even though it is not certain that all the SDS are ionized at the interface. At concentrations close to the cmc, the correspondence is considered good, but an increasing discrepancy can be seen in the low SDS concentration. This discrepancy could be due to the fact that both methods measure different species (SFS measures charged and uncharged sulfate groups while ζ-potential overall charges).

4.3.6 Other Surfactants

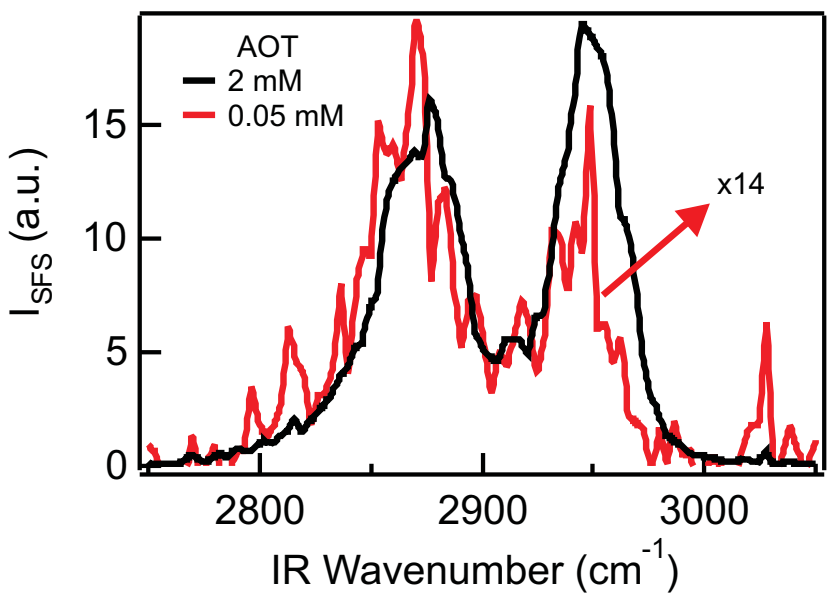

Figure 4.5: SFS spectra of the surfactant AOT at the oil droplet-water interface at different concentrations. The emulsion consisted of 1 vol% dC16-in-D_2O and was prepared using the constant size approach. The polarization combination was ssp.

We observed similar behavior with another ionic surfactant, namely sodium bis (2-ethylhexyl)

[1] For instance, see [26] and references therein.

sulfosuccinate (AOT). The SFS spectra of the interfacial AOT is shown in Fig. 4.5 for the CH stretch region. The emulsion consisted of 1 vol% dC16-in-D_2O and was prepared using the constant size approach (see Chapter 2). As it can be seen, the signal increases ≈14 times as we increase the bulk concentration by a factor of 40. Altough this increase in signal as a function of concentration is stronger than the SDS case, the signal strength at concentrations close to their cmc are comparable (cmc of AOT=2.8 mM [27]). If AOT had the same density as observed in a planar interface experiment (∼60 Å^2 [28]), the signal intensity would be expected to be at least 10 times stronger which is not observed. Also, the droplet size of emulsions prepared with AOT (average radius 106 nm) were comparable to the ones obtained using SDS as surfactant. Therefore, the density of AOT should be in the same order of magnitude as the SDS.

4.3.7 Role of impurities

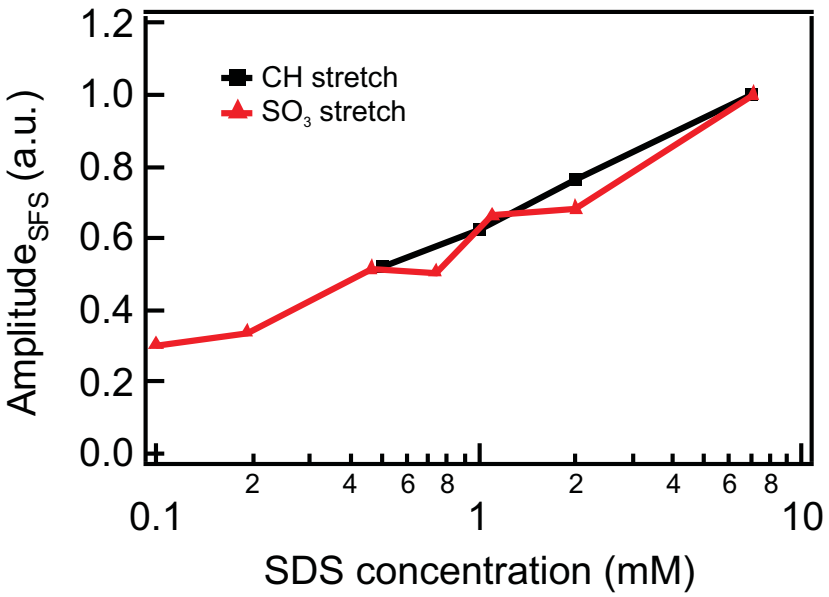

Figure 4.6: SFS response of the SO_3 symmetric stretch and CH stretches as a function of SDS concentration. The spectra of the CH stretch response is shown in Chapter 5. The polarization combination was *ssp*. Both data sets (CH and SO_3) were normalized to the intensity measured at 7 mM.

SDS in aqueous solutions undergoes a chemical reaction (hydrolysis) in which it has a small amount of dodecanol as product [29]. This is a major concern in studies of the planar air-water interface [30], where the surface activity of dodecanol is comparable to SDS, or can be even higher [31]. However, in our SFS experiments we do not expect that dodecanol competes with SDS upon adsorption. Emulsions systems have much higher area to volume ratio, therefore more impurities levels are needed to interfere in our experiments. Additionally, dodecanol is highly soluble in the oil phase [29, 32]. Also, the free energy of

adsorption of dodecanol at the oil-water interface is smaller than SDS [33]. Furthermore, we used the purest chemicals available and we did not observe any difference in the results if SDS was further purified by recrystallization.

Nevertheless, we checked if dodecanol plays a role by comparing the SFS spectra of the CH stretch region to the SO_3 stretch region. If dodecanol is present at the oil droplets-water interface, we expect a different shape of the isotherm [31] of the CH stretch region from the SO_3 stretch region. This is due to the fact that in the CH stretch region both species (SDS and dodecanol) contribute to the measured signal whereas in the SO_3 stretch region only SDS contributes. We plot in Fig. 4.6 the SFS amplitudes of the CH stretch and SO_3 stretch regions as a function of SDS concentration. As can be clearly seen in Fig. 4.6, both spectral regions show very similar increase in SFS amplitude as the SDS concentration increases (spectra of the CH stretch region are shown in Chapter 5). The similar changes in amplitude as a function of concentration in both spectral regions (CH and SO_3) indicate that the co-adsorption of dodecanol is negligible.

4.4 Implications on Ostwald Ripening

A consequence of our results is to explain the difference between theory and experiments of Ostwald Ripening on emulsions. Ostwald ripening is the process in which larger droplets increases their size at the expense of smaller ones. Molecules from the smaller droplets diffuses through the continuous phase towards the larger droplets [9]. The Ostwald ripening rate can be calculated according to the Lifshitz-Slyozov-Wagner (LSW) model [9, 34]. The average radius as a function of time $\bar{R}(t)$ can be written as:

$$\bar{R}(t) = (\bar{R}^3_{(t=0)} + \frac{8\gamma D c_{r\to\infty} V_m^2 t}{9 R_g T})^{1/3} \tag{4.6}$$

where γ is the interfacial tension at the oil-water interface, D is the diffusion coefficient of the oil through the aqueous phase, $c_{r\to\infty}$ is the solubility of the oil in the aqueous phase, V_m is the molar volume of the oil, R_g is the gas constant and T is the absolute temperature.

The dashed-dotted lines curve in Fig. 4.7 shows a calculation of the increase in droplet radius due to Ostwald ripening. For this calculation we have taken values for the solubility, the diffusion constant, the molar volume and the interfacial tension from Ref. [9]. It can be seen that indeed the Ostwald ripening rate for this system is very slow. It should be noted however that the measured Ostwald ripening rate presented in Ref. [9] is much larger than what is calculated using Eq. 4.6. For an emulsion of 5 wt % hexadecane oil in water with 20 mM SDS it was measured that the average radius increased from 51 nm to 63 nm in 480 hours (20 days). This data is represented in Fig. 4.7 by the dashed line. Although the measured rate is much higher than predicted by the calculation it is still very low change in droplet size. If we repeat the calculation with Eq. 4.6, with an interfacial tension value of 52 mN/m we

arrive at an Ostwald ripening rate that is much closer to the measured value, as can be seen from the continuous line in Fig. 4.7.

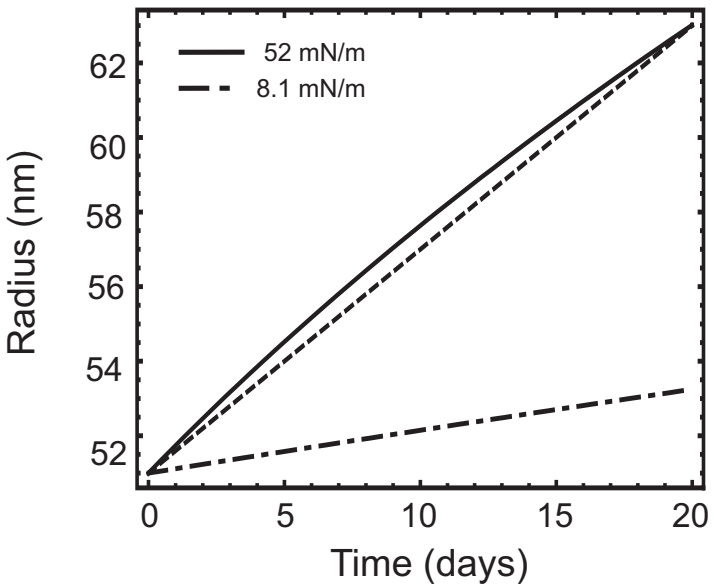

Figure 4.7: The calculated Ostwald ripening rate using Eq. 4.6, using different values for the oil-water interfacial tension (γ). The dashed line corresponds to data points taken from Ref. [9].

4.5 Conclusions

Although on a planar interface the interfacial tension drops dramatically due to surfactant action, this clearly does not happen on the corresponding nanoscopic droplet interface. Our data are in agreement with ζ-potential measurements and our findings would explain the discrepancy between calculated and measured Ostwald ripening rates. In the next chapter we discuss a mechanism to explain this surprisingly low interfacial density.

Bibliography

[1] R J Hunter. *Zeta Potential in Colloid Science: Principles and Applications*. Colloid Science. Academic Press, 1981.

[2] S. A. Nespolo, M. A. Bevan, D. Y. C. Chan, F. Grieser, and G. W. Stevens. Hydrodynamic and electrokinetic properties of decane droplets in aqueous sodium dodecyl sulfate solutions. *Langmuir*, 17(23):7210, 2001.

[3] M Messmer, J Conboy, and G Richmond. Observation of molecular ordering at the liquid-liquid interface by resonant sum-frequency generation. *J. Am. Chem. Soc.*, 117(30):8039, 1995.

[4] J. C. Conboy, M. C. Messmer, and G. L. Richmond. Investigation of surfactant conformation and order at the liquid-liquid interface by total internal reflection sum-frequency vibrational spectroscopy. *J. Phys. Chem.*, 100(18):7617–7622, 1996.

[5] J Conboy, M Messmer, and G Richmond. Effect of alkyl chain length on the conformation and order of simple ionic surfactants adsorbed at the D_2O/CCl_4 interface as studied by sum-frequency vibrational spectroscopy. *Langmuir*, 14(23):6722, 1998.

[6] S. J. Rehfeld. Adsorption of sodium dodecyl sulfate at various hydrocarbon-water interfaces. *J. Phys. Chem.*, 71(3):738–745, 1967.

[7] J. W. Goodwin. *Colloids and interfaces with surfactants and polymers: an introduction*. John Wiley & Sons, 2004.

[8] A. W. Adamson and A. P. Gast. *Physical Chemistry of Surfaces*. 6th edition, 1997.

[9] J. Weiss, N. Herrmann, and D. J. McClements. Ostwald ripening of hydrocarbon emulsion droplets in surfactant solutions. *Langmuir*, 15:6652, 1999.

[10] H. Wang, E. C. Y. Yan, E. Borguet, and K. B. Eisenthal. Second harmonic generation from the surface of centrosymmetric particles in bulk solution. *Chem. Phys. Lett.*, 259(1-2):15–20, 1996.

[11] H Wang, E Yan, Y Liu, and K Eisenthal. Energetics and population of molecules at microscopic liquid and solid surfaces. *J. Phys. Chem. B*, 102(23):4446, 1998.

[12] J Dadap, J Shan, K Eisenthal, and T Heinz. Second-harmonic Rayleigh scattering from a sphere of centrosymmetric material. *Phys. Rev. Lett.*, 83(20):4045, 1999.

[13] H. F. Wang, T. Troxler, A. G. Yeh, and H. L. Dai. In situ, nonlinear optical probe of surfactant adsorption on the surface of microparticles in colloids. *Langmuir*, 16:2475–2481, 2000.

[14] N Yang, W Angerer, and A Yodh. Angle-resolved second-harmonic light scattering from colloidal particles. *Phys. Rev. Lett.*, 87(10):103902, 2001.

[15] K. B. Eisenthal. Second harmonic spectroscopy of aqueous nano- and microparticle interfaces. *Chem. Rev.*, 106(4):1462, 2006.

[16] S. Roke, W. G. Roeterdink, J. E.G. J.Wijnhoven, A. V. Petukhov, A. W. Kleyn, and M. Bonn. Vibrational sum frequency scattering from a submicron suspension. *Phys. Rev. Lett.*, 91:258302, 2003.

[17] S. Roke. Nonlinear optical spectroscopy of soft matter interfaces. *ChemPhysChem*, 10(9-10):1380–1388, 2009.

[18] A. B. Sugiharto, C. M. Johnson, I. E. Dunlop, and S. Roke. Delocalized surface modes reveal three-dimensional structures of complex biomolecules. *J. Phys. Chem. C*, 112(20):7531–7534, 2008.

[19] P. Guyot-Sionnest, J. H. Hunt, and Y. R. Shen. Sum-frequency vibrational spectroscopy of a Langmuir film: Study of molecular-orientation of a two-dimensional system. *Phys. Rev. Lett.*, 59(14):1597, 1987.

[20] Y Shen. Surface-properties probed by 2nd-harmonic and sum-frequency generation. *Nature*, 337(6207):519, 1989.

[21] S. Roke, M. Bonn, and A. V. Petukhov. Nonlinear optical scattering: The concept of effective susceptibility. *Phys. Rev. B*, 70:115106, 2004.

[22] C Johnson and E Tyrode. Study of the adsorption of sodium dodecyl sulfate (SDS) at the air/water interface: targeting the sulfate headgroup using vibrational sum frequency spectroscopy. *Phys. Chem. Chem. Phys.*, 7(13):2635, 2005.

[23] D Hore, D Beaman, and G Richmond. Surfactant headgroup orientation at the air/water interface. *J. Am. Chem. Soc.*, 127(26):9356, 2005.

[24] R C Tolman. The effect of droplet size on surface tension. *J. Chem. Phys.*, 17(3):333, 1949.

[25] F O Koenig. On the thermodynamic relation between surface tension and curvature. *J. Chem. Phys.*, 18(4):449, 1950.

[26] K Marinova, R Alargova, N Denkov, O Velev, D Petsev, and I Ivanov. Charging of oil-water interfaces due to spontaneous adsorption of hydroxyl ions. *Langmuir*, 12(8):2045, 1996.

[27] R Aveyard, P Cooper, and P Fletcher. Solubilization of hydrocarbons in surfactant monolayers. *J. Chem. Soc. Faraday Trans.*, 86(21):3623–3629, 1990.

[28] R. Aveyard, B. P. Binks, P. Cooper, and P. D. I. Fletcher. Incorporation of hydrocarbons into surfactant monolayers. *Adv. Colloid Interface Sci.*, 33(2-4):59–77, 1990.

[29] A Javadi, N Mucic, D Vollhardt, V Fainerman, and R Miller. Effects of dodecanol on the adsorption kinetics of SDS at the water-hexane interface. *J. Colloid Interface Sci.*, 351(2):537–541, 2010.

[30] R. J. Hunter. *Foundations of Colloid Science*. Oxford, 2002.

[31] R Ward, P Davies, and C Bain. Coadsorption of sodium dodecyl sulfate and dodecanol at a hydrophobic surface. *J. Phys. Chem. B*, 101(9):1594–1601, 1997.

[32] P Joos, D Vollhardt, and M Vermeulen. Interfacial-tension of sodium dodecyl-sulfate solutions at the hexane water interface. *Langmuir*, 6(2):524–525, 1990.

[33] R Aveyard and B Briscoe. Adsorption of n-alkanols at alkane/water interfaces. *J. Chem. Soc. Faraday Trans. 1*, 68:478, 1972.

[34] I Lifshitz and V Slyozov. The kinetics of precipitation from supersaturated solid solutions. *J. Phys Chem. Solids*, 19(1-2):35–50, 1961.

Chapter 5

Surface structure of SDS and oil at the oil droplets interface

We present sum frequency scattering spectra on kinetically stabilized emulsions consisting of nanoscopic oil droplets in water, stabilized with sodium dodecyl sulfate (SDS). We have measured the interfacial structure of the alkyl chains of the surfactant molecules, the alkyl chain of the oil molecules, the weakly dispersive D_2O response, and the interference between SDS and the oil. We find a big difference in chain conformation: SDS has many chain defects, whereas the oil has very few. Our spectra are interpreted to originate from a surface structure with oil molecules predominantly oriented parallel with respect to the plane of the interface. Such a conformation of surfactant occupies a surface area of several hundreds of squared Ångstroms.

5.1 Introduction

If surfactants are added to an oil/water system they will occupy the interfacial region until a significant portion of the surface layer is packed with surfactant. When the maximum coverage is reached, the surfactant will form micelles in the bulk phase (this is called the critical micelle concentration) [1]. This idea was proposed in the early 20th century [2, 3], and originated from surface tension measurements that could be explained by a theory for oriented adsorption. Oriented adsorption in an oil/water system occurs with molecules that are amphiphilic, i.e. partially hydrophilic and partially hydrophobic. Such molecules have an affinity for both the oil and the water phase and are therefore highly surface active. The explanation for the lowering of surface tension was directly transferred to explain the experimental observation that emulsions appear to be stabilized by the same molecules that would reduce the surface tension [4]. From experiments on planar oil/water systems and microemulsions it is widely accepted [1] that (i) in most cases a large amount of surfactant is needed to stabilize emulsions, that (ii) below the critical micelle concentration surfactants primarily reside as a somewhat oriented layer at the interface of the oil droplet in water, and (iii) that the hydrophobic tail will mix with the oil, while the hydrophilic head group will mix with the water.

In the past decades this general picture has been refined by numerous experiments reviewed in e.g. Refs. [5–7], involving X-ray diffraction [7–13], neutron scattering [9, 14–22], (dynamic) surface tension measurements [6, 23–25], viscoelastic measurements [26–29], second harmonic generation [30], ellipsometry [11, 31–33], and sum frequency generation [34–48]. The anionic surfactant sodium dodecylsulfate (SDS) has been studied with SFG at the air/water interface [34, 38, 42, 43, 47] and at the CCl_4-water interface [35, 37]. Cationic alkyltrimethylammonium bromide surfactants have been studied with SFG at the air/water interface [49–52], and the hexadecane/water interface [40, 46]. Neutron reflection measurements have also been performed [22] as well as ellipsometry measurements of the temperature dependent wetting of hexadecane [33]. These measurements have shown that three phases exist on this alkane/water/ dodecyltrimethylammonium bromide (DTAB) interface: a 2D gas phase, a liquid phase comprising a mixed monolayer of hexadecane and the surfactant and a 2D 'solid' phase. Surfactants can also induce surface freezing [31], which occurs on alkane/air interfaces [53], but for reasons that are unclear, not on alkane/water interfaces [9]. Surfactant surface areas are reported in the range of 40 - 70 $Å^2$, whereby the occupied surface area is found to be larger on the oil/water interface than on the air/water interface.

The properties of kinetically stabilized emulsions are generally understood with the above described behavior in mind [54, 55]. Kinetic stability refers to the fact that, although the lifetime of an emulsion can be years, emulsions ultimately undergo a phase separation. Some observations can be interpreted as pointing towards a situation that requires a surfactant

surface density that is much lower than 40 - 70 $Å^2$. For example, when droplet size in a kinetically stabilized emulsion is reduced down to the nanometer scale the surface area becomes so large that the amount of surfactant in the sample is not enough to create interfaces with an area per surfactant of 40 - 70 $Å^2$. Instead, the calculated area per surfactant is 10 to 100 times lower [54]. Nevertheless nanoemulsions are very stable. It has also been reported [56–58] that stable emulsions can be prepared that do not require surfactant. The charge density needed to stabilize an emulsion is estimated to be in the range of 0.016 e^-/nm^2 (Ref. [59]) - 0.3 e^-/nm^2 (Ref. [60]).

Commonly employed techniques for the study of fundamental processes that determine the structure and stability of kinetically stabilized emulsions typically probe parameters such as surface tension or overall charge (zeta potential) [57, 61–63], which are not direct measurements of the droplet interfacial molecular structure. For most molecular probes the surrounding medium forms an impenetrable barrier. As a result, the molecular interfacial properties of emulsion droplets are still unknown [54, 55, 61].

Since the mid-90s pioneering work by the Eisenthal group has shown that Second Harmonic Scattering (SHS) could be used to elucidate the hidden properties of solid particles or droplets in solution [64, 65]. Vibrational Sum Frequency Scattering [66, 67] (SFS) spectroscopy builds upon those developments. It relies on the same principles as SHS with the additional feature that a vibrational spectrum can be recorded for any of the species that reside at the interface. In SFS experiments there are two important length scales: the molecular length scale of the molecules on the droplet interface and the size of the droplets. The latter is what makes scattering experiments distinctly different from reflection experiments from a planar interface (see Ref. [68] for a discussion of the differences). When droplets are in the size range of $\sim$ 100 nm they are large enough for the generated SF field to experience a different phase at different parts of the droplet surface. Thus, coherent addition of the generated SF photons on the droplet surface will lead to a non-vanishing SF signal that appears with a maximum scattering angle in a certain non-phase matched direction.

The molecular length scale is important as well. On the molecular length scale the local inversion symmetry determines whether an SF photon will be generated. An alkyl chain with an all-trans conformation and an even number of CH_2 groups has inversion symmetry centers between each inter-chain C-C bond. Selection rules dictate that there will be no SF photons emitted from the symmetric CH_2 stretch vibration (d^+ mode). In contrast, surface bound all-trans chains are terminated by ordered CH_3 groups, so that coherent addition of the SF electric field components will result in a strong signal at the frequency of the symmetric CH_3 stretch vibration (r^+ mode). A collection of all-trans alkyl chains will therefore have an amplitude ratio of the d^+ mode and r^+ mode close to 0. If chain defects are present in the alkyl chains the inversion symmetry centers are removed, and the intensity of the symmetric CH_2 stretch vibration will increase. Coherent addition of the SF electric field components of a collection of randomly oriented methyl groups will result in a weak symmetric CH_3 stretch

signal [66, 69, 70]. A collection of disordered alkyl chains will therefore have an amplitude ratio of the d^+ mode and r^+ mode that is large. The order in alkyl chains on a surface can therefore be represented by the d/r-ratio.

This d/r-ratio has been determined for n-hexadecane at the hexadecane/air interface (at room temperature, 24 °C) where d/r = 3.3 [71]. For SDS adsorbed on the water/CCl_4 interface in various amounts compared to the critical micelle concentration (cmc) the d/r-ratio ranges from d/r=1.5 for SDS concentrations of 0.1 mM SDS, down to d/r= 1 - 0.76, for SDS concentrations of 1 - 10 mM SDS [35]. The cmc of SDS is 8.1 mM at 298 K. For hexadecyltrimethylammonium bromide (CTAB) adsorbed on the n-hexadecane-d_{34}/ D_2O planar interface values are reported ranging from d/r = 1.6 for CTAB concentrations of 0.05 mM, down to d/r= 0.5, for CTAB concentrations of 0.6 mM. For CTAB adsorbed on the air/D_2O interface values are reported ranging from d/r = 1.75 for CTAB concentrations of 0.05 mM down to d/r = 0.8 for CTAB concentrations of 0.9 mM at 298 K [40]. The cmc of CTAB is 0.9 mM.

In the previous chapter, we have conducted SFS experiments on the oil droplet-water interface stabilized by SDS, in which we followed the change in surface density as a function of SDS concentration by monitoring the sulfate symmetric stretch scattered SF signal. For an emulsion series prepared with constant droplet concentration and size we found that the SF amplitudes change only by a factor of three when the total SDS concentration is varied from 50 μM to 10 mM. We concluded that the interfacial density of adsorbed SDS is at least one order of magnitude lower than the interfacial density at a corresponding planar interface.

In this chapter, we present SF scattering spectra on similar kinetically stabilized emulsions of sub-micron oil droplets in water. Because we measure vibrational resonances, selective deuteration can be used to measure the interfacial structure of the alkyl chains of the surfactant SDS molecules, the alkyl chain of the oil molecules, the weakly dispersive nonresonant response, and the interference between SDS and the oil. We have determined the SDS alkyl chain conformation and the oil chain conformation, for different concentrations of SDS and different oil chain lengths. We find a big difference in chain conformation. SDS has many chain defects, and the oil has very few. Interference experiments, and structure determination of SDS and oil as a function of oil chain length are also described. We explain our observations using time scale arguments.

5.2 SF scattering background

In an SF scattering experiment, mid-infrared (IR) and visible (VIS) pulsed laser beams are overlapped inside a cuvette containing dispersed particles in a liquid or solid matrix [72, 73]. At the droplet interface, a second-order nonlinear polarization is created which oscillates at the sum of IR and VIS frequencies. This polarization is small but does not vanish because there is a phase difference between the polarization generated on different parts of the droplet surface. Therefore, sum frequency (SF) photons can be emitted. Interference of the SF field

that is generated on different positions on the surface of the droplet generates a scattering pattern in the far-field. The scattering pattern depends on the droplet size [74–77] which for the size range used in this study has a broad maximum intensity at a scattering angle (θ) of $\theta \approx 60^\circ$ as measured from the direction of the sum of IR and VIS wave vectors.

The SF intensity contains surface structural information and is resonantly enhanced when the energy of the IR photons equals the energy of a vibrational transition. Using a broad band femtosecond IR pulse, multiple vibrational resonances within a frequency range of $\sim$ 150 cm^{-1} are excited and subsequently upconverted by a narrow band width VIS pulse. The resulting scattered spectrum represents the average vibrational spectrum of the interface of all droplets in the region where both laser pulses overlap.

In order to obtain the contribution of each vibrational mode, the spectra can be described with the following well-known expression, in complete analogy [67] with SFG experiments in reflection mode from planar interfaces [69]:

$$I_{SFS}(\omega,\theta) \propto \left| \sum_n \left(A_{NR} f(\omega,\theta) e^{i\Delta\phi} + \frac{A_n(\theta)}{(\omega - \omega_{0n}) + \mathrm{i}\Upsilon_\mathrm{n}} \right) \right|^2, \tag{5.1}$$

with A_{NR} the amplitude of a weakly dispersive background,
$f(\omega,\theta)$ the spectral shape of the weakly dispersive background,
n a vibrational mode with resonance (RES) frequency ω_{0n},
$A_n(\theta)$ the angle dependent amplitude,
Υ_n the half width at half maximum of vibrational mode n
$\Delta\phi$ the phase difference between the resonant and weakly dispersive background signal.
For the experiments described here, the spectral shape of the weakly dispersive background $f(\omega,\theta)$ can be measured by deuterating all components in the sample. For this case the SF signal will be proportional to $|f(\omega,\theta)|^2$.

5.3 Experimental details

5.3.1 Materials and emulsion preparation

The oil-in-water emulsions for the concentration dependent SFS measurements (Fig. 5.2) were made using the constant size approach. The stock emulsion was a 2 vol% hexadecane-in-D_2O 1 mM SDS. The other SFS measurements were done with emulsions prepared using the standard approach. See Chapter 2 for more details.

The Polytetrafluoroethylene (PTFE) dispersions were prepared as follows. 1 vol% PTFE particles in the form of powder were added to an aqueous solutions containing the desired surfactant. The powder does not disperse and floats on the solution. Dispersion of the particles was achieved by adding a 20 vol% of ethanol to the solution in a drop wise manner. As the ethanol was added the particles in the powder were readily dispersed. The dispersion was dried to remove the aqueous solution and ethanol and consequently added D_2O

to redisperse it again. We confirmed integrity of the particle by DLS measurements after the dispersion was made. The particles in the dispersions had a radius of 118 nm.

Polystyrene aqueous dispersions were purchased from Polysciences. The dispersion was dried to replace H_2O to D_2O containing the desired concentration of surfactant. The PS particle size was 262 nm.

5.3.2 SFS experiments

The SFS measurements were done with the emulsions placed in a CaF_2 cuvette with an optical path length of 200 μm. The SF scattering experiments were performed using IR pulses centered around $\sim$2900 cm^{-1} (8 - 12 μJ, 150 fs, FWHM bandwidth 120 cm^{-1}) spatially and temporally overlapped with 800 nm VIS pulses (8 - 15 μJ, FWHM bandwidth 5 - 13 cm^{-1}) in a cuvette containing the emulsion (see Chapter 2 for more details). The selectively polarized IR and VIS pulses were incident in the horizontal plane in respect to the optical table. The SF scattered light was measured in the same plane at a scattering angle of 60° with an acceptance angle of 20°. Fluctuations in laser power and stability were accounted for by measuring a reference sample between samples (see Fig. 3.5).

5.4 Results

5.4.1 Surfactant vs oil SF spectra

In order to compare the structure of the surfactant alkyl and oil alkyl chains we have made use of selective deuteration of the surfactant, the oil, or both. Fig. 5.1 shows SF scattering spectra of emulsions prepared with 8 mM h-SDS and d-C16 (top panel) or 8 mM d-SDS and h-C16 (middle panel) in D_2O. The left panels display polarization combination ssp and the right panels display polarization combination ppp. From top to bottom the graphs show the signal of the SDS alkyl chains (using perdeuterated hexadecane, d-C16), the signal of the hexadecane alkane chains (using deuterated SDS, d-SDS), and the 'non-resonant' or broadly dispersive background of the D_2O (using d-SDS and d-C16).

The spectra were fit using Eq. 5.1, whereby the polynomial fit to the measured response of the fully deuterated samples was used as $A_{NR}f(\omega,\theta)$. For both hexadecane and SDS, the resonant part is composed of the five well-known spectral features of the C-H stretch modes: The symmetric methylene stretch vibration (d^+, at 2855 cm^{-1}), the symmetric methyl stretch mode (r^+, at 2878 cm^{-1}), the Fermi resonance of the CH_3 bending mode overtone with the CH_3 stretch mode (r^{FR+}, at 2939 cm^{-1}) and the asymmetric methyl stretch mode (r^-, at 2959 cm^{-1}). These values correspond well with those reported for hexadecane at the air/hexadecane interface, the D_2O/CTAB/hexadecane interface [46] and SDS at the CCl_4/water interface [35, 71]. In these spectra there is also a clear peak at 2980 cm^{-1}, which is not present in the mentioned references.

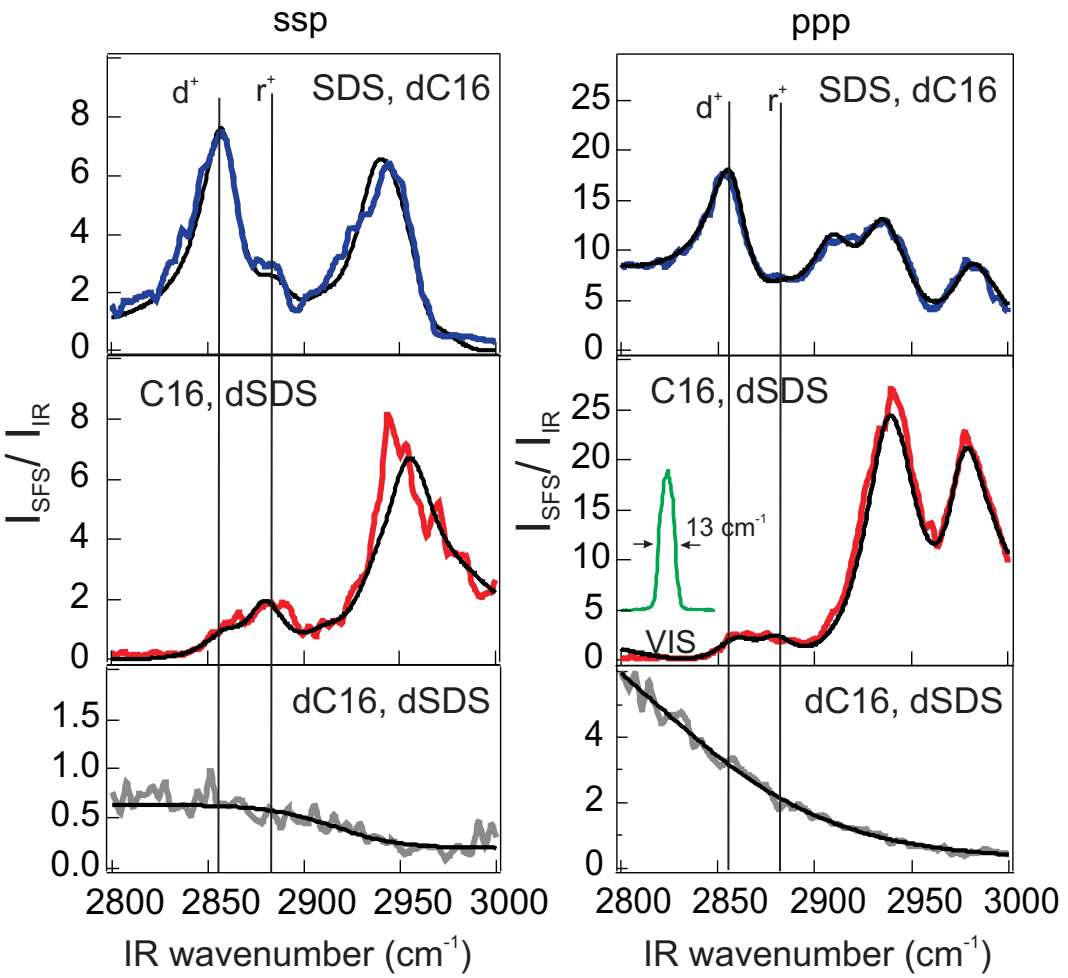

Figure 5.1: SF scattering spectra of the oil-in-water liquid/liquid interface of small droplets composed of 1 vol% n-hexadecane dispersed in D_2O and 8 mM SDS. Top: The h-SDS signal (using deuterated hexadecane). The droplets had an average radius of 103 nm. Middle: The h-C16 signal (using deuterated SDS). The droplets had an average radius of 103 nm. Bottom: the weakly dispersive non-resonant background, obtained using d-SDS and d-C16. The left (right) panel shows the ssp (ppp)-polarization. The black lines are fits as described in the text.

If we divide the vibrational response of the d^+ mode by that of the r^+ mode we get d/r ratios that can be used to quantify the order in the alkyl chains (i.e. a measure of the number of non-all-trans bonds). For n-hexadecane we obtained, by averaging over 11 data sets, a d/r-ratio of 0.88±0.42 and a phase difference $\Delta\phi$ between the weakly dispersive part and the resonance part of 0±10°. In contrast, the spectrum of h-SDS has a peak at the symmetric CH_3 stretch mode with lower relative intensity and the obtained d/r ratio is 4.3± 0.42 (determined by averaging over 8 data sets). The obtained best fit for the phase difference $\Delta\phi$ between the weakly dispersive part and the resonances was 113±10°. Both ppp and ssp data sets were fit with the same value of $\Delta\phi$, whereby we have used the weakly dispersive response that was measured for each polarization combination (displayed in the bottom part of Fig. 5.1).

5.4.2 The effect of surfactant concentration

To get more insight into the large mismatch in d/r ratios (4.3 for h-SDS vs 0.88 for h-C16) we have taken SF spectra for emulsions prepared with changing bulk concentrations of SDS, and followed the response of both the SDS (Fig. 5.2, left panel) and the oil (Fig. 5.2, right top panel). The left panel shows SFS spectra for different total concentrations of SDS, prepared with constant droplet density and total interfacial area. From 0.5 mM (0.06 × cmc) up to 8 mM (0.99 × cmc) the SF signal increases, which reflects an increase in SDS density at the interface. The change in intensity is a direct indication of a change in SDS interfacial density of a factor of ∼2.6. The oil spectra are shown in the top right panel and show no change in intensity or spectral shape if the SDS concentration is increased.

For the SDS spectra the d/r ratios were determined in the same way as described above, and varied from 4.2 up to 15 (from averaging over 5 data sets). The error bar at d/r = 15 indicates that the amplitude of the sym. CH_3 stretch mode has become so small that it is below the noise level. The d/r values for SDS are plotted in the bottom right panel of Fig. 5.2. The surface areas per SDS molecule on the x-axis are upper limit values determined from Chapter 4. Literature data for SDS on the D_2O/CCl_4 planar interface were taken from Ref. [37] and the values from the hexadecane/air interface were taken from Ref. [71].

5.4.3 Interference between the oil and the SDS SF response

In order to compare the signal strength of both the oil and the surfactant we have prepared emulsions with D_2O, hydrogenated oil (h-C16) and hydrogenated SDS (h-SDS) as constituents. Fig. 5.3 shows the ssp spectra for three different samples: d-C16 + h-SDS, h-C16 + d-SDS and h-C16 + h-SDS. It can be seen that the spectrum of the h-C16 + h-SDS sample has an extremely low intensity. This low intensity is caused by the interference of the electric field components of the CH stretch modes of the oil and surfactant molecules on the interface. The phase difference between the oil and surfactant field causes destructive in-

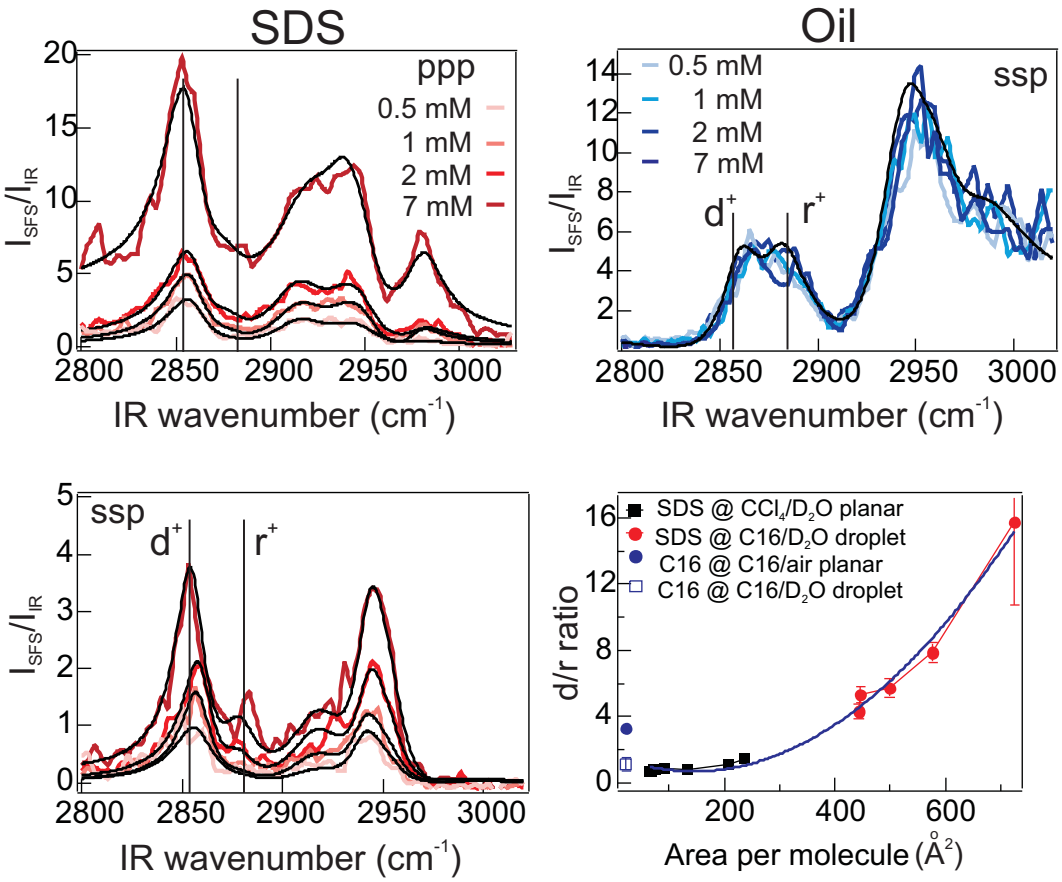

Figure 5.2: SF scattering spectra of the oil-in-water liquid/liquid interface of small droplets composed of 1 vol% n-hexadecane in D_2O and various amounts of SDS. Left panel: *ppp*-polarization (top) and *ssp*-polarization (bottom), for an emulsion made with SDS and fully deuterated oil, using 0.5, 1, 2 and 7 mM SDS (average radius=120 nm). Right panel, top: SF spectra in *ssp*-polarization for an emulsion made with deuterated SDS at the same concentrations and non-deuterated n-hexadecane (average radius 130 nm). The bottom right panel shows a summary of d/r order parameters (red points) measured on the oil/water droplet interface for SDS surfactant and hexadecane oil, plotted against the surface area per molecule that was determined from Chapter 4. The black points for the SDS at the D_2O/CCl_4 planar interface were taken from Ref. [37] and the hexadecane/air interface was taken from Ref. [71]. The solid line is a guide to the eye.

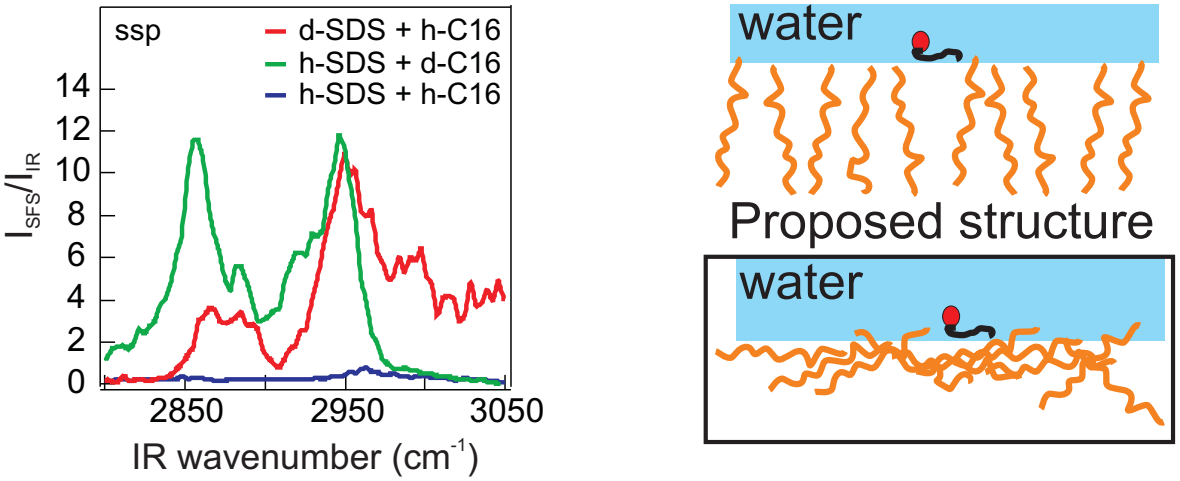

Figure 5.3: Left: Interference of SDS and C16. The green spectrum shows the *ssp* signal for droplets prepared with d-C16 oil and h-SDS. The red spectrum shows the *ssp* signal for droplets prepared with h-C16 oil and d-SDS. The blue spectrum shows the ssp signal for droplets prepared with h-C16 oil and h-SDS. Right: Illustration of possible surface scenarios. Top: The SF field of SDS molecule and oil molecules cancel each other. The majority of oil molecules determines the signal. This scenario does not explain the data. Bottom: The SF field of one SDS molecule has a comparable magnitude (but different phase), as the SF field generated by many oil molecules, resulting in near cancelation of the signal.

terference, which results in a nearly vanishing signal. Since the resultant field has almost vanished, the SF field from the SDS and the oil molecules is of nearly equal strength. The same result can be achieved starting from a surfactant free emulsion, prepared with D_2O and h-C16. Adding h-SDS to the emulsion reduces the signal to the level observed in Fig. 5.3.

5.4.4 The effect of oil alkyl chain length

In order to get more insight into the structure of the alkane layer and its interaction with the SDS at the interface, we have changed the oil alkane chain length and measured, again by selective deuteration, the response of both the SDS and the oil. The left panel of Fig. 5.4 displays the h-SDS alkyl chain conformation in both *ppp* and *ssp* polarization, measured with d-C12, and d-C16 oil. It can be seen that when the oil chain length is decreased from d-C16 to d-C12, the SDS SF spectra are almost identical.

For the case of reversed deuteration, the SF spectra for hexadecane (h-C16), dodecane (h-C12), and hexane (h-C6) droplets prepared with 8 mM d-SDS are plotted in the top left panel of Fig. 5.4. It can be seen that the signal changes dramatically at the high frequency side when the chain length is decreased. The relative intensity of the asym. CH_3 mode increases significantly. The intensity of the sym. CH_3 mode increases as well but this is less pronounced, as the r^+ and d^+ mode have a weak response in all h-alkane spectra. The bottom right panel displays the amplitude of the asym. CH_3 stretch mode, determined from spectral fitting.

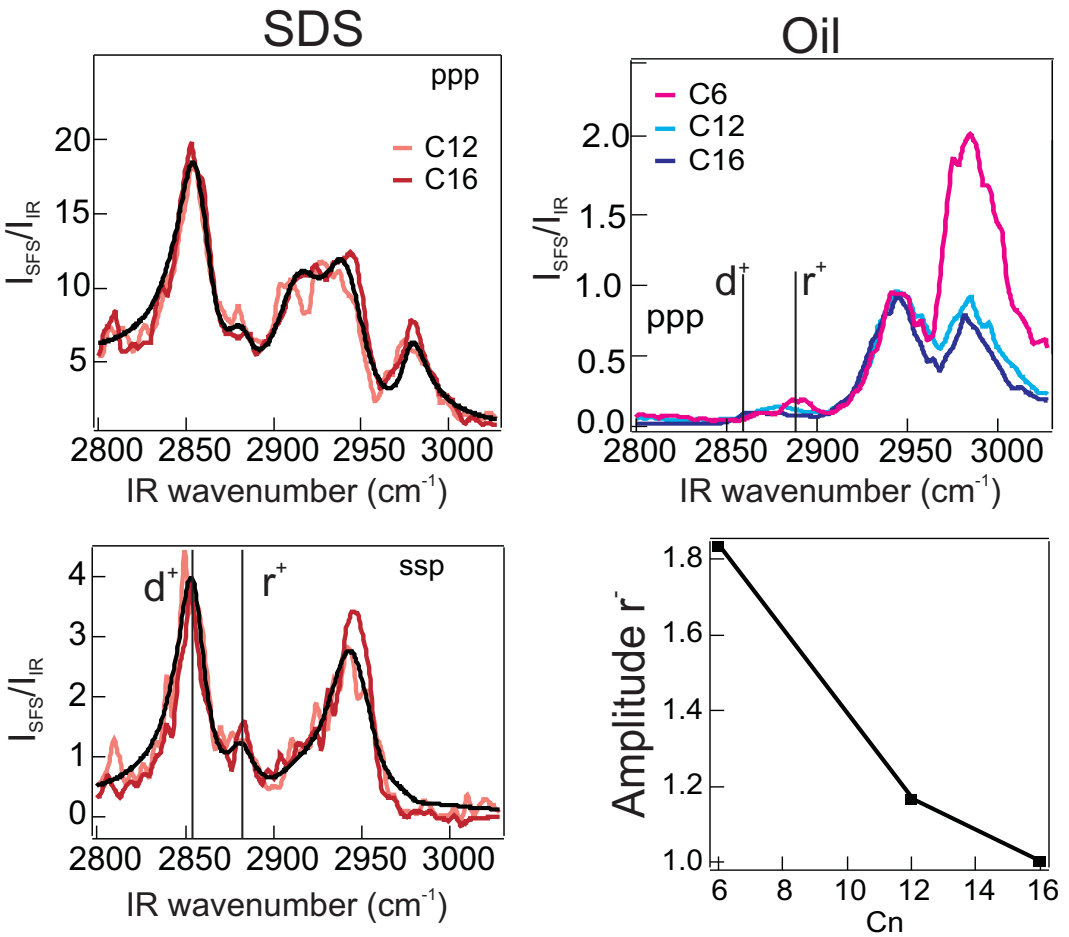

Figure 5.4: Left panel: SDS response as a function of oil chain length. SF scattering spectra of h-SDS on the oil-in-water liquid/liquid interface of droplets composed of either 1 vol % d-C16 in D_2O and 8 mM h-SDS (average radius=95 nm), or 1 vol% d-C12 in D_2O and 8 mM h-SDS (average radius=90 nm). Right panel top: Oil response as a function of oil chain length. SF spectra for emulsions composed of 1 vol% h-C16, h-C12, and h-C6 in D_2O prepared with 8 mM d-SDS. Right bottom panel: Amplitude of the asymmetric stretch mode for different alkane chain lengths.

5.5 Discussion

5.5.1 Interpretation of the data

Here, we will discuss the implications of the measurements done on the structure of the oil, the surfactants, and the interference measurements. We will describe our interpretation of the data, keeping the low surface densities measured in Chapter 4 in mind.

From the SF spectra in Fig. 5.1 we have seen that the chain order in the alkane chains of the hexadecane is large so that the alkane chains that generate our spectra posses only a few gauche defects. The d/r-ratio of 0.88 $\pm$ 0.42 is smaller than the value reported by Esenturk et al. (d/r=3.3, Ref [71]) for the hexadecane/air interface. This means that the hexadecane alkyl chains at the droplet oil/water interface are well ordered, and a bit more ordered than hexadecane at the hexadecane/vapor interface. In contrast, the SDS at the interface (at 8 mM) has a d/r ratio of 4.3 which is indicative of a high number of gauche defects, and a structure that is more disordered.

Clearly visible in the ppp spectra of SDS and C16, as well as in the ssp C16 spectrum is a peak at 2980 cm^{-1}, which has not been reported for either SDS on CCl_4/water or hexadecane/air interface. It is most likely due to the asymmetric stretch mode of the CH_3 groups. Further analysis on the exact assignment is needed, but it could be related to the interaction of CH_3 groups and water as suggested by Scheiner et al. [78].

Fig. 5.2 (left panel) shows that if we increase the concentration of SDS (while keeping the droplet size distribution constant) the spectral intensity increases, which is indicative of an increased surface density. The SDS interfacial density is increased by a factor of $\sim$2.6. This factor is in agreement with the data in Fig. 4.2. Fig. 5.2 (bottom right) shows the d/r values from our study plotted against the lower limit for the area per molecule as estimated earlier. The d/r values increase from 4.3 to 15, which means that the SDS becomes more disordered at lower concentrations, and thus higher available surface areas. This is a consistent observation: a larger molecular area scales with a larger amount of conformational freedom. The d/r values reported for SDS at the planar CCl_4-D_2O interface [37] are plotted in the same figure. One can observe a trend in the molecular area vs d/r ratio curves that holds for both data sets: a more densely packed surface will have a more ordered conformation. The fit through the data points is a guide to the eye.

The oil spectra in Fig. 5.2 (top right) show no change in intensity or spectral shape if the SDS concentration is increased. Thus, SDS does not strongly influence the interfacial oil SF response. This could be due to several effects:
(1) - The SDS with its low interfacial density perturbs only a tiny amount of the oil molecules. Therefore, the signal change that results from SDS/oil interaction is within the noise of the measurements.
(2) - The SF signal originates from the second oil layer and not from the first.
(3) - The SDS is not interacting strongly with the oil molecules.

The most likely of these three scenarios can be deduced by performing an SF scattering experiments on a sample prepared with hydrogenated SDS (h-SDS) and hydrogenated oil (h-C16). Since the SF field components of oil and SDS are out of phase, there will be destructive interference between the electric SF field components generated from the oil and the SDS. If the SDS is at a too low concentration to perturb the oil signal (irrespective of orientation) or if we are measuring SF photons from the second oil layer only, the h-SDS + h-C16 spectrum will not be significantly different from the d-SDS + h-C16 spectrum. If, on the other hand, there is enough SDS on the surface to generate a signal comparable to the oil signal the h-SDS + h-C16 spectrum will be much lower in intensity than the d-SDS+h-C16 spectrum. Fig. 5.3 shows that the h-SDS + h-C16 spectrum is much lower in intensity than the d-SDS+h-C16 spectrum. This indicates that there is enough SDS on the surface to interact with the oil. If the SDS would perturb the oil structure we would have to see a change in the oil spectra in the top right panel of Fig. 5.2.

The question that now arises is: How can such a low density of surfactant have such a large effect in the interference experiment? On the oil/water surface the projected surface area of an alkane molecule perpendicular to the interface is $\sim$22 Å^2. A parallel oriented molecule would have a larger projected area (up to $\sim$80 Å^2). Thus, depending on the orientation, there are between 7-20 hexadecane molecules per SDS molecule on the droplet surface. The signal of one SDS molecule can compete with the signal of 7-20 oil molecules if there is a difference in orientation. Since the SF intensity is proportional to $N_s^2 < \cos\phi >^2$, (with N_s the interfacial density, ϕ the angle between the C-C backbone and the surface normal, and $<>$ the orientational average) [68], we need only a factor of $< \cos\phi >\sim$0.05-0.2 to explain the difference in signal. This can easily be achieved if the average orientational distribution of the oil would be such that the oil orients with an angle of $\sim$78-85° with respect to the surface normal.

In contrast to an oil molecule oriented perpendicular to the interface, a parallel oriented oil molecule would display a change in the methyl mode stretch intensity if the alkane chain length is varied (because the number of surface CH_3 groups changes). The result of changing the oil chain length on the oil SF signal can be seen in Fig. 5.4. It shows that the spectral shape is preserved, with the most pronounced difference in the amplitude of the asym. CH_3 stretch mode. If the chain length is reduced from C16 to C6, the relative amplitude increases from 1 to 1.9. This would happen only if the oil molecules are oriented away from the surface normal.

5.5.2 The structure of the SDS stabilized oil/water interface

Considering all the experimental data, we arrive at a surface structure where the oil molecules are on average oriented nearly parallel to the surface plane. It is difficult to estimate the exact average orientation, but the observation of a change in the amplitude of the asym. CH_3 stretch mode is in agreement with a structure with oil molecules that are preferentially

lying flat on the surface. The small d/r ratio indicates that they have a small number of chain defects. The blue shift observed in the asymmetric CH_3 stretch mode indicates that at least a portion of the CH_3 groups of the oil are in contact with the water. X-ray diffraction studies have shown that surface freezing is absent on the alkane/water interface [9], while it occurs on the alkane/air interface [31, 53]. This could be due to parallel oriented oil when it is in contact with water. Furthermore, theoretical simulations of the neat oil/water interface predict a parallel oriented oil [79].

The SDS molecules have a low surface density and a large number of gauche defects. The sulfate head group consists of four O atoms that can act as hydrogen bond acceptors. Since hydrogen bonds are energetically more favorable than the van der Waals interactions between alkyl chains, it is likely that the head group is fully surrounded by water molecules and therefore adopts an orientation with its symmetry axis lined up on average with the surface normal. The oil is hydrophobic and non-polar and it is therefore reasonable to assume that there will be some distance between the O atom in the sequence S-O-C and the surface. The CH_2-CH_2 bond that follows will therefore be reasonably perpendicular. For the remainder of the SDS alkyl tail to be in contact with the oil, at least two chain defects are needed to bend the alkyl tail towards the surface. The blue shift observed in the asymmetric CH_3 stretch mode indicates that at least a portion of the CH_3 groups of the SDS are in contact with the water.

Summarizing our discussion, the SF data is consistent with a parallel oriented oil. SDS resides mainly on the water side, with its sulfate group interacting with water molecules. The alkyl tail can lie parallel on top of the oil only if it has chain defects. In such a structure the CH_3 groups are partially exposed to water, which result in a blue shift of the asymmetric stretch mode. The bottom right panel of Fig. 5.3 shows an illustration of this scenario. SDS molecules in such a conformation can have projected surface areas of a few squared nanometers, if they are allowed to be free to rotate around the direction of the surface normal. This matches with our finding that the *smallest* projected area per SDS molecule at the cmc was 4.25 nm^2.

5.5.3 Non-mixing of surfactant chains with oil chains

To further test the hypothesis of noninteracting oil and surfactant, we performed the SFS experiments using a fluorocarbon polymer and polystyrene as substrate instead of oil. By such a chemical modification it is possible to ensure that no mixing occurs between the alkyl chains of the surfactant and the moieties of the polymer. Thus, they are ideal candidates to tweak interactions of the surfactants with the oil phase. Here, we used polytetrafluoroethylene (PTFE) and polystyrene (PS) particles dispersed in D_2O. The structure of PS and PTFE are depicted in Fig. 5.5. Neither PTFE nor PS has a structure that is chemically comparable to C16.

Fig. 5.5 shows SFS spectra of SDS adsorbed at different interfaces. The spectra shown

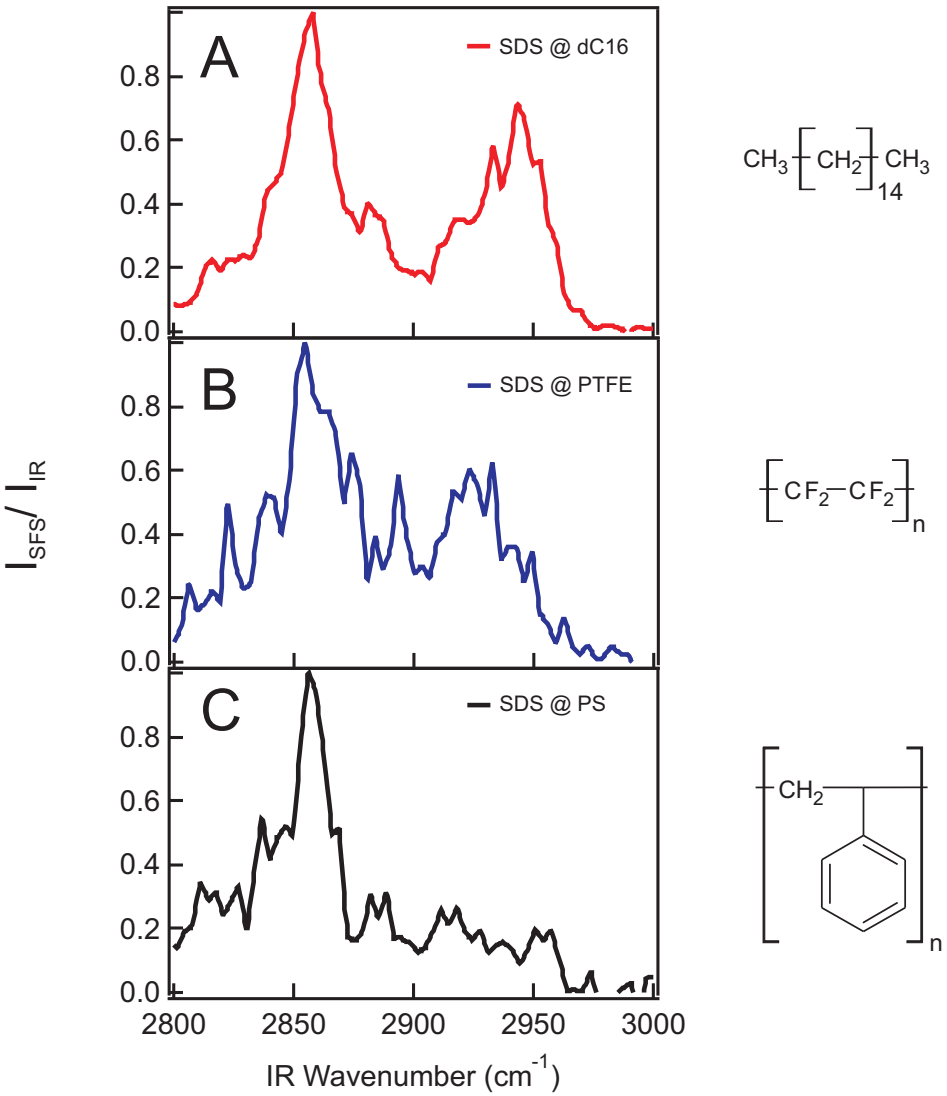

Figure 5.5: SF scattering spectra SDS adsorbed at different interfaces. A) d-C16-D_2O liquid-liquid interface of droplets composed of 1 vol% d-C16 dispersed in D_2O. B) PTFE-D_2O interface. C) PS-D_2O interface. The polarization combination was *ssp*.

were taken in ssp polarization combination and normalized by the symmetric methylene stretch resonance. In Fig. 5.5.A we also show the spectrum of SDS at the d-C16-D_2O interface for comparisson. Fig. 5.5.B shows the spectrum of SDS adsorbed at the PTFE-D_2O interface. PTFE does not have vibrational resonances in this spectral region. Therefore the resonances observed are only from SDS. Fig. 5.5.C shows the spectrum of SDS adsorbed at the PS-D_2O interface. Although PS has also methylene groups, their intensity is generally much lower than the resonances of adsorbates [80, 81]. This is probably due to a random distribution of the methylene groups at the interface and/or a transition dipole moment parallel to the interface. In fact, the neat interface shows signal levels comparable to the noise level (not shown). Addition of SDS considerably increases the signal therefore indicating that the resonances are due to the surfactant.

The symmetric modes d^+ and r^+ shows similar relative intensity regardless of the chemical structure of the interface. This means that SDS conformation at these interfaces is very disordered and probably have low interfacial densities. The observation of similar conformation corroborates the interpretation of a weak interaction of SDS and hexadecane.

5.5.4 Comparison to planar oil/water systems and microemulsions

The number of experiments done on planar oil/surfactant/water systems and microemulsions is enormous (see e.g. [5–22, 30–48]) and it is beyond the scope of our current work to treat them all here. There are however a few important differences between the experiments described here and measurements on planar systems and microemulsions:

(i) Microemulsions are thermodynamically stable, but microscopically kinetically unstable mixtures of oil, water, surfactant(s), and/or salt. Kinetic instability here refers to the possibility that the droplet interfaces can merge so that new droplets can be formed, and exchange of contents between droplets is possible [82]. Typically the interfacial tension is ultralow and the droplets are small with diameters usually below 30 nm. The mixture can be characterized as a point in a phase diagram, and by changing the composition different mixtures and phases can be prepared. Microemulsions cannot be prepared with oil, water and a single chained surfactant such as SDS [83], but need the presence of a co-surfactant, or a salt, or both, in order to be thermodynamically stable. A microemulsion can be considered as a solution of solubilized water or solubilized oil. An alternative name that has been suggested is 'swollen micelles' [84]. In contrast, the emulsions studied here are true emulsions: they are kinetically stable (i.e. no exchange is possible between the contents of the droplets on the time scale of the experiments), but thermodynamically metastable and consist of oil droplets surrounded by water.

(ii) Experiments on planar systems are often done on the air-water surface, which has been covered with surfactant. This layer is subsequently wetted by oil molecules. This gives a clear picture of solubilization of alkanes in surfactant layers (and it would be a comparable system to study the interactions in microemulsions). In our system, however, we have a pristine wa-

ter/oil interface that interacts with surfactant. Such a neat interface can only with difficulty be prepared in a planar geometry (see e.g. [9, 40]). In comparison, our sample contain several 100 cm^2 of interfacial area that is prepared in solution (without being exposed to air).
(iii) A planar oil/surfactant/water interface cannot spontaneously emulsify. It is therefore not necessarily comparable to the alkane/surfactant/water interfaces that we measure in our experiments, which is a kinetically stable, but ultimately thermodynamically metatable state.
(iv) Most surface specific measurements have not been performed with SDS, but with trimethylammonium (TA) salts (C_nTAB) [25, 38, 43]. Besides being of opposite charge, there is a distinct difference in the chemical structure of the head groups: the sulfate head group consist of oxygens that can hydrogen bond with the water, whereas the TA head group cannot form strong hydrogen bonds through the C-H groups. The interaction energy with water is therefore much larger for SDS (whereby electrostatic interaction and hydrogen bonding plays a role) than for C_nTAB (whereby electrostatic interaction will be the dominant driving force).
(v) Droplets experience Brownian motion and rotation while a planar surface is static.

5.5.5 Explanation of low surface coverage and structure

We can offer a tentative explanation for the low density and structure of the interfacial layer by considering the time scales involved for making a surface and for the refreshment of the surface layer. The timescale needed to form a planar/static surface layer can be estimated from dynamic surface tension measurements. In a dynamic surface tension measurement, the surface tension is measured as a function of time by e.g. analysis of the droplet shape of a newly formed hanging droplet. Dynamic surface tension measurements of aqueous SDS solutions against hexane show that the thermodynamic surface equilibrium state is reached in a time scale of seconds [6, 24, 25]. For a hanging droplet (with a size of a few mm) of an aqueous solution of 0.5 mM SDS that is newly formed in hexane the hexane/water surface tension is reduced from its initial value of 51.1 mN/m to 48 mN/m in 0.01 s, to 38 mN/m in 0.1 s and to its lowest value of 24 mN/m in a time scale of a few seconds. From this measurement we can conclude that the formation of a (static) surface that is in thermodynamic equilibrium takes a few seconds.

The oil droplet interfaces in our emulsions undergo continuous changes due to droplet rotation and translation. The timescale on which the interface refreshes can be estimated from the diffusion timescale. From our DLS autocorrelation traces, we can deduce that on average the oil droplets have a mean square displacement of 200 nm in a timescale of 100 ms. In general (from Stoke-Einstein equation), a 100 nm droplet makes a complete rotation in 260 ms. Taking these numbers, on average it takes the droplet 0.72 ms to make a rotation of one degree, which corresponds to translation over a surface distance of 17 Å.

This crude estimate of timescales shows that the timescale needed to reach an interfacial

equilibrium state is longer than the timescale at which the surface is changing. It is therefore feasible that the interfacial layer cannot reach a thermodynamic equilibrium state. The equilibration of the surface structure is therefore not reached, and the surface structure is stuck at a state that is, under the non-equilibrium conditions, energetically and entropically the most favorable one.

Interestingly, Ichikawa et al have shown that [85] application of a 10 kHz +20 V/-20 V square wave to a dense oil-in-water emulsion does not accelerate demulsification whereas application of a 20 V/0 V square wave of the same frequency shortens the demulsification time from hours to only 1 min. The phenomenon was explained by the migration of (surface) charges that happens on the same time scale as the on/off switching of the kHz block pulse. This behavior is completely in line with our observations, as it implies that a surface charge reorganization happens on a timescale (0.1 ms) that is shorter than what is needed for the formation of an interfacial layer in thermodynamic equilibrium.

5.6 Conclusions

In conclusion, the oil/water interface in a kinetically stabilized emulsion does not display the kind of structure that would be expected. The classical picture of emulsion stabilization requires that a large amount of surfactant is needed to stabilize emulsions, and that below the critical micelle concentration a charged surfactant forms an oriented monomolecular layer at the interface of the oil droplet in water, with the apolar tails interdigitated in the oil phase and the polar head group mixed with the water phase.

Vibrational SF scattering spectra contain information about the molecular structure of the nanoscopic oil droplet-water interface. Because vibrational resonances are measured, selective deuteration can be used to measure either the interfacial structure of the alkyl chains of the surfactant SDS molecules or the alkyl chain of the oil molecules. We have determined the SDS alkyl chain conformation and the oil chain conformation, for different concentrations of SDS and different oil chain lengths. We find a big difference in chain conformation. SDS has many chain defects, while the oil has very few. Interference experiments, and structure determination of SDS and oil as a function of oil chain length are also described.

All data can be explained by a surface structure in which the oil is predominantly oriented parallel with respect to the interface. The SDS head group is surrounded by water molecules, and the alkyl tail needs a few chain defects in order to be in contact with the oil. Such a conformation of surfactant requires a surface area of several hundreds of squared Angstroms. We can explain our observations by considering the interaction between oil and water and surfactant, whereby we take into account the timescales of Brownian motion and droplet rotation and compare it to the timescale on which an interface reaches its equilibrium state. Since the time scale needed to equilibrate a surface layer is longer than the timescale on which the interfacial structure changes (due to Brownian motion and droplet rotation) the

surface state of the droplets cannot reach the same equilibrium as the planar interface. The interface will therefore have a low density of surfactant.

Bibliography

[1] A. W. Adamson and A. P. Gast. *Physical chemistry of surfaces*. Wiley-interscience, 1997.

[2] I Langmuir. The constitution and fundamental properties of solids and liquids. II. Liquids. *J. Am. Chem. Soc.*, 39:1848–1906, 1917.

[3] W Harkins, F Brown, and E Davies. The structure of the surfaces of liquids, and solubility as related to the work done by the attraction of two liquid surfaces as they approach each other. (Surface tension V). *J. Am. Chem. Soc.*, 39:354–364, 1917.

[4] E Fischer and W Harkins. Monomolecular films. the liquid-liquid interface and the stability of emulsions. *J. Phys. Chem.*, 36(1):98–110, 1932.

[5] C D Bain. Studies of adsorption at interfaces by optical techniques: ellipsometry, second harmonic generation and sum-frequency generation. *Curr. Opin. Colloid Interface Sci.*, 3(3):287–292, 1998.

[6] J Eastoe, A Rankin, R Wat, and C Bain. Surfactant adsorption dynamics. *Int. Rev. Phys. Chem.*, 20(3):357–386, 2001.

[7] M. L. Schlossman and A. M. Tikhonov. Molecular ordering and phase behavior of surfactants at water-oil interfaces as probed by x-ray surface scattering. *Annu. Rev. Phys. Chem.*, 59(1):153–177, 2008.

[8] A Tikhonov, D Mitrinovic, M Li, Z Huang, and M Schlossman. An x-ray reflectivity study of the water-docosane interface. *J. Phys. Chem. B*, 104(27):6336–6339, 2000.

[9] M Schlossman. Liquid-liquid interfaces: studied by x-ray and neutron scattering. *Curr. Opin. Colloid Interface Sci.*, 7(3-4):235, 2002.

[10] E Sloutskin, X. Z. Wu, T. B. Peterson, O. Gang, B. M. Ocko, E. B. Sirota, and M. Deutsch. Surface freezing in binary mixtures of chain molecules. I. Alkane mixtures. *Phys. Rev. E*, 68(3):031605, 2003.

[11] E Sloutskin, Z. Sapir, C. D. Bain, Q. Lei, K. M. Wilkinson, L. Tamam, M. Deutsch, and B. M. Ocko. Wetting, mixing, and phase transitions in langmuir-gibbs films. *Phys. Rev. Lett.*, 99(13):136102, 2007.

[12] K Kashimoto, J Yoon, B Hou, C Chen, B Lin, M Aratono, T Takiue, and M Schlossman. Structure and depletion at fluorocarbon and hydrocarbon/water liquid/liquid interfaces. *Phys. Rev. Lett.*, 101(7):076102, 2008.

[13] M Mezger, F Sedlmeier, D Horinek, H Reichert, D Pontoni, and H Dosch. On the origin of the hydrophobic water gap: An X-ray reflectivity and MD simulation study. *J. Am. Chem. Soc.*, 132(19):6735–41, 2010.

[14] B Cabane, R Duplessix, and T Zemb. High-resolution neutron-scattering on ionic surfactant micelles: SDS in water. *J. Phys.*, 46(12):2161–2178, 1985.

[15] S Chen. Small-angle neutron-scattering studies of the structure and interaction in micellar and microemulsion systems. *Annu. Rev. Phys. Chem.*, 37:351–399, 1986.

[16] J LU, I PURCELL, E LEE, E SIMISTER, R THOMAS, and A RENNIE. The composition and structure of sodium dodecyl-sulfate dodecanol mixtures adsorbed at the air-water-interface - a neutron reflection study. *Journal of colloid and interface science*, 174(2):441–455, 1995.

[17] J Eastoe, K Hetherington, D Sharpe, J Dong, R Heenan, and D Steytler. Mixing of alkanes with surfactant monolayers in microemulsions. *Langmuir*, 12(16):3876–3880, 1996.

[18] J Hines, R Thomas, P Garrett, G Rennie, and J Penfold. A study of the interactions in a ternary surfactant system in micelles and adsorbed layers. *J. Phys. Chem. B*, 102(48):9708–9713, 1998.

[19] E. Staples, J. Penfold, and I. Tucker. Adsorption of mixed surfactants at the oil-water interface. *J. Phys. Chem. B*, 104(3):606, 2000.

[20] R Thomas. Neutron reflection from liquid interfaces. *Annu. Rev. Phys. Chem.*, 55:391–426, 2004.

[21] P Reynolds, M Henderson, and J White. A small angle neutron scattering study of the interface between solids and oil-continuous emulsions and oil-based microemulsions. *Colloids Surf. A*, 232(1):55–65, 2004.

[22] A Zarbakhsh, J Webster, and J Eames. Structural studies of surfactants at the oil-water interface by neutron reflectometery. *Langmuir*, 25(7):3953, 2009.

[23] R. Aveyard, B. P. Binks, P. Cooper, and P. D. I. Fletcher. Incorporation of hydrocarbons into surfactant monolayers. *Adv. Colloid Interface Sci.*, 33(2-4):59–77, 1990.

[24] V Fainerman. Adsorption-kinetics from concentrated micellar solutions of ionic surfactants at the water air interface. *Colloids Surf.*, 62(4):333–347, 1992.

[25] A Javadi, N Mucic, D Vollhardt, V Fainerman, and R Miller. Effects of dodecanol on the adsorption kinetics of SDS at the water-hexane interface. *J. Colloid Interface Sci.*, 351(2):537–541, 2010.

[26] A Bonfillon and D Langevin. Viscoelasticity of monolayers at oil-water interfaces. *Langmuir*, 9(8):2172–2177, 1993.

[27] D Langevin. Influence of interfacial rheology on foam and emulsion properties. *Adv. Colloid Interface Sci.*, 88(1-2):209–222, 2000.

[28] J. N. Wilking and T. G. Mason. Irreversible shear-induced vitrification of droplets into elastic nanoemulsions by extreme rupturing. *Phys. Rev. E*, 75(4):041407, 2007.

[29] D Georgieva, V Schmitt, F Leal-Calderon, and D Langevin. On the possible role of surface elasticity in emulsion stability. *Langmuir*, 25(10):5565–5573, 2009.

[30] J Conboy, J Daschbach, and G Richmond. Studies of alkane water interfaces by total internal-reflection 2nd-harmonic generation. *J. Phys. Chem.*, 98(39):9688, 1994.

[31] Q Lei and C Bain. Surfactant-induced surface freezing at the alkane-water interface. *Phys. Rev. Lett.*, 92(17):176103, 2004.

[32] J Day and C Bain. Ellipsometric study of depletion at oil-water interfaces. *Phys. Rev. E*, 76(4):041601, 2007.

[33] H Matsubara, E Ohtomi, M Aratono, and C Bain. Wetting and freezing of hexadecane on an aqueous surfactant solution: Triple point in a 2-D film. *J. Phys. Chem. B*, 112(37):11664–11668, 2008.

[34] R Ward, D Duffy, P Davies, and C Bain. Sum-frequency spectroscopy of surfactants adsorbed at a flat hydrophobic surface. *J. Phys. Chem.*, 98(34):8536–8542, 1994.

[35] M Messmer, J Conboy, and G Richmond. Observation of molecular ordering at the liquid-liquid interface by resonant sum-frequency generation. *J. Am. Chem. Soc.*, 117(30):8039, 1995.

[36] J. C. Conboy, M. C. Messmer, and G. L. Richmond. Investigation of surfactant conformation and order at the liquid-liquid interface by total internal reflection sum-frequency vibrational spectroscopy. *J. Phys. Chem.*, 100(18):7617–7622, 1996.

[37] J Conboy, M Messmer, and G Richmond. Effect of alkyl chain length on the conformation and order of simple ionic surfactants adsorbed at the D_2O/CCl_4 interface as studied by sum-frequency vibrational spectroscopy. *Langmuir*, 14(23):6722, 1998.

[38] B Casson and D Colin. Phase transitions in mixed monolayers of sodium dodecyl sulfate and dodecanol at the air/water interface. *J. Phys. Chem. B*, 102(38):7434–7441, 1998.

[39] L. F. Scatena and G. L. Richmond. Orientation, hydrogen bonding, and penetration of water at the organic/water interface. *J. Phys. Chem. B*, 105(45):11240, 2001.

[40] M. M. Knock, G. R. Bell, E. K. Hill, H. J. Turner, and C. D. Bain. Sum-frequency spectroscopy of surfactant monolayers at the oil-water interface. *J. Phys. Chem. B*, 107(39):10801–10814, 2003.

[41] M Brown, D Walker, E Raymond, and G Richmond. Vibrational sum-frequency spectroscopy of akane/water interfaces: Experiment and theoretical simulation. *J. Phys. Chem. B*, 107(1):237–244, 2003.

[42] D Hore, D Beaman, and G Richmond. Surfactant headgroup orientation at the air/water interface. *J. Am. Chem. Soc.*, 127(26):9356, 2005.

[43] C Johnson and E Tyrode. Study of the adsorption of sodium dodecyl sulfate (SDS) at the air/water interface: targeting the sulfate headgroup using vibrational sum frequency spectroscopy. *Phys. Chem. Chem. Phys.*, 7(13):2635, 2005.

[44] D Walker and G Richmond. Depth profiling of water molecules at the liquid-liquid interface using a combined surface vibrational spectroscopy and molecular dynamics approach. *J. Am. Chem. Soc.*, 129(30):9446–9451, 2007.

[45] F Moore and G Richmond. Integration or segregation: How do molecules behave at oil/water interfaces? *Acc. Chem. Res.*, 41(6):739, 2008.

[46] Katherine M. Wilkinson, Lei Qunfang, and Colin D. Bain. Freezing transitions in mixed surfactant/alkane monolayers at the air-solution interface. *Soft Matter*, 2:66–76, 2006.

[47] K Harper and H Allen. Competition between DPPC and SDS at the air-aqueous interface. *Langmuir*, 23:8925–8931, 2007.

[48] C McFearin and G Richmond. The role of interfacial molecular structure in the adsorption of ions at the liquid-liquid interface. *J. Phys. Chem. C*, 113(50):21162–21168, 2009.

[49] C Bain, P Davies, T Ong, R Ward, and M Brown. Quantitative-analysis of monolayer composition by sum-frequency vibrational spectroscopy. *Langmuir*, 7(8):1563–1566, 1991.

[50] G Bell, C Bain, and R Ward. Sum-frequency vibrational spectroscopy of soluble surfactants at the air/water interface. *J. Chem. Soc. Faraday Trans.*, 92(4):515–523, 1996.

[51] B Casson and C Bain. Phase transitions in mixed monolayers of cationic surfactants and dodecanol at the air water interface. *J. Phys. Chem. B*, 103(22):4678–4686, 1999.

[52] M Knock and C Bain. Effect of counterion on monolayers of hexadecyltrimethylammonium halides at the air-water interface. *Langmuir*, 16(6):2857–2865, 2000.

[53] X Wu, B Ocko, E Sirota, S Sinha, M Deutsch, and B Cao. Surface-tension measurements of surface freezing in liquid normal-alkanes. *Science*, 261(5124):1018–1021, 1993.

[54] T Mason, J Wilking, K Meleson, C Chang, and S Graves. Nanoemulsions: formation, structure, and physical properties. *J. Phys.: Condens. Matter*, 18(41):R635, 2006.

[55] D McClements. Critical review of techniques and methodologies for characterization of emulsion stability. *Crit. Rev. Food Sci. Nutr.*, 47:611–649, 2007.

[56] R Aveyard, B Binks, and J Clint. Emulsions stabilised solely by colloidal particles. *Adv. Colloid Interface Sci.*, 100:503–546, 2003.

[57] J Beattie and A Djerdjev. The pristine oil/water interface: Surfactant-free hydroxide-charged emulsions. *Angew. Chem., Int. Ed.*, 43(27):3568, 2004.

[58] M Leunissen, J Zwanikken, R van Roij, P Chaikin, and A van Blaaderen. Ion partitioning at the oil-water interface as a source of tunable electrostatic effects in emulsions with colloids. *Phys. Chem. Chem. Phys.*, 9(48):6405–6414, 2007.

[59] K Karraker and C Radke. Disjoining pressures, zeta potentials and surface tensions of aqueous non-ionic surfactant/electrolyte solutions: theory and comparison to experiment. *Adv. Colloid Interface Sci.*, 96(1-3):231–264, 2002.

[60] J Beattie, A Djerdjev, and G Warr. The surface of neat water is basic. *Faraday Discuss.*, 141:31, 2009.

[61] R. J. Hunter. *Foundations of Colloid Science*. Oxford, 2002.

[62] A Djerdjev and J Beattie. Electroacoustic and ultrasonic attenuation measurements of droplet size and zeta-potential of alkane-in-water emulsions: effects of oil solubility and composition. *Phys. Chem. Chem. Phys.*, 10(32):4843, 2008.

[63] P Creux, J Lachaise, A Graciaa, J Beattie, and A Djerdjev. Strong specific hydroxide ion binding at the pristine oil/water and air/water interfaces. *J. Phys. Chem. B*, 113(43):14146–14150, 2009.

[64] H. Wang, E. C. Y. Yan, E. Borguet, and K. B. Eisenthal. Second harmonic generation from the surface of centrosymmetric particles in bulk solution. *Chem. Phys. Lett.*, 259(1-2):15–20, 1996.

[65] K. B. Eisenthal. Second harmonic spectroscopy of aqueous nano- and microparticle interfaces. *Chem. Rev.*, 106(4):1462, 2006.

[66] S. Roke, W. G. Roeterdink, J. E.G. J.Wijnhoven, A. V. Petukhov, A. W. Kleyn, and M. Bonn. Vibrational sum frequency scattering from a submicron suspension. *Phys. Rev. Lett.*, 91:258302, 2003.

[67] S. Roke. Nonlinear optical spectroscopy of soft matter interfaces. *ChemPhysChem*, 10(9-10):1380–1388, 2009.

[68] A de Beer and S Roke. Obtaining molecular orientation from second harmonic and sum frequency scattering experiments in water: Angular distribution and polarization dependence. *J. Chem. Phys.*, 132(23):234702, 2010.

[69] P. Guyot-Sionnest, J. H. Hunt, and Y. R. Shen. Sum-frequency vibrational spectroscopy of a Langmuir film: Study of molecular-orientation of a two-dimensional system. *Phys. Rev. Lett.*, 59(14):1597, 1987.

[70] M Gurau, E Castellana, F Albertorio, S Kataoka, S Lim, and R Yang. Thermodynamics of phase transitions in langmuir monolayers observed by vibrational sum frequency spectroscopy. *J. Am. Chem. Soc.*, 125(37):11166–11167, 2003.

[71] O Esenturk and R A Walker. Surface vibrational structure at alkane liquid/vapor interfaces. *J. Chem. Phys.*, 125(17):174701, 2006.

[72] S Roke, J Buitenhuis, J van Miltenburg, M Bonn, and A van Blaaderen. Interface-solvent effects during colloidal phase transitions. *J. Phys.: Condens. Matter*, 17(45):S3469, 2005.

[73] A. G. F. de Beer, H. B. de Aguiar, J. F. W. Nijsen, A. B. Sugiharto, and S. Roke. Detection of buried microstructures by nonlinear light scattering spectroscopy. *Phys. Rev. Lett.*, 102(9):095502, 2009.

[74] S. Roke, M. Bonn, and A. V. Petukhov. Nonlinear optical scattering: The concept of effective susceptibility. *Phys. Rev. B*, 70:115106, 2004.

[75] J Dadap, H de Aguiar, and S Roke. Nonlinear light scattering from clusters and single particles. *J. Chem. Phys.*, 130(21):214710, 2009.

[76] S Jen, G Gonella, and H Dai. The effect of particle size in second harmonic generation from the surface of spherical colloidal particles. I: Experimental observations. *J. Phys. Chem. A*, 113(16):4758, 2009.

[77] S Jen, H Dai, and G Gonella. The effect of particle size in second harmonic generation from the surface of spherical colloidal particles. II: The nonlinear Rayleigh-Gans-Debye model. *J. Phys. Chem. C*, 114(10):4302, 2010.

[78] S Scheiner, S Grabowski, and T Kar. Influence of hybridization and substitution on the properties of the CH – O hydrogen bond. *J. Phys. Chem. A*, 105(46):10607, 2001.

[79] F Bresme, E Chacon, P Tarazona, and K Tay. Intrinsic structure of hydrophobic surfaces: The oil-water interface. *Phys. Rev. Lett.*, 101(5):056102, 2008.

[80] K Gautam, A Schwab, A Dhinojwala, D Zhang, S Dougal, and M Yeganeh. Molecular structure of polystyrene at air/polymer and solid/polymer interfaces. *Phys. Rev. Lett.*, 85(18):3854–3857, 2000.

[81] J Kim, A Opdahl, K Chou, and G Somorjai. Hydrophobic-interaction-induced alignment of polymers at the solid/liquid interface studied by infrared-visible sum frequency generation. *Langmuir*, 19(23):9551–9553, 2003.

[82] J. Eastoe. *Colloid Science, principles methods and applications*. Blackwell publishing, 2005.

[83] R Aveyard, B Binks, and J Mead. Interfacial-tension minima in oil-water surfactant systems: Effects of cosurfactant in systems containing sodium dodecyl-sulfate. *J. Chem. Soc. Faraday Trans. 1*, 83:2347–2357, 1987.

[84] S Friberg, L Mandell, and M Larsson. Mesomorphous phases, a factor of importance for properties of emulsions. *J. Colloid Interface Sci.*, 29(1):155–156, 1969.

[85] T Ichikawa, T Dohda, and Y Nakajima. Stability of oil-in-water emulsion with mobile surface charge. *Colloids Surf., A*, 279(1-3):128, 2006.

Chapter 6

Probing surface charges and surface potentials *via* SFS

This chapter is devoted to explore electrostatics aspects of the liquid-liquid interface and how can we probe by SFS. We show that the dispersive nonresonant background response due to the tail of the OD vibrational stretch is related to the strength of the surface potential. The surface charges are due to adsorption of the surfactant sodium dodecylsulphate (SDS) which is probed by the SO_3 stretch response of the headgroup. Since both the equilibrium adsorption of surfactants and the surface potential are sensitive to the ionic strength, one needs to probe these quantities independently. At surfactant concentrations at the critical micelle concentration (cmc), increasing the ionic strength decreases the surface potential, but the surface charge density stays constant. At 1.5 mM, the surface potential is insensitive to an increase in ionic strength, whereas the surface charge densities increases. The results are explained based solely on the Gouy-Chapman model and rationalized due to an interplay between charging of the interface and screening effects. Furthermore, the changes in surface potential are in qualitative agreement with ζ-potential measurements.

6.1 Introduction

Electrostatic interactions are widely recognized to play a role in colloidal and interfacial science. For instance, critical micelle concentration, protein stability, emulsions stability and surface tension all depend on a delicate balance of electrostatic and non-electrostatic interactions. These interactions are mainly determined by the molecular structure of the interface. Consequently, there is an increasingly interest in the characterization of interfacial properties of colloidal systems [1]. A particularly important quantity, which characterizes the strength of electrostatic interactions, is the surface potential due to adsorption of charged species at colloidal interfaces.

Emulsions are nonequilibrium thermodynamic systems. Nevertheless, they can be kinetically stable for days, months or even years. This kinetic stability can be explained by the Derjaguin-Landau-Verwey-Overbeek (DLVO) theory which combines attractive dispersive interactions (van der Waals) and repulsive electrostatic interactions [2]. The DLVO interaction potential gives the change in free energy ΔF_T as two spheres of radius R approach each other

$$\Delta F_T = 2\pi\epsilon_r\epsilon_0 R\phi_0^2 \exp(-\kappa_{DH}x) - \frac{A_{121}R}{12x} \tag{6.1}$$

where A_{121} is the Hamaker constant of media 1 dispersed in media 2, κ_{DH} is the inverse of the Debye-Hückel screening length, ϵ_0 is the vacuum permittivity and ϵ_r is the dielectric constant. A key parameter in the DLVO theory is the surface potential ϕ_0. To illustrate how sensitive the stability of the droplets is with respect to the (electrostatic) surface potential, we plot in Fig. 6.1 the free energy given by Eq. 6.1 as a function of interparticle distance for different values of surface potential. One can see that a change of only 20% in the surface potential decreases the barrier height of the interaction energy by more than a factor of 2.

At the interface of the droplets, there is an excess of charges due to the preferential adsorption of surfactants. The profile of the electrostatic potential due to these surface charges is schematically sketched in Fig. 6.2. For simplicity, we only plot the potential in one phase. The potential at the interface is the surface potential. Further into the solution, the potential is screened by the surrounding counter-ions and has a characteristic screening length given by $1/\kappa_{DH}$.

Surface potential cannot be directly measured in colloidal systems. However, it can be inferred from force vs. distance measurements. The surface potential is obtained by using Eq. 6.1 to fit the measured force vs. distance curve [1, 3]. The surface potential can also be inferred from a related potential called ζ-potential [4] (see Fig. 6.2). The ζ-potential (ϕ_ζ) is defined as the electrostatic potential measured at a distance from the particle surface where the fluid velocity attains the same value as the particle velocity. This distance where the ζ-potential is located is called the shear plane. Its distance is not known but generally evaluated on a case-by-case basis.

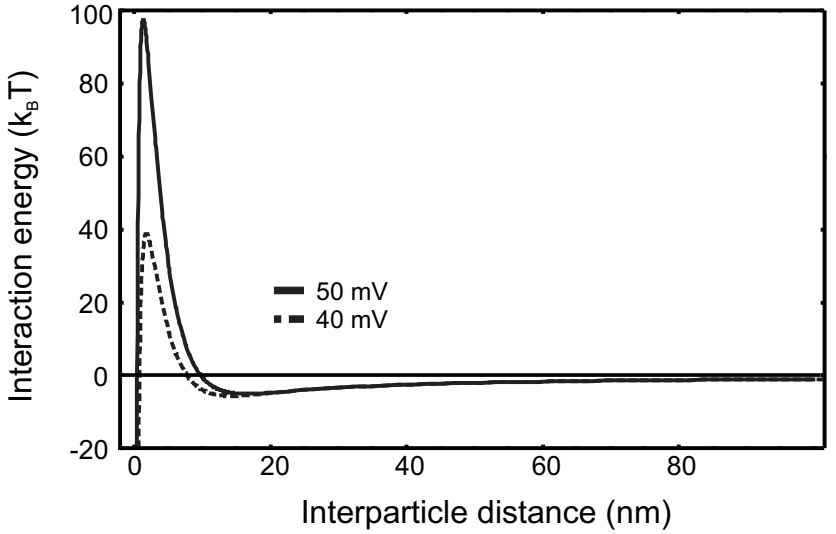

Figure 6.1: Free energy change of two hexadecane oil droplets (100 nm radius) in water for different surface potentials. The Debye-Hückel screening length is 3 nm. The Hamaker constant is 6×10^{-20} J.

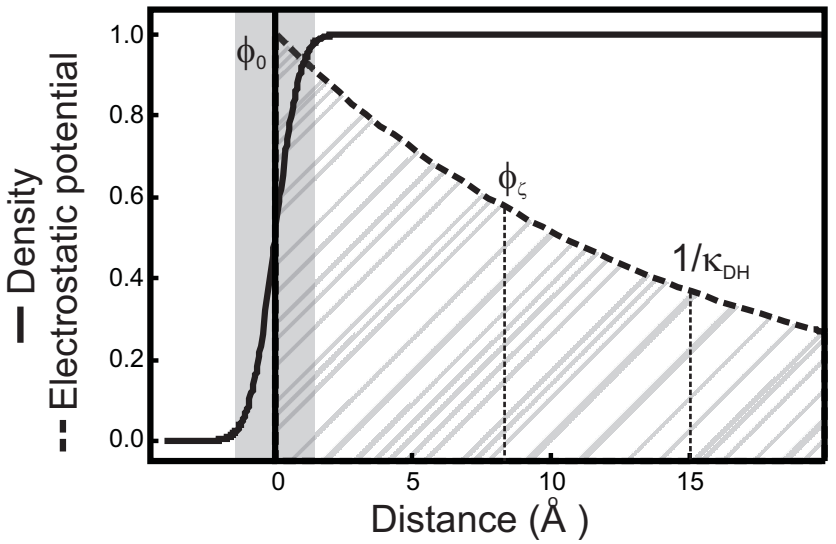

Figure 6.2: Sketch of the density (continuous line) and electrostatic potential (dashed line) profiles. $\chi^{(2)}$ processes generally occur within the shaded area, whereas $\chi^{(3)}$ processes occur within the hatched area.

In the early 90's, Eisenthal's group pioneered the use of Second-Harmonic Generation (SHG) to probe electrostatic properties of interfaces [5, 6]. The strong electrostatic field created by interfacial charges acts as a third input electric field of zero frequency. Together with the incoming electromagnetic fields from the laser, a third-order polarization can be induced. Since third order processes are symmetry-allowed in centrossymetric media, the measured signal can have a contribution from an interface specific signal ($\chi^{(2)}$) and a bulk signal ($\chi^{(3)}$). It was shown by SHG experiments on planar surfaces that the intensity is related to the electrostatic potential at the interface (surface potential). This technique is commonly referred to as the $\chi^{(3)}$-method.

After the observation of Second-Harmonic Generation from the surface of centrossymetric particles [7], the $\chi^{(3)}$-method was extended to probe colloidal systems [8]. However, SHG does not have specificity to discern if the contributions to the signal are either $\chi^{(2)}$ (surface) or $\chi^{(3)}$ (bulk). The reason is because the light generated at the second-harmonic is non-resonant, so both $\chi^{(3)}$ and $\chi^{(2)}$ cannot be distinguished. Conversely, Sum-Frequency Generation can probe selectively chemical moieties through their vibrational resonances, which allows one the separation of the bulk from the interfacial nonlinear response.

We show here that SFS is a unique technique capable of probing both surface potential and surface charge density, independently. We first introduce the so-called Eisenthal's $\chi^{(3)}$-method as a background together with the Gouy-Chapman model. In the second part, we show that the dispersive nonresonant background response (see Chapter 5) is a $\chi^{(3)}$ related signal, from which we can retrieve the surface potential. Surface charge density changes are probed by measuring the SO_3 stretch resonance of the SDS headgroup.

6.2 $\chi^{(3)}$-method background

In these experiments, in addition to a second order nonlinear polarization $\mathbf{P}^{(2)}$ excited at the interface, there is a third order nonlinear polarization $\mathbf{P}^{(3)}$ in the bulk which is excited by the incoming electromagnetic fields together with the electrostatic field (DC). The total nonlinear polarization can be written as

$$\begin{aligned} \mathbf{P}(\omega_0) &= \mathbf{P}^{(2)}(\omega_0) + \mathbf{P}^{(3)}(\omega_0) + \ldots, \\ \mathbf{P}^{(2)}(\omega_0 = \omega_1 + \omega_2) &= \chi^{(2)}\mathbf{E}_1(\omega_1)\mathbf{E}_2(\omega_2), \\ \mathbf{P}^{(3)}(\omega_0 = \omega_1 + \omega_2) &= \chi^{(3)}\mathbf{E}_1(\omega_1)\mathbf{E}_2(\omega_2)\mathbf{E}_{DC}(\omega_3 = 0), \end{aligned} \tag{6.2}$$

where $\mathbf{E}_n(\omega_n)$ are the pump electric field of frequency ω_n, $\mathbf{E}_{DC}(0)$ is the electrostatic field, $\chi^{(2)}$ is the second order susceptibility and $\chi^{(3)}$ is the third order susceptibility. Here, we only show the response of the polarization oscillating at the sum of the frequencies. As explained in Chapter 1, $\boldsymbol{\chi}^{(2)}$ is only nonvanishing at interfaces. Therefore, $\mathbf{P}^{(2)}$ is only excited at the interface where centrosymetry is broken. This region from where the $\chi^{(2)}$ is nonvanishing is schematically depicted by the shaded area in Fig. 6.2. It typically extends over few molecular

layers. The third order polarization in Eq. 6.2 has a spatial dependence: it decays to zero in the bulk solution. Integration of the third order polarization of Eq. 6.2 from the interface up to the bulk solution leads to

$$\int_0^\infty \chi^{(3)}\mathbf{E}_1(\omega_1)\mathbf{E}_2(\omega_2)\mathbf{E}_{DC}(0)dz = -\chi^{(3)}\mathbf{E}_1(\omega_1)\mathbf{E}_2(\omega_2)[\phi(\infty)-\phi(0)]$$
$$= \chi^{(3)}\mathbf{E}_1(\omega_1)\mathbf{E}_2(\omega_2)\phi_0, \tag{6.3}$$

where we use the relation $\mathbf{E}_{DC} = -\nabla\phi$, ϕ_0 is the (electrostatic) potential at the surface ($\phi(0)$) and $\phi(\infty)$ is the potential in the bulk solution, which is set to zero.

$\chi^{(3)}$ effects in scattering

The intensity measured at ω_0 is proportional to the strength of second and third oder effective particle susceptibility

$$I(\omega_0) \propto \left|\Gamma^{(2)}(\omega_0) + \Gamma^{(3)}(\omega_0)\right|^2. \tag{6.4}$$

$\Gamma^{(2)}$ is the effective interfacial response and the equations for a sphere are given in Chapter 1. $\Gamma^{(3)}$ is the effective response from the bulk and is given by [9]

$$\Gamma^{(3)}(\omega_0) = F_1(qR)\chi^{(3)}\phi_0. \tag{6.5}$$

The form factor function $F_1(qR)$ is given by Eq. 1.10. We can rewrite it in the form:

$$I(\omega_0) = \left|A(\omega_0) + B(\omega_0)\phi_0\right|^2. \tag{6.6}$$

Eq. 6.6 shows that there are two contributions to the signal at ω_0. The $B(\omega_0)$ term is a surface potential dependent response ($\Gamma^{(3)}$) and the A term a surface potential independent response ($\Gamma^{(2)}$).

Eq. 6.6 contains two variables: A and B. In order to see how the surface potential changes an easy adjustable parameter to tune its strength is the ionic strength of the solution. The Gouy-Chapman model relates the surface potential to the ionic strength. From the solution of the Poisson-Boltzmann equation, the surface potential ϕ_0, ion concentration c and surface density of charges σ_0 are related as [4]

$$\phi_0 = \frac{2k_B\,T}{e}\sinh^{-1}\left(\frac{\sigma_0}{11.74\sqrt{c}}\right), \tag{6.7}$$

where k_B is the Boltzmann Constant, T is temperature and e is the elementary charge. The monovalent ion concentration ionic strength is in mol l^{-1}, σ_0 is in $\mu\mathrm{C\,cm}^{-2}$ and ϕ_0 in V.

The Gouy-Chapman model is an analytical solution of the Poisson-Boltzmann equation for flat interfaces. For curved interfaces (spherical symmetry), the Poisson-Boltzmann Equation

does not have an analytical solution, but there is an approximation for small surface potentials (the so-called Debye-Hückel approximation). Nevertheless, the Gouy-Chapman model has been demonstrated to work well for spherical particles with screening lengths (κ_{DH}^{-1}) much smaller than the particle radius (R) [8].

Eq. 6.7 in combination with Eq. 6.6 gives

$$I = \left| A + B\frac{2k_B T}{e} \sinh^{-1}\left(\frac{\sigma_0}{11.74\sqrt{c}}\right)\right|^2 . \tag{6.8}$$

Eq. 6.8 shows that the response of the B term decreases as the ion concentration increases at a constant surface charge density. Frequently in SHG experiments, one assumes that the surface charge density is constant as the ionic strength changes. However, in the case of equilibrium adsorption of ionic species, the free energy of adsorption has an electrostatic contribution which depends on the ionic strength, thus changing the equilibrium between species adsorbed and in solution. Therefore, a change in ionic strength will unavoidably change the amount of (ionic) species adsorbed, which in turn change the surface potential. Since SHG can not selectively probe surface potential and surface charge densities independently, a change in ionic strength and the use of the Gouy-Chapman model can lead to erroneous conclusions.

6.3 Experimental details

Emulsions preparation

The emulsions were prepared using the constant size approach with a stock emulsion made out of 2 vol% perdeuterated hexadecane (dC16) in D_2O solution containing 1 mM dSDS. The droplets had a radius of 180 nm.

SFS experiments

The SFS measurements were done with the emulsions placed in a cuvette with optical path lengths of 200 μm and 100 μm for experiments in the CH and SO_3 stretches spectral regions, respectively. The experiments were performed using 10 μJ IR pulses centered either around 2900 cm^{-1} or 1100 cm^{-1} and 10 μJ VIS pulses. Fluctuations in laser power and stability were accounted for by measuring a reference sample between samples (see Chapter 2).

6.4 Results and discussion

6.4.1 ζ-potential measurements

In order to get a first idea of the qualitative behavior of the electrostatics in the vicinity of the interface, we performed ζ-potential measurements. Although the ζ-potential is not measured

at the same position as the surface potential, it gives a qualitative information on how the surface potential responds to different ionic strengths and surfactant concentrations.

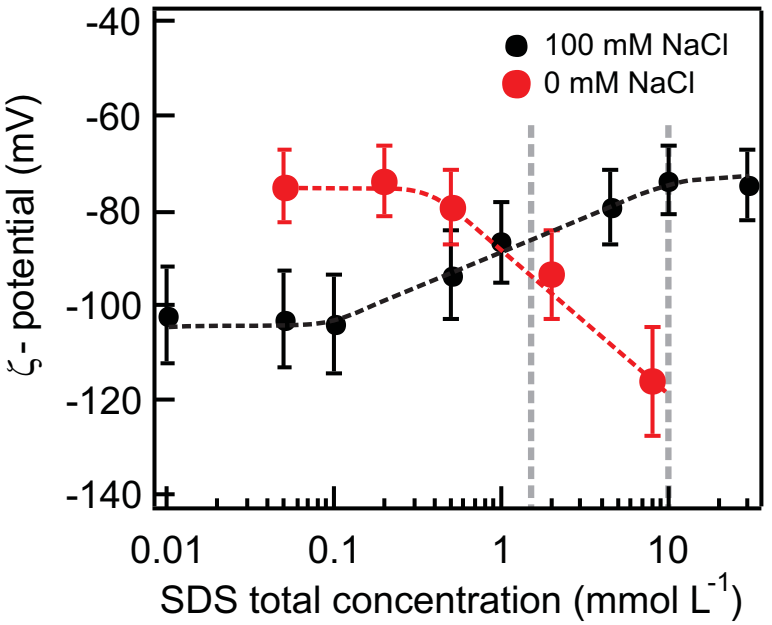

Figure 6.3: ζ-potential measurements as a function of SDS concentration for different NaCl concentration. The emulsion was 0.1 vol% C16-in-water. The vertical dashed grey lines depict concentrations where SFS experiments were performed. The dashed red and black lines are guides to the eye.

Fig. 6.3 shows the ζ-potential as a function of SDS concentration for two different NaCl concentration. The emulsion consisted of 0.1 vol% C16-in-water. At 0 mM NaCl, the modulus of the ζ-potential continuously increases (modulus) as a function of SDS concentration. The ζ-potential with no surfactant and no electrolyte added has the value of -60 mV. The most common explanation for this negative potential is assigned to a preferential adsorption of ions at the oil droplet-water interface [10–13]. The ζ-potential up to 0.5 mM SDS does not seem to change strongly. This can be rationalized if one considers competitive adsorption of both ions and SDS. As the SDS concentration increases, it replaces the adsorbed ions. Since both species carry negative charges, the ζ-potential does not change. Above 0.5 mM SDS, SDS has replaced most of the ions and continues to populate the interface. In fact, if one adds SDS to a surfactant-free emulsion the pH increases, because the SDS displaces the ions at the interface, which will therefore go into the solution [11]. At 100 mM NaCl, the ζ-potential stays at -105 mV up to SDS concentrations around 0.2 mM. As the concentration increases, the ζ-potential modulus decreases until it levels off at ∼-80 mV for 10 mM SDS concentration.

The ζ-potential measurements indicate that there is a complex interplay between surface charge density and ionic strength. We highlight two features from Fig. 6.3. Firstly, at 1-2 mM SDS concentration, the ζ-potential at 0 and 100 mM NaCl is the same. This indicates that

the surface potential is constant at this SDS concentration. Secondly, at 10 mM SDS concentration the ζ-potential modulus decreases as the NaCl concentration increases. We therefore performed SFS experiments at these two SDS concentrations: 1.5 mM, at which the surface potential is constant, and 10 mM around the cmc.

6.4.2 At the cmc of SDS

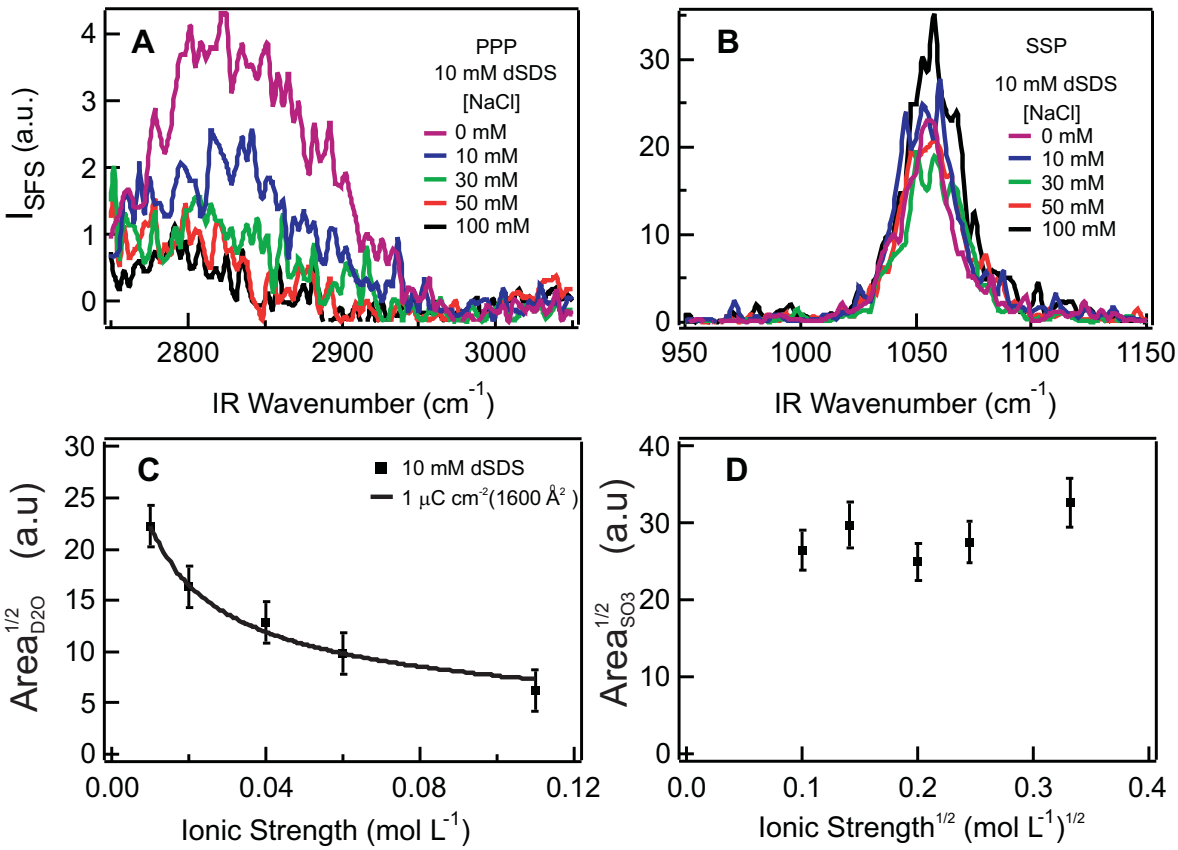

Figure 6.4: Response of the SFS spectra to the ionic strength at a 10 mM dSDS concentration. The emulsion consisted of 1 vol% dC16-in-D_2O. (A) SFS spectra of the CH stretch region in *ppp*-polarization combination. (B) SFS spectra of the symmetric SO_3 headgroup stretch in *ssp*-polarization combination. (C) Squared-root of the integrated spectrum of the OD-stretch response as a function of the ionic strength. (D) Squared-root of the integrated spectrum of the SO_3-stretch response as a function of the ionic strength. Note that these measurements are performed in the same sample.

Fig. 6.4 shows SFS spectra at different ionic strength but constant dSDS concentration (10 mM) for the spectral regions of the OD stretch and SO_3 symmetric stretch. The ionic strength was controlled by the NaCl salt. Fig. 6.4.A shows that the strength of the SFS signal decreases continuously as the ionic strength increases. The signal strength decreases a factor of 3-4 as the ionic strength increases by one order of magnitude.

Fig. 6.4.B shows the strength of the symmetric SO_3 stretch for the *same samples* as in Fig. 6.4.A. It can be seen that the intensity of the SO_3 stretch resonance stays constant as the ionic strength increases. This observation shows indeed that the interfacial density is not changing, thus the surface charge density is constant at 10 mM dSDS concentration. This reduces the number of variables that affects the surface potential.

Fig. 6.4.C shows the square root of the integrated OD stretch response as a function of ionic strength. As it can be seen in Fig. 6.4.C the signal strength decreases more strongly for small ionic strengths and seems to level off at a higher concentration.

6.4.3 At the constant surface potential concentration

Both surface charge density and surface potential change with surfactant concentration and ionic strength [14]. Fortunately, at the cmc the surface charge density does not increase since an increase in SDS concentration would create more micelles, and not increase the interfacial excess. For SDS concentrations below 10 mM, a change in ionic strength shows an interplay between surface charge density increase and increase in screening length.

The SFS results for the SDS concentration (1.5 mM dSDS) are shown in Fig. 6.5 for different ionic strengths. In Fig. 6.5.A the OD stretch strength seems to increase slightly at 30 mM NaCl and then keeps constant again as the ionic strength increases. The observed constancy is in qualitative agreement with the ζ-potential measurements. Nevertheless, the observed constancy of the surface potential at this SDS concentration is still puzzling since it should decreased based on Eq. 6.7.

The constancy of the surface potential can be explained by an increase in surface charge density. Fig. 6.5.B shows the response of the SO_3 symmetric stretch. The intensity of the signal increases a factor $\approx$6 as the NaCl concentration changes from 0 to 100 mM. Since we did not observe any systematic variation in the ssp/ppp-ratio, the increase in the signal strength is related to an increase in interfacial excess. At 1.5 mM dSDS concentration, the interfacial excess is not close packed (Chapter 4). Therefore, an increase in interfacial excess is plausible.

6.4.4 Discussion

The signal strength of the OD stretch vibration at the cmc decreases a factor of 3-4 as the ionic strength increases by one order of magnitude. This behavior can be understood as follows. The Debye-Hückel screening length is inversely proportional to the square root of the ionic strength. Therefore, the extension of the electrostatic field into the solution decreases as the ionic strength increases, if the surface charge density is constant. A shorter extension of the electrostatic field decreases the amount of water dipoles within the region where this higher order process take place. Fig. 6.6 illustrates this explanation.

The results in Fig. 6.4 can be nicely described by the Gouy-Chapman model. Eq. 6.7

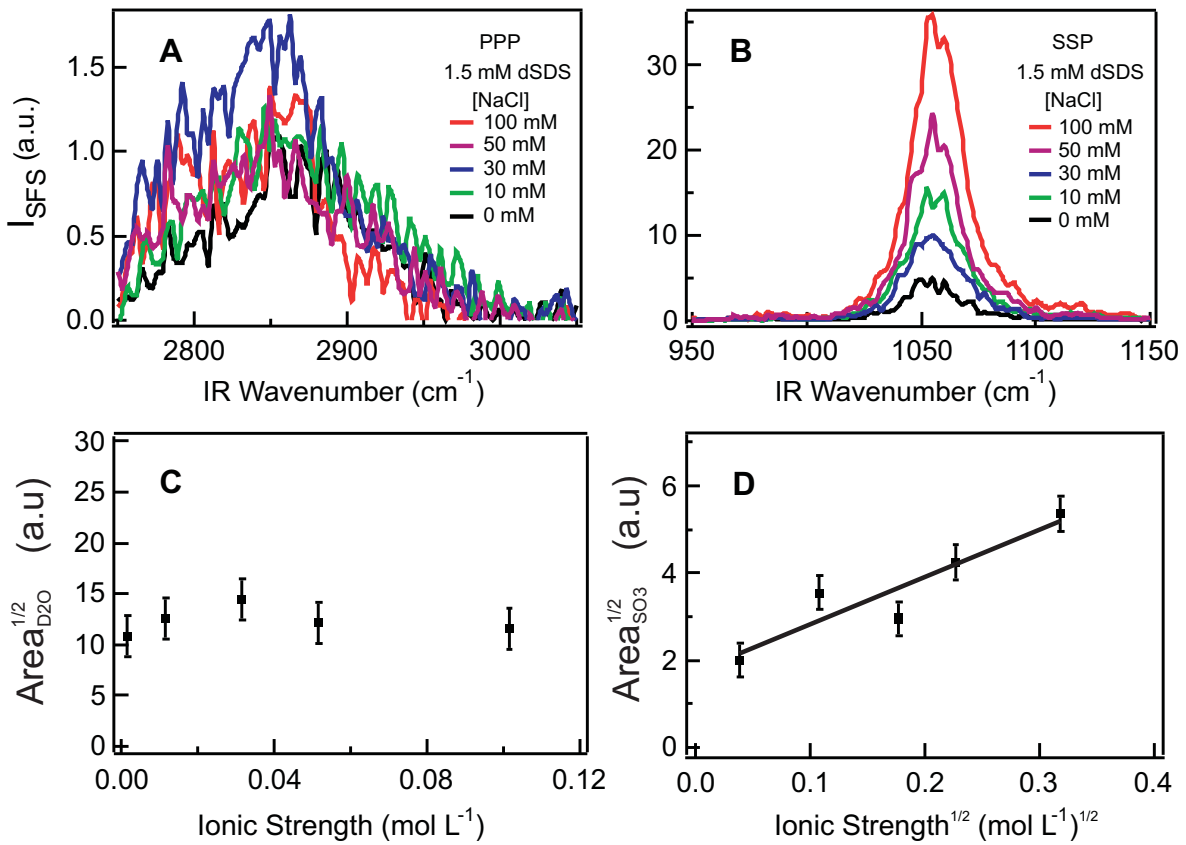

Figure 6.5: Response of the SFS spectra to the ionic strength at a 1.5 mM dSDS concentration. The emulsion consisted of 1 vol% dC16-in-D_2O(A) Response of the OD-stretch in *ppp*-polarization combination. (B) Response of the SO_3 headgroup stretch in *ssp*-polarization combination. (C) Squared-root of the integrated spectrum of the OD-stretch response as a function of the ionic strength. (D) Squared-root of the integrated spectrum of the SO_3-stretch response as a function of the ionic strength. The continuous line is a linear fit.

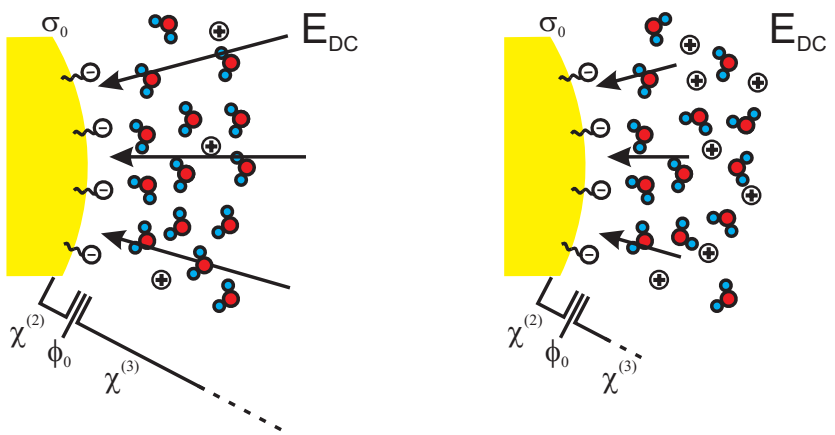

Figure 6.6: Illustration of the effect of the ionic strength on the strength of the electrostatic field. Upon increasing the salt concentration, the electrostatic field is screened more decreasing its extent into the solution.

relates surface potential and ionic strength. The signal strength in Fig. 6.4.A is proportional to the surface potential [15], and from a fit using Eq. 6.8 we can retrieve a surface charge density. Table 6.1 shows the obtained values from the fitting. The surface charge density σ of $1\pm0.5\,\mu$C cm^{-2} (or 1600 Å^2 per charge) corresponds to a surface potential of 40 mV (1.5 k_BT) at 10 mM SDS.

A	0
B	583±282
σ	$1\pm0.5\,\mu$C cm^{-2}

Table 6.1: Parameters obtained from the fittings to the data presented in Fig. 6.4.C with Eq.6.8

Remarkably, the obtained surface potential compares very well to 45 mV measured by Leal-Calderon et al using the Magnetic Chaining Technique [3]. However, the surface potential retrieved from SFS strongly disagrees with ζ-potential measurements which show a "surface potential" of -120 mV. Nevertheless, the ζ-potential measurements qualitatively agree with SFS results, both showing a decrease in potential for 10 mM dSDS and the constancy of the potential at 1-2 mM dSDS as the ionic strength changes.

The apparent baseline at higher ionic strength is not a consequence of a surface potential *independent* response which would give rise to a baseline (ionic strength independent) as a function of ionic strength (the A term in Eq. 6.6) [6]. This is due to the $\sinh(x^{-0.5})$ dependence, which only decreases to zero for very high ionic strength. The negligible contribution of a surface potential independent response is further supported by measurements performed with positively charged surfactants (not shown) which also shows a decrease in the strength of the OD stretch signal with an increase of ionic strength. Since the signal decreases for both cases, we can conclude that the surface-potential independent signal is negligible. This is not the case for SHG studies because the second-harmonic signal is non-resonant, therefore one cannot distinguish between the A and B terms. In a SFS experiment we can selectively probe molecular vibrations of species that gives rise to a signal that is predominantly either from the B term (the outnumbering bulk water) or A term (interfacial species such as SDS).

Using the retrieved surface charge density and the interfacial excess of Chapter 4, a lower limit for the degree of ionization can be obtained for SDS at the cmc. The corresponding area per charge is 1600 Å^2 and the area per SDS is 425 Å^2. The degree of ionization is $\sim$25%.

At 1.5 mM dSDS concentration the interfacial excess is not yet close packed and can be increased by changing the ionic strength. If the degree of ionization is constant, the observed increase in interfacial excess is directly related to an increase in surface charge density. Consequently, an increase in surface charge density increases the surface potential. However, as the ionic strength increases the screening length shortens, therefore the surface potential decreases. These two effects, increase in surface charge density and decrease in surface potential as the ionic strength increases, seem to cancel each other at 1.5 mM dSDS concentration

making the surface potential constant.

The results at the 1.5 mM dSDS concentration can also be nicely described by the Gouy-Chapman model. According to Eq. 6.7, if the surface potential is constant, then the surface charge density should be linearly related to the square root of the ionic strength. Fig. 6.5.C shows the square root of the SO_3 resonance integrated intensity as a function of (ionic strength)$^{1/2}$. The observed linearity corroborates the assumption of a constant degree of ionization.

The ζ-potential measurements agrees qualitatively with the SFS results. At 10 mM dSDS concentration, i. e. close to the cmc, both techniques show a decrease in potentials as the ionic strength increases. Around 1-2 mM ζ-potential shows the same potential for 0 and 100 mM NaCl and SFS shows a constant potential. Moreover, the surface-potential retrieved from the SFS results is in quantitative agreement with Magnetic Chaining Technique. However, the ζ-potential is quantitatively different, showing a higher values (modulus) even though it is expected that the potential measured at the shear plane to be *smaller* than the surface potential as schematically depicted in Fig. 6.2. An issue of ζ-potential measurements is that the shear plane is ill-defined and changes for every system [4]. For example, ζ-potentials of hexane droplets stabilized with SDS are considerably lower than hexadecane droplets with the same concentration of SDS [16]. However, one would expect that the ζ-potentials to be the same as well, based on Eq. 6.7, because the SDS interfacial density at both interfaces are the same [17]. At this point, we cannot offer and explanation for the discrepancy, but we can conclude that there is very good qualitative agreement between the techniques.

6.5 Conclusions

This chapter has focused on the electrostatics of the liquid-liquid droplet interface and how can we probe it with SFS. The strength of the OD stretch response was related to the surface potential. By measuring the vibrational resonances of the surfactant molecules at the interface, we could probe the surface charge density independently. The surface potential was sensitive to the ionic strength, but also to the surface charge density. At surfactant concentrations at the critical micelle concentration, an increase in the ionic strength decreases the surface potential, but the surface charge density remains constant. At 1.5 mM, the surface potential showed to be insensitive to ionic strength, whereas the surface charge density increases. The results could be explained based on the Gouy-Chapman model, from which we obtained a surface charge density of $1 \pm 0.5\ \mu C\,cm^{-2}$ at 10 mM corresponding to a surface potential of 40 mV. Moreover, the changes in surface potential are in qualitative agreement with ζ-potential measurements.

Bibliography

[1] J. Bibette, F. Leal Calderon, and P. Poulin. Emulsions: basic principles. *Rep. Prog. Phys.*, 62(6):969, 1999.

[2] J. W. Goodwin. *Colloids and interfaces with surfactants and polymers: an introduction*. John Wiley & Sons, 2004.

[3] F Calderon, T Stora, O Monval, P Poulin, and J Bibette. Direct measurement of colloidal forces. *Phys. Rev. Lett.*, 72(18):2959, 1994.

[4] R J Hunter. *Zeta Potential in Colloid Science: Principles and Applications*. Colloid Science. Academic Press, 1981.

[5] S. W. Ong, X. L. Zhao, and K. B. Eisenthal. Polarization of water-molecules at a charged interface: 2nd harmonic studies of the silica water interface. *Chem. Phys. Lett.*, 191(3-4):327–335, 1992.

[6] X. L. Zhao, S. W. Ong, and K. B. Eisenthal. Polarization of water-molecules at a charged interface - 2nd harmonic studies of charged monolayers at the air-water-interface. *Chem. Phys. Lett.*, 202(6):513, 1993.

[7] H. Wang, E. C. Y. Yan, E. Borguet, and K. B. Eisenthal. Second harmonic generation from the surface of centrosymmetric particles in bulk solution. *Chem. Phys. Lett.*, 259(1-2):15–20, 1996.

[8] E Yan, Y Liu, and K Eisenthal. New method for determination of surface potential of microscopic particles by second harmonic generation. *J. Phys. Chem. B*, 102(33):6331, 1998.

[9] A. G. F. de Beer, R. K. Campen, and S. Roke. Separating surface structure and surface charge with second-harmonic and sum-frequency scattering. *Phys. Rev. B*, 82(23):235431, 2010.

[10] J Stachurski and M Michalek. The effect of the zeta potential on the stability of a non-polar oil-in-water emulsion. *J. Colloid Interface Sci.*, 184(2):433–436, 1996.

[11] J Beattie and A Djerdjev. The pristine oil/water interface: Surfactant-free hydroxide-charged emulsions. *Angew. Chem., Int. Ed.*, 43(27):3568, 2004.

[12] K Marinova, R Alargova, N Denkov, O Velev, D Petsev, and I Ivanov. Charging of oil-water interfaces due to spontaneous adsorption of hydroxyl ions. *Langmuir*, 12(8):2045, 1996.

[13] J Beattie, A Djerdjev, and G Warr. The surface of neat water is basic. *Faraday Discuss.*, 141:31, 2009.

[14] V V Kalinin and C J Radke. An ion-binding model for ionic surfactant adsorption at aqueous-fluid interfaces. *Colloids Surf., A*, 114:337, 1996.

[15] G Wurpel, M Sovago, and M Bonn. Sensitive probing of DNA binding to a cationic lipid monolayer. *J. Am. Chem. Soc.*, 129(27):8420–8421, 2007.

[16] A Djerdjev and J Beattie. Electroacoustic and ultrasonic attenuation measurements of droplet size and zeta-potential of alkane-in-water emulsions: effects of oil solubility and composition. *Phys. Chem. Chem. Phys.*, 10(32):4843, 2008.

[17] S. J. Rehfeld. Adsorption of sodium dodecyl sulfate at various hydrocarbon-water interfaces. *J. Phys. Chem.*, 71(3):738–745, 1967.

Summary and outlook

Summary

Emulsions are colloidal systems composed of liquid droplets floating in another immiscible liquid. Due to emulsion relevancy in our daily lives, a number of fundamental and applied studies have been performed since the 19th century. Most of these studies aimed to understand emulsions at a fundamental level and ultimately to control its properties and stability. Nowadays, it is well known that interfacial properties of the droplets determine the stability of emulsions. However, there still lacks a molecular level description of the droplet interface. Part of this problem is due to the experimental challenge of probing droplets interfaces with interface specificity. Even though new experimental techniques capable of differentiate interfacial species from bulk species exist, there is the additional and inherent nature of the droplets: they are buried in a liquid phase that is impenetrable for the probes with interface specificity. Consequently, most of our understanding of the droplets interface at a molecular level was build based on outcomes and extrapolations of results from planar liquid interfaces experiments.

In this thesis, we used SFS to gain a molecular level description of the droplets in oil-in-water emulsions. SFS is an interface specific technique which can measure a vibrational spectrum of the species at the droplet interface. Here, we present a summary of our results.

In Chapter 3, we presented a detailed description of the SFS experiment. We also discussed competing processes that occurs within the sample and how to discern them from the SFS response of the droplets. We characterized the SFS signal to different experimental parameters: scattering pattern, cuvette path length, droplet density, IR energy and penetration depth. After a thorough analysis, we concluded that our SFS spectra are free of artifacts and represent the vibrational response of the interfacial molecules that constitute the liquid-liquid oil droplet-water interface.

As discussed in the Introduction of this thesis, surfactants are believed to populate the oil droplets interface in the same density as it is found for planar oil-water interfaces. Since the SFS response is proportional to the interfacial density of molecules, we presented in Chapter 4 the response of symmetric SO_3 stretch of the headgroup of the surfactant Sodium dodecylsulfate (SDS) as a function of the concentration. We found a surprisingly low interfacial density of surfactants at the oil droplets interface, one order of magnitude lower than

at the corresponding planar interface. We used the Gibbs adsorption equation that relates interfacial tension, surfactant concentration and interfacial density to retrieve the changes in interfacial tension. As a consequence of such a low interfacial density, the interfacial tension barely changes from the value of the neat oil-water interface. The results further explained the discrepancies in Ostwald ripening rates reported on literature. We also observed similar interfacial density for the anionic surfactant sodium bis(2-ethylhexyl) sulfosuccinate.

SFS is a powerful technique to study molecular order of the alkyl chains. In Chapter 5 we selectively probed the CH stretch of the alkyl chains of the surfactants and oil. From the spectral analysis of the CH stretch response we could infer the molecular order of SDS and the oil molecules at the interface. We showed that SDS is very disordered as expected based on the very low interfacial density found in the Chapter 4. In contrast, the alkyl chains of the oil molecules at the interface was much more ordered than the surfactants. To understand the origin of this difference in order, we measured the response of both SDS and oil to the SDS concentration. The increase in SDS response in CH stretch regiong was in agreement with the one founds for the SO_3 response. In contrast, the response of the oil molecules did not change while increasing the interfacial density of SDS. We interpreted these results as the SDS chains not interacting with the oil chains. This was further supported by the similar degree of order of SDS when adsorbed at polymer particles interface (PTFE and polystyrene beads). From an interference experiment of the response of the oil with the SDS molecules, we concluded that the oil molecules are predominantly oriented parallel with respect to the plane of the interface. We finalize the chapter giving a possible explanation to the observed low interfacial density based on the timescales of Brownian motion and droplet rotation and comparing it to the timescale on which an interface reaches its equilibrium state as observed from planar interface experiments.

In Chapter 6, we used SFS to probe the electrostatic properties of the droplets interface. We showed that we can measure independently the surface potential and the surface charge density. The strength of the OD vibrational stretch was proportional to the surface potential. The surface charge density was probed by measuring the SO_3 vibrational response of the SDS headgroup adsorbed at the droplet interface. Since both the equilibrium adsorption of ionic surfactants and the surface potential are sensitive to the ionic strength, the independent measurement of these quantities was vital to separate the changes in surface potential due to charging of the interface from changes due to screening effects. We demonstrated this by measuring the response of the surface potential and surface charge density to the ionic strength in solution. We chose two SDS concentrations: one where the charge density was constant and another where the surface potential was constant. The results were explained based on the Gouy-Chapman model and were in good quantitative agreement with other techniques that can measure surface potentials. However, the results were only in qualitative agreement with ζ-potential measurements.

Outlook

This thesis presented the first vibrational spectra of the species at the oil droplets-water liquid-liquid interface. We hope that with this work we can start bridging the gap between emulsion and interfacial science. These results also pave the way for further studies in aqueous dispersion, like vesicles, polymer particles etc. Although some results presented were surprising, we could only provide a tentative explanation. Further theoretical work is necessary to clearly understand what is the fundamental reason in the discrepancy between planar interfaces and emulsion droplets.

Due to the very low interfacial density of surfactants, the oil droplet-water interface behaves more like the neat interface. This offers the opportunity to study the neat alkane-water interface, one of the simplest chemical structure of oil-water interfaces. With the intrinsic sensitivity of SFS to molecular order, one can try to elucidate what is the origin of the order of the alkane-water interface as measured by X-Ray Reflectivity and Second-Harmonic Generation.

From a perspective of the electrical double-layer effects, Chapter 6 shone some light in this widely studied phenomena. Now that it is possible to separate the two important quantities that characterizes the double-layer, one can use more conclusive measurements together with more complicated models of the double-layer apart from the Gouy-Chapman model.

Acknowledgements

This might be the hardest part of the thesis, since there are too many people that helped me until here in many different ways. The list here is far from being complete. For those who I forgot: Thank you! First of all I'd like to thank Sylvie Roke for believing in me and giving me this opportunity of performing my PhD abroad in a great scientific environment. Our discussions certainly helped me to boost my scientific arguments, perspective and accuracy. The guys from the lab for helping me out one way or another: Albert, Anneke, Magnus and Luca for the initial help in understanding the laser setup and fruitful discussions; Joerg and Lalinda. Special thanks to Matt and Alex who taught me a lot of Physics and Chemistry during this PhD, helping me to understand more about the fabulous Nature. The latest group members Mireia, Jean and Rudy for the friendship, help in proof-reading and translations, gràcies, merci and danke, respectively. The people from the Max-Planck that help me with technical comments, giving directions in the institute and/or just simply having fun in the night: Julien, Roberto, Stefan, Kristen, Carla, Maggie, Kasya and Claudio; The Southside team Burak (tough, but fair), Burcu, Jaysen and Eduardo, you guys should all continue to behave. My friends back in Brazil that continuously support me online or offline =) May the force be with you!: Ézio, Júlia e família, Luciano e família, Lucinalda e Neto, Memel e família, Marlon e família, Tadeu, Suellen e família, Duardo e família, Larissa, HT e família, Lu Piteca, Felipe, Léo Levi, Marcelo Caju, Najara, Tony and X. Carol who gave me support in many important moments: My sincere best wishes in your new path. The numerous friendships I've made during my staying in Stuttgart. People from the beginning of my journey to Germany that help me out adapting to the new life abroad: Karsten, Wieland, Fabian, Carlos, Mattias/Jenny and family; The brazilian dudes Dani and Ciro, Chris, Thais, Willian, Thomas Tigrão and Sandra (valeu rapaziada!); The latest ones (but not least) Madeleine, Salome, Amelie and Jan, cumpadre PY and cherie Caro (the frenchship will never sink), Yannis and cumadre Jovana; A special thanks to Silvia who was always very cheerful when welcoming me in the Traditional Jazz Hall, as well as the others. Those nights will certainly continue to keep vivid in my mind . . . without all of you, there wouldn't be any magic in this life.

To my family that supported me all the way until here. Seu Beto, Dona Angela, Jonatas e Davy, o melhor grupo do qual ja participei e os quais me ensinaram a sempre ter fé em Deus; Tia Carmen e família. Durante o meu percurso de vida, a distância física foi grande,

mas os ensinamentos que todos vocês me deram foram fundamentais para mantê-los sempre por perto, de um jeito ou de outro...

...that's all folks!

Curriculum Vitae

Hilton Barbosa de Aguiar

PERSONAL INFORMATION

Nationality: Brazilian
Date of birth: 01/08/1980
Address: Nonlinear Spectroscopy Group, Max-Planck Institute for Metals Research, Heisenbergstrasse 3, 70569 Stuttgart, Germany
E-mail: haguiar@mf.mpg.de, hiltonbarbosa@gmail.com

EDUCATION

2007-11 **PhD candidate in Photonics**, École Polytechnique Fédérale de Lausanne (EPFL), Switzerland (expected June 2011)

- **Thesis:** *Vibrational Sum-Frequency Scattering studies of oil-in-water emulsions*
- **Advisor:** Sylvie Roke

2005-07 **MS in Materials Science and Engineering**, Universidade de São Paulo, Brazil.

- **Dissertation:** *Alguns Aspectos Acerca da Adsorção de Alcanotióis e Bases Nitrogenadas em Ouro via Espectroscopia Não-Linear e Microscopia de Tunelamento de Elétrons*
- **Advisor:** Paulo B. Miranda

2001-05 **Undergraduation in Physics Licenciate**, Universidade Federal de Sergipe, Brazil.

AWARDS and FELLOWSHIPS

2008 Best poster in the Biomaterials Interfaces Division at the American Vacuum Society 55th International Symposium.

2003- Member of the Brazilian Physical Society.

PROFESSIONAL EXPERIENCE

- **Teaching Assistantship**, Physics I at Universidade de São Paulo/USP, Brazil (2006).
- **Scholarships for Undergraduate Scientific Projects**, at Universidade Federal de Sergipe, São Cristovão, Brazil (2002-2005).
- **Receptionist**, Resort Parque dos Coqueiros, Aracaju, Brazil (2000-2002).
- **Administrative Assistant**, Construtora Celi (1998-2000).

SCIENTIFIC and GENERAL INTERESTS

- **Experimental Techniques**: Scanning Tunneling Microscopy, Nonlinear Spectroscopy (Vibrational Sum-Frequency Generation), Dynamic and Static Light Scattering, Cyclic Voltammetry, FTIR, Raman Scattering.
- **Research Areas**: Emulsions, Colloids, Self-Assembled Monolayers, Liquid-Liquid and Solid-Liquid Interfaces, Nonlinear Optics, Light Scattering.
- **Cultural Activities**: Musical and Audiovisual production.
- **Sports/Hobbies**: Soccer and Aikido.

PUBLICATIONS

- H. B. de Aguiar, M. L. Strader, A. G. F. De Beer and S. Roke. **Surface structure of SDS Surfactant and oil at the oil-in-water droplet liquid/liquid interface: A manifestation of a non-equilibrium surface state**. *J. Phys. Chem. B*, 115 (2011), 2970.
- M. L. Strader, H. B. de Aguiar, A. G. F. De Beer and S. Roke. **Label-free Spectroscopic Detection of Vesicles in Water using Vibrational Sum Frequency Scattering**. *Soft Matter*, 7 (2011), 4959.
- R. Vacha, P. Jungwirth, S. W. Rick, A. G. F. de Beer, H. B. de Aguiar, J.-S. Samson, and S. Roke. **The orientation and charge of water at the hydrophobic oil droplet-water interface**. *Accepted in J. Am. Chem. Soc.*, 2011.
- H. B. de Aguiar, J.-S. Samson and S. Roke. **Probing nanoscopic droplet interfaces in aqueous solution with vibrational sum-frequency scattering: a study of the effects of path length, droplet density and pulse energy**. *Submitted to Chem. Phys. Lett.*, 2011.
- H. B. de Aguiar, A. G. F. de Beer and S. Roke. **Phase matched vs non-phase matched SFG: A comparison between sum frequency scattering and reflection from a dispersion of nanoscopic droplets in aqueous solution**. *In preparation*, 2011.
- H. B. de Aguiar, A. G. F. de Beer and S. Roke. **Measurements of surface potentials and surface charges by Vibrational Sum-Frequency Scattering**. *In preparation*, 2011.

- H. B. de Aguiar and S. Roke. **Ultrasensitive detection of buried nanostructures: Nonlinear Light Scattering reveals cristalinity in amorphous Polylactic Acid**. *In preparation*, 2011.
- H. B. de Aguiar, A. G. F. De Beer, M. L. Strader and S. Roke. **The Interfacial Tension of Nanoscopic Oil Droplets in Water Is Hardly Affected by SDS Surfactant**. *J. Am. Chem. Soc. (Communication)*, 132 (2010), 2122.
- H. B. de Aguiar, F. Cunha, F. Nart, P. B. Miranda. **Adsorption Behavior of 5-fluorouracil on Au(111): an in-situ STM Study**. *J. Phys. Chem. C*, 114 (2010), 6663.
- J. I. Dadap, H. B. de Aguiar and S. Roke. **Nonlinear light scattering from clusters and single particles**. *J. Chem. Phys.*, 130 (2009), 214710.
- A. G. F. de Beer, H. B. de Aguiar, J. F. W. Nijsen, S. Roke. **Detection of Buried Microstructures by Nonlinear Light Scattering Spectroscopy**. *Phys. Rev. Lett.*, 102 (2009), 095502.
- A. B. Sugiharto, C. Magnus Johnson, H. B. de Aguiar, L. Alloatti, S. Roke. **Generation and application of high power femtosecond pulses in the vibrational fingerprint region**. *Appl. Phys. B, Lasers and Optics*, 91 (2008) 315.
- H. B. Aguiar, A. C. Santanna, M. L. A. Temperine, P. Corio, F. Cunha. **Surface Enhanced Raman Spectroscopy Analysis Of The Adsorption Of 2-Thiouracil To Au, Ag And Cu Electrodes: Surface Potential Dependence**. *Vibrational Spec.*, 40 (2006), 127.
- J. E. Andrade, H. B. Aguiar, F. Cunha. **Silver Nanoparticles Self Assembled On HOPG: Unusual Behavior As Probed By Scanning Tunneling Microscopy**. *Microscopy and Microanalysis*, 11, S03 (2005), 158.
- H. B. De Aguiar, P. Corio, A. C. Santanna, M. L. A. Temperine, F. C. Nart, F. Cunha. **Adsorção da Timina em Ag: Estudo da Influência do pH Via SERS**. *Scientia Plena*, 1 (2005), 20.
- L. Almeida, H. B. De Aguiar. **Uma escolha nada retrô (box: LP x CD)**.*Contexto*, São Cristovão/SE, 8 (2006).

COMPUTER EXPERIENCE

- LaTeX, Mathematica, CorelDraw, IgorPro, Pascal, MS Office, Adobe Photoshop.